The Pennsylvania State University

The Graduate School

Energy and Geo-environmental Engineering

# ROLES OF ZEOLITE SUPPORT AND NOBLE METAL IN SULFUR-TOLERANT CATALYST FOR LOW TEMPERATURE HYDROGENATION OF AROMATICS

A Dissertation in

Energy and Geo-environmental Engineering

by

Hyun Jae Kim



Submitted in Partial Fulfillment
of the Requirements
for the Degree of

Doctor of Philosophy

August 2011

The dissertation of Hyun Jae Kim was reviewed and approved* by the following:

Chunshan Song
Distinguished Professor of Fuel Science and Professor of Chemical Engineering
Dissertation Advisor
Chair of Committee

Yaw D. Yeboah
Professor of Energy and Mineral Engineering
Department Head of Energy and Mineral Engineering

Yongsheng Chen
Assistant Professor of Energy and Mineral Engineering

Adri van Duin
Associate Professor of Mechanical Engineering

*Signatures are on file in the Graduate School

## ABSTRACT

This dissertation focuses on fundamental understanding of the roles of supports and noble metals in the sulfur-tolerant catalysts for low-temperature hydrogenation of aromatics in the presence of sulfur. Emphasis was placed on investigating the effect of supports and supported metals for high sulfur tolerance and verifying a catalyst design concept for the sulfur-tolerant noble metal catalyst based on shape selective exclusion of sulfur and hydrogen spillover for low-temperature hydrogenation of aromatics [C.S. Song, Chemtech, 29 (1999) 26-30].

The effect of supports was explored for sulfur tolerance of the supported Pd catalyst on tetralin hydrogenation in the presence of benzothiophene by varying the Pd catalysts on different supports (mordenite, zeolite Y, zeolite A, amorphous silica-alumina). The pore structures and pore sizes were both found to be the important factors in determining the catalytic activity of sulfur-tolerant metal catalyst. Among the catalysts tested, the acidic zeolite Y-supported Pd catalyst showed excellent sulfur tolerance while maintaining high catalytic activity, which may be mainly due to its high surface area, acidity and three-dimensional zeolite framework.

The hybrid zeolite-supported Pd catalyst was prepared to improve sulfur tolerance, based on the proposed catalyst design concept. The hybrid catalyst consists of Pd supported on Y and A type zeolites. For further investigation on small pore system in hybrid catalyst, surface metal passivation by silica coating and pore size control by potassium ion exchange were employed to zeolite A-supported Pd catalyst. Although Pd on Zeolite A showed no catalytic activity for hydrogenation of tetralin, adding the small-pore catalyst to Pd/Y significantly enhanced sulfur tolerance of the catalyst for both naphthalene and tetralin hydrogenation in the presence of sulfur in the form of benzothiophene. Sulfur tolerance of the hybrid catalyst is mainly attributed to the

small pore system, inducing size-selective exclusion of bulky sulfur compounds as well as hydrogen spillover from metal inside small pore component. Hydrogen spillover plays two roles in maintaining high sulfur tolerance of the hybrid catalyst: first, regeneration of sulfur-poisoned metal active sites in the large pores of Pd/Y as well as hydrodesulfurization of aromatic sulfur compounds over the zeolite Y support.

The effect of metal species for the zeolite Y-supported metal catalyst was investigated using various group 10 metals (Ni, Pd, Pt) as well as Pd-Pt bimetal. The metal type also has major impact on sulfur tolerance of the zeolite supported catalyst for tetralin hydrogenation. Even Pd shows better sulfur-tolerance than other monometallic catalysts, Pd-Pt bimetallic catalyst exhibited exceptionally high sulfur-tolerance, maintaining 100% conversion for tetralin hydrogenation in the presence of sulfur, which can be ascribed to high metal dispersion and electron-deficiency of Pd-Pt. Addition of small pore catalyst (silica-coated Pd/KA catalyst) to Pd-Pt/Y also enhances sulfur tolerance of the Pd-Pt catalyst on tetralin hydrogenation even in the presence of 300ppmw sulfur as benzothiophene.

On the basis of the above results and discussion focusing on the importance of the supports and metal types for improving sulfur tolerance, the hybrid catalyst system based on the new design concept of sulfur tolerant catalyst is applicable in the development of sulfur tolerant catalysts for low-temperature hydrogenation of aromatics.

# TABLE OF CONTENTS

# LIST OF FIGURES

# LIST OF TABLES

# ACKNOWLEDGEMENTS

I am sincerely grateful to my advisor, Professor Chunshan Song for his continued faith and encouragement notwithstanding long period of poor returns. My Ph.D. degree would not have been possible without his generous investment of time, energy and wisdom.

I greatly benefited from my thesis committee members and sincerely thank Prof. Yaw Yeboah, Prof. Yongsheng Chen and Prof. Adri van Duin for their time and insightful and valuable advice and for serving as committee members.

I am also grateful to past and current members of our laboratory, Clean Fuels and Catalysis Program (CFCP) at Energy Institute for their knowledge, encouragement, patience and friendship. Especially, I'd like to thank Dr. Xiaoliang Ma, Dr. Cigdem Shalaby, Junichiro Kugai, Ramanathan Sundararaman, Jiahua Guo and Chao Xie for helpful discussion and Dr. Xiaoxing Wang and Dr. Dongxiang Wang for technical support. In particular, I owe a special debt of gratitude to Dr. Jae Hyung Kim in Sűd Chemie, Dr. Shyamal Kumar Saha in Dow Corning for sharing their profound knowledge with me. I also wish to thank the previous members of our laboratory, Andrew Schmitz, Ming Guo, Michael Sprague, and Brian Senger for their work on naphthalene and tetralin hydrogenation which helped to establish a base for data verification.

I wish to thank Dr. Trevor Clark, Ms. Nicole Wonderling and Dr. Maria Klimkiewicz in Material Characterization Lab for technical support that I received for the catalyst characterization in this work.

Finally, I gratefully acknowledge U.S. Department of Energy-National Energy Technology Laboratory and the Pennsylvania State University for sponsoring work presented in this thesis.

I dedicate this dissertation to my family, especially

to my parents for encouragement

to my wife Hyeran for love and understanding

to my son Jason for sharing your happiness

to my sister Taeyun for infusing optimism

## Chapter 1

# Introduction

The world demand for transportation fuels has been increasing for the past three decades while the world oil reserves have been gradually depleted. It leads to the use of lower-grade, higher sulfur and more aromatic feedstock for transportation fuel production, which is undesirable since the sulfur and aromatics contribute to the formation of environmental harmful emission including SOx and particulate matters in exhaust gases from combustion engines [1, 2]. In accordance with increasing awareness towards the health risks related to the fuel, sulfur and aromatic contents have been a target for the recent transportation fuel regulations [3]. In many countries, the specifications for diesel fuel already limit the sulfur contents strictly, and it is expected that the upcoming regulation related to the sulfur and aromatics content will be more stringent than before [4]. Thus, refineries are taking measures to meet the fuel specification along with the required aromatic contents, and considerable attention is currently being paid to deep desulfurization and aromatic hydrogenation of distillate fuels.

Conventional hydrotreating processes are widely employed in the refining industry to achieve target levels of sulfur and aromatics contents [1]. Reduction of aromatic content in addition to sulfur content is desired for better diesel fuel quality since reducing aromatics in diesel fuel increases cetane level as well as improved combustion characteristics [1, 2]. The existing hydrotreating processes predominantly utilize Co-Mo and Ni-Mo sulfide catalysts operating at relatively high temperature (>350 ℃) under high pressure. However, since deep aromatic hydrogenation favors lower temperature, these catalysts are not suitable to overcome

thermodynamic limitation of hydrogenation of aromatics. Recently, the noble metal catalyst candidates for deep hydrogenation have shown high catalytic activity at low temperature, but the typical noble metal catalyst has serious problem, i.e. rapid deactivation even when it is exposed to sulfur at trace sulfur level [5]. For these reasons, the noble metal catalysts in current hydrotreating processes require ultra deep hydrodesulfurization and multi stage hydrotreating to prevent sulfur poisoning.

Considerable research has been dedicated to the development of sulfur-resistant noble metal catalysts. For years, there have been two main approaches suggested to improve sulfur resistance. One is the introduction of acidic zeolite support. It was reported that noble metal catalysts supported on acidic zeolite are more sulfur tolerant than those on silica- or alumina-supports due to the stronger electron transfer to the acidic sites of the zeolite, making noble metal particles more electron-deficient [6-14]. This electron transfer causes weaker sulfur-metal bonding and improves sulfur tolerance of the zeolite supported noble metal catalyst.

The other approach is metal alloy. It has been proposed to improve the sulfur resistance of supported noble metal by adding another metal that either enhances metal support interactions or removes electron density from noble metal. Several bimetallic Pt or Pd catalysts (Co-Pt, Mo-Pt, Ni-Pt, Re-Pt, Ag-Pt, Pd-Pt, Pd-Rh, Pd-Ir, Pd-Au and Pd-Mo) were suggested for the improvement of hydrogenation activity or sulfur resistance on the catalyst [8, 15-23]. In the case of bimetallic Pt catalysts, Co-Pt, Ni-Pt, and Pd-Pt catalysts were reported to have the improved sulfur resistance on aromatic hydrogenation [15, 23, 24]. Pd metal and its alloy were also studied promisingly owing to the reversible nature of sulfur poisoning and easy hydrogen dissociation over Pd surface [18, 21, 25-28]. Overall, it is suggested that, since alloy formation causes electronic interaction between electronically different metal component, electrophilic metals tend to remove electron density from the noble metal in a bimetallic system and improves sulfur

resistance. However, the major problem related to these approaches is that the metal active sites are still exposed to and poisoned by organosulfur compounds remaining in the fuel feed.

A new design concept involving the support and metal with different pore configuration of support was suggested for sulfur-tolerant noble metal catalyst on zeolites for low-temperature aromatic hydrogenation by Song [4, 29, 30].

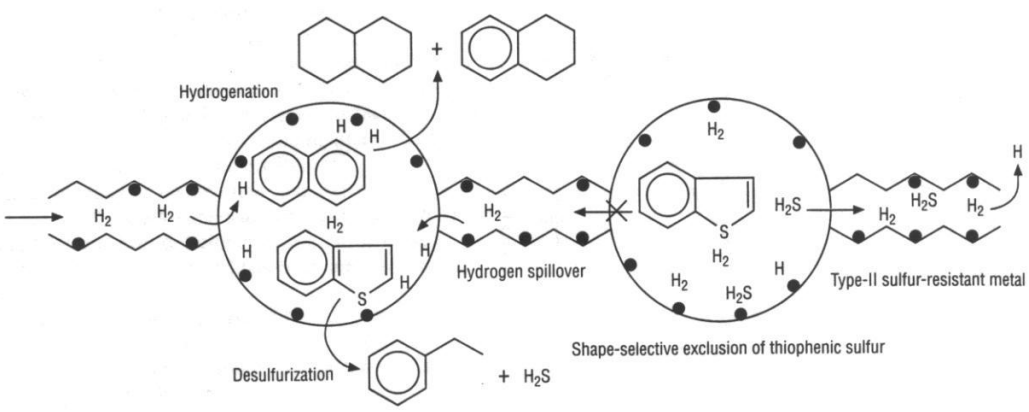


Figure **1-1**: Proposed catalyst design concept for aromatic hydrogenation. Adapted from [29]

As shown in Figure 1-1, the concept invokes different pore structures of zeolites as support matrix for noble metal catalysts and utilizes shape selective exclusion of sulfur compound and hydrogen spillover. According to the concept, noble metals are supported on zeolite material possessing bimodal pore size distributions. The large pore system (> 6Å) allows hydrogenation of polyaromatics and hydrodesulfurization of aromatic sulfur compounds, while bulky aromatics and organic sulfur compounds such as thiophenic molecules are selectively excluded from the small pore system (< 5Å). $H_2$ molecules can enter both large and small pores, be dissociated on metal sites and be transported between both pore systems by hydrogen spillover. When metal in

the large pore systems becomes inactive by adsorbed sulfur molecules, spillover hydrogen from the small pores can recover the poisoned metal sites by elimination of organic sulfur compound.

However, there are a number of scientific question that remain to be answered and several design issues remain to be clarified. Based on the discussion above, the main objective of the present study is to clarify the roles of support and metals on sulfur-tolerance of the noble metal catalysts for low-temperature hydrogenation of aromatics including the following aspects:

(1) Effect of zeolite supports and supported metals on hydrogenation of aromatics in the presence of aromatic sulfur

(2) Influence of hybrid zeolites and supported metals on the hydrogenation activity and sulfur resistance of metal catalysts

(3) Role of hydrogen spillover in improving sulfur tolerance of the catalyst

## Chapter 2

# Literature Review

### 2-1. Current industrial hydrotreating process

In the refining industry, conventional hydrotreating processes are widely employed to achieve acceptable levels of sulfur removal and the associated aromatic saturation [1]. These processes predominantly utilize sulfided Ni-Mo, Co-Mo or Ni-W catalysts supported on alumina in a hydrotreater operating at relatively high temperature (>350 °C) and high pressure [31]. However, this high reaction temperature limits aromatic conversion. Furthermore, severe operating conditions result in higher operation cost and additional process equipment which incurs high capital cost [32]. The performances of sulfided Co-Mo/$Al_2O_3$, Ni-Mo/$Al_2O_3$, and Ni-W/$Al_2O_3$ catalysts were compared in dearomatization of light cycle oil and found that it is impossible to meet stringent aromatics specifications in a single-stage reactor even under severe operating conditions with these catalysts [33].

The use of noble metal catalysts containing such metals as Pt and Pd has a potential to overcome these operating barriers in achieving deep aromatics reduction. Noble-metals are more active than conventional hydrotreating catalysts for aromatic hydrogenation and exhibit much higher turnover frequencies compared to metal sulfides at significantly lower temperature and pressure [2]. However, the biggest problem existing on noble metal catalysts is that it is easily poisoned by sulfur and nitrogen compound in the feedstock [5, 34].

For this reason, the commercial hydrogenation processes have been developed to employ two or multi-stage design. In the first stage, hydrodesulfurization is carried out over a traditional Co-Mo or Ni-Mo catalyst to reduce sulfur and nitrogen content of the distillate to very low levels. This stage is followed by intermediate removal of byproduct gases such as $H_2S$ and $NH_3$ before second stage. Deep hydrogenation over noble metal catalyst can thus be employed in the second stage where the sulfur content is low [35-37]. The commercial examples of two-stage or multi-stage hydroprocessing technology are listed in Table 2-1 and their flow diagram are shown in Figure 2-1~4.

Table **2-1**: Current commercial process for ultra deep HDS and hydrogenation [38]

| Licensor | Process | Purpose |
|---|---|---|
| Shell | Shell middle distillate hy drogenation process | Deep desulfurization and aromatic saturation |
| Topsøe | Two stage process for improving disel quality | Deep HDS and aromatic hydrogenation of diesel blends |
| | Ultra deep HDS process (UD HDS) | Two stage process for producing low sulfur and low aromatic diesel fuel |
| IFP/Axen | IFP deep HDS and HAD | Diesel deep HDS and aromatic hydrogenation |
| | Axen (IFP) Prime-D | Producing diesel fuel with low sulfur and reduced polycyclic aromatic compounds and boosted cetane rating |
| UOP | MQD Unionfining | High-quality low sulfur diesel fuel by combining base metals and noble metal catalyst in the first and second stages. |
| Criterion & ABB Lummus | SynSat | Ultra deep HDS, aromatic saturation |
| | SynShift | Ultra deep HDS, density reduction, cetane increase, distillation shift, polyaromatic saturation |

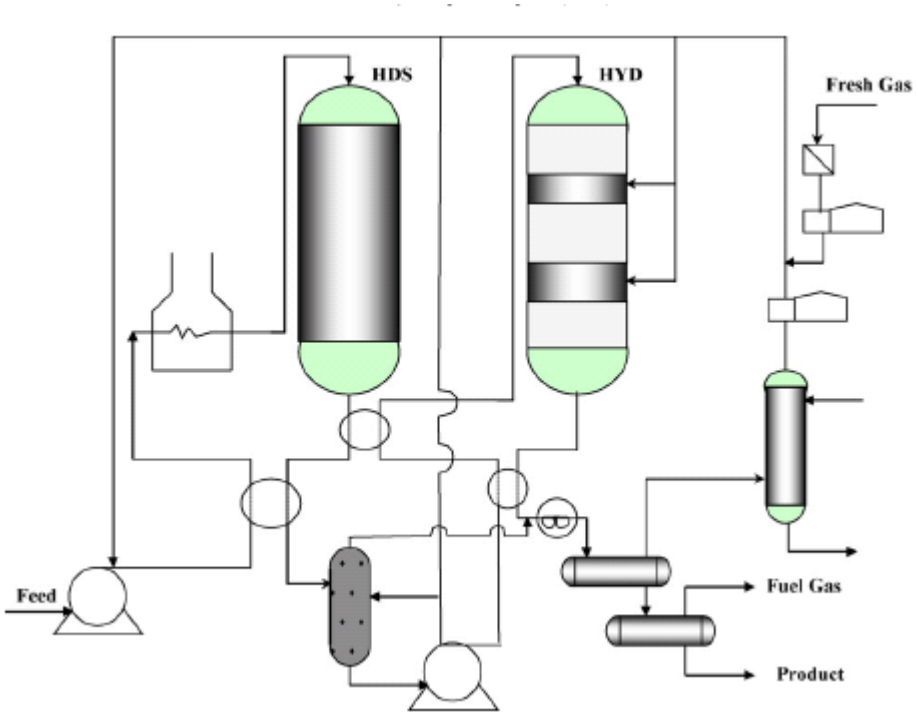


Figure **2-1**: Shell middle distillate hydrotreating Process adopted from [38]

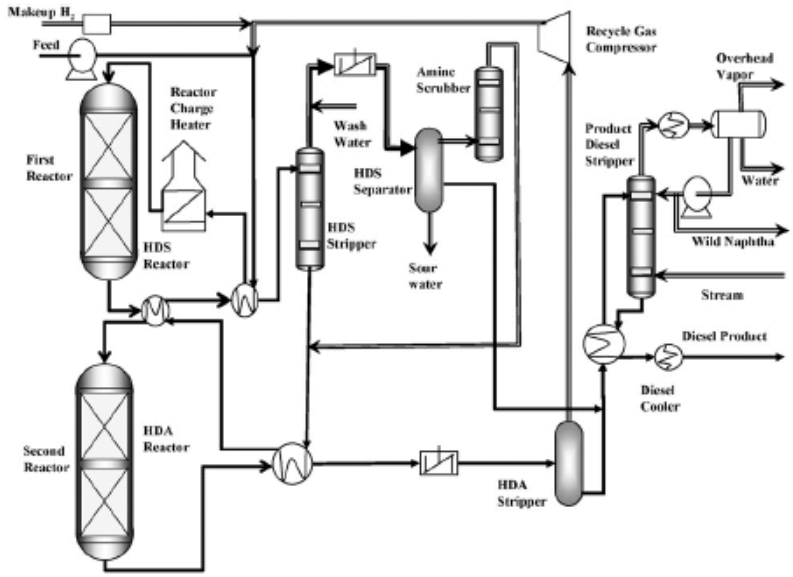


Figure **2-2**: Haldor-Topsoe two-stage process for diesel aromatics removal adopted from [38]

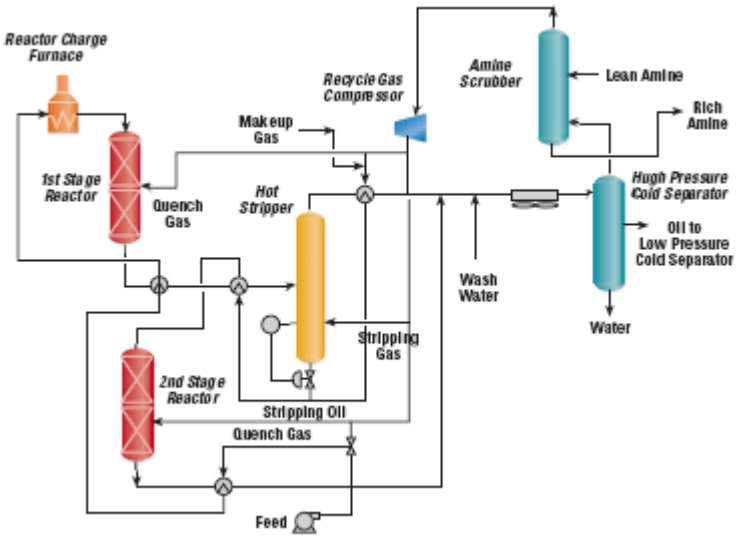


Figure **2-3**: Integrated Two stage MQD Unionfining Process for noble metal catalyst system [39]

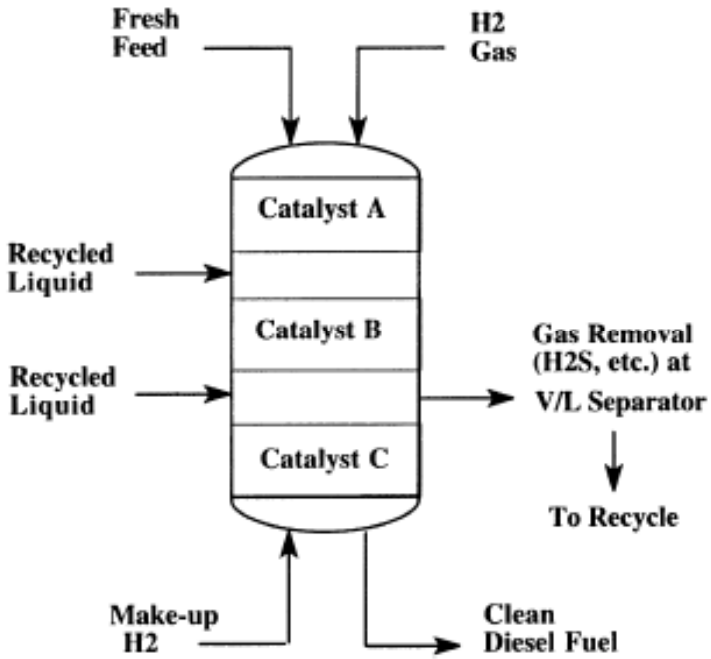


Figure **2-4**: The Criterion / ABB Lummus Crest SynSat/SynShift process, from [35]

Among these processes, SynSat Process (short for synergetic saturation) by Criterion / ABB Lummus Global, is considered to be an innovative technology [40]. The process configuration is the same as the two stage-design mentioned before, but it adopts just one reactor shell with several different catalyst beds in it and there is intermediate removal of by-product gases between the catalysts beds. The upper and the bottom catalyst beds (Catalyst A and C in Figure 2-4) contain the hydrodesulfurization catalysts such as Ni-Mo or Co-Mo sulfide and the noble-metal catalyst for dearomatization, respectively. The SynShift process was developed to supplement the SynSat process with a ring-opening process. Typical operating conditions for the SynSat/SynShift process are 315 – 400 °C and 450 – 900 psig, depending on feedstock composition and output specifications [35, 41, 42]. These Syn- technologies have the flexibility to be operated for desulfurization, desulfurization with dearomatization and even for mild hydrocracking [35, 43].

However, even though there are several processes developed for removing sulfur and aromatic compounds at the same time, there is no report of noble metal catalysts that can operate without first stage hydrodesulfurization [34]. It is expected in future that the enhanced noble metal catalysts with high sulfur tolerance will lead to significant improvement in terms of efficiency and economics of refinery, which will allow the hydrotreating at lower temperature and pressure, or be used for new processing schemes or even in stacked bed within a single reactor shell.

## 2-2. Sulfur poisoning

As previously mentioned, one of the biggest problems in application of noble metal to commercial hydrotreating is sulfur poisoning. The noble metal catalysts are easily and rapidly poisoned by even a few ppm of sulfur present in industrial fuel feedstock. It has been reported that adsorption of sulfur on the catalytic active sites inhibits adsorption of reactants such as $H_2$, CO, NO, aromatics and olefins on Pd surfaces, thus prevent reaction by steric effect. For example, adsorption capacity of $H_2$ is diminished proportional to the fraction of sulfur coverage on the surface [44]. Sulfur poisoning results from strong bonding between the electronegative sulfur atoms and metal atoms of noble metal catalyst. It is caused by donation of unshared electrons of sulfur to unfilled d-orbital on the transition metal, forming α-bond, and a synergistic back donation of electron from filled d-orbital on the metal to unfilled orbital on sulfur, inducing π-bond [45]. The adsorption energy of atomic sulfur on transition metal surface is between 80-140kcal/mol and it decreases as S coverage increases. At low sulfur coverage, where only minor interactions between sulfur atoms exist, sulfur adsorbs on metal sites with the highest binding energy. Each sulfur atom is bonded with three or four metal atoms and placed in the highest coordination site. As coverage increases, the metal-sulfur bond is weakened [5].

The extent of sulfur poisoning is varied by the kinds of sulfur compounds. It was reported that the unshielded structures, such as $H_2S$, are more toxic than shielded structures, such as $SO_4^{2-}$, [44]. In the case of poisoning caused by organic sulfur species, the thiophenic organosulfur species cause stronger poisoning effects than $H_2S$ and the relative preference for adsorption on the active site is $H_2S$<thiophenic compounds [29, 46]. Maxted and Evans also found the relative sulfur poisoning in the following order: $H_2S < CS_2 <$ thiophene [47], which was explained that the

toxicity of sulfur increases with the molecular size of sulfur species. In general, the toxicity of sulfur increases with molecular weight and size of the poison and the stability of the adsorbed sulfur compound on the metal surface. The suggested mechanism is that the sulfur molecule is adsorbed by sulfur atom anchorage, around which the free rotation of the carbon chain inhibits the adsorption of reactant on the adjacent surface [5]. Furthermore, the more highly condensed thiophenic structures, such as dibenzothiophene and especially their alkyl-substituted derivatives are more difficult to be removed in fuel feedstock by hydrodesulfurization. Especially, for aromatic hydrogenation in hydrotreating process, sulfur is mainly present as refractory organosulfur compounds, such as alkylated DBT.

The removal of adsorbed sulfur for regeneration of poisoned catalysts depends on the metal-sulfur binding energy and thermodynamic properties of the surface metal-sulfur interface. High temperature and hydrogen pressure affect the equilibrium shifting to desorption. Generally, an increase of temperature will favor more reversible adsorption, resulting in sulfur tolerance.

## 2-3. Strategies for enhancing sulfur tolerance of noble metal catalysts

Considerable research has been dedicated to development of sulfur-tolerant noble metal catalysts and several strategies have been suggested to improve sulfur resistance of noble-metal catalysts with two main approaches, i.e., metal and support.

### 2.3.1. Effect of support

#### *Influence of support*

A surface area of a support is closely related with a high metal dispersion. The support produces highly efficient catalysts with maximum specific metal surface area in most cases. Furthermore, the support acidity is related to the catalytic activity and directly related to the small metal clusters in anchoring or stabilizing on the support, thus preventing sintering and agglomeration of metal clusters [48].

#### *Electron deficiency*

A supported metal catalyst, an acidic support in combination with a transition metal was named as bifunctional catalysts owing to their unique characteristics. [49]. The acid sites on support and the metal sites induce synergistic effect, where the acid sites affect the electronic property of the supported transition metal clusters. The term “electron deficiency” was introduced to explain the exceptionally high hydrogenation activity of zeolite Y-supported platinum catalyst

[50]. It was attributed to an electron withdrawing effect from metal clusters to the acidic zeolite support. [48, 51, 52]. Thus, electron deficient metal particles display enhanced catalytic activity of hydrogenation, hydrogenolysis with sulfur resistance [52].

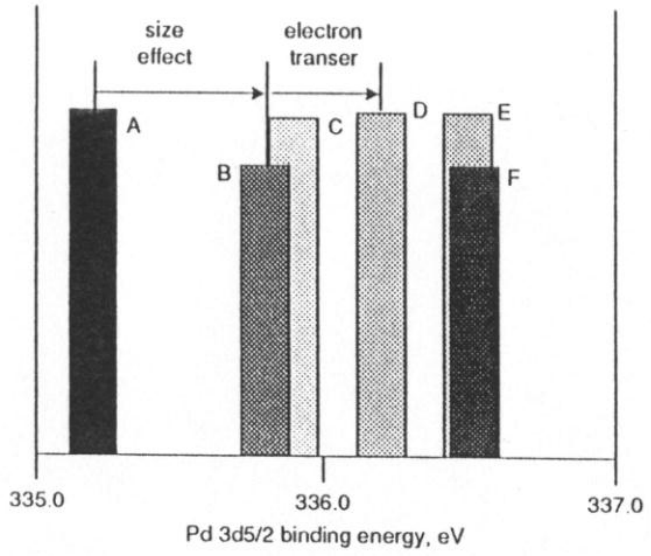


Figure **2-5**: Binding energies of Pd $3d_{5/2}$ electrons for (A) bulk Pd, (B) Pd/NaY neutralized with $NH_3$, (C) Pd/NaY neutralized with NaOH, (D) Pd/NaY, (E) Pd/MgY, and (F) Pd/Y (proton form). [53]

Figure 2-5 shows the electron deficiency of Pd particles with the effect of the metal particle size and the electron transfer. The binding energy of Pd $3d_{5/2}$ in Pd/NaY are shifted to higher values as compared with bulk Pd, which represents small Pd particles are electron deficient. Moreover, the binding energy of Pd/Y is shifted to even higher binding energy compared with Pd/NaY. The difference in binding energies between a series of Pd/NaY and Pd/Y is due to the acid site concentration, which makes the metal clusters more electron deficient.

***Electron deficiency and sulfur tolerance***

It is also reported that the zeolite-supported noble metal catalysts is more sulfur tolerant than silica- or alumina- supported catalysts due to the stronger electron transfer to the acidic sites of the zeolite, which makes noble metal clusters more electron deficient [6-14]. This electron deficiency of noble-metal particles improves sulfur tolerance of noble-metal catalysts. It was suggested that the sulfur tolerance is due to a weaker interaction between sulfur (an electron acceptor) and electron deficient noble-metal particles [50].

The degree of electron deficiency for metal particles is related with Brønsted acid concentration, where electron deficiency of the metal clusters increases as acid site strength and density increases [48, 53]. However, increasing acidity also promotes coke formation on the catalyst surface [10, 54], which was explained by the relative contributions of acid site concentration of the support on benzene hydrogenation in the presence of sulfur (Figure 2-6). If acid site concentration is low, overall hydrogenation rate will be low. On the other hand, if acid site concentration is high, it will promote strong reactant adsorption due to highly electron deficient metal particles and lead to self inhibition and formation of a carbonaceous overlayer on metal particles, which induce coke formation and reduces overall catalytic activity. For this reason, a balance of Brønsted acid site concentration should be obtained for optimum hydrogenation rates.

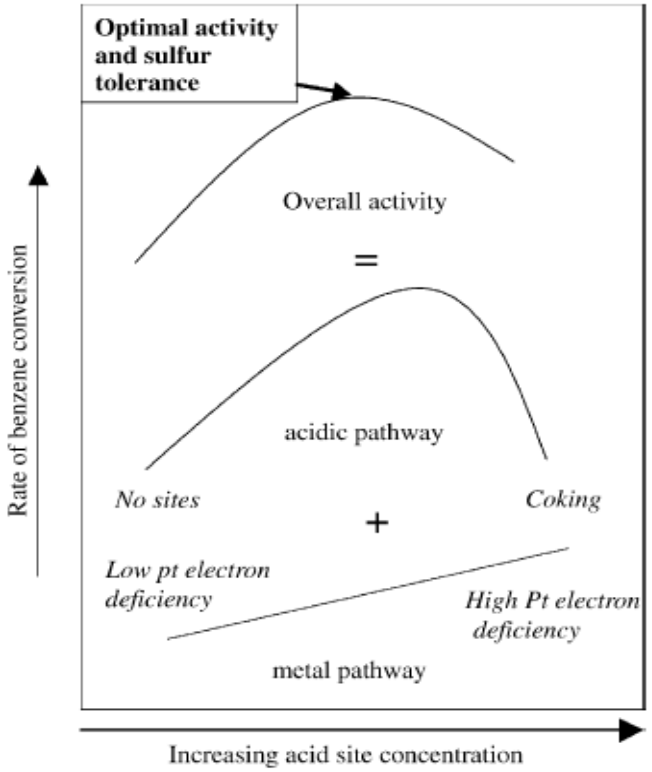


Figure **2-6**: Relative contribution of active site concentrations to the rate of aromatic hydrogenation. [54]

### 2.3.2. Effect of noble metal

***Influence of metal***

The most active metal catalysts are those in group 8, 9, 10(group VIII B). This is rationalized in terms of adsorption, which is called Sabatier principle [55]. When the strength of adsorption was compared among group 5 (VB), 6 (VIB), 11 (IB) and 8-10(VIIIB), group 5 and 6 metals are too strong, group 11 metals is too weak or nonexistent. In the case of group 8, 9, 10 metal, interactions between the catalyst and the reactant is "just right"; neither too strong nor too

weak. The six elements in the platinum group are all hydrogenation catalysts which is exceptionally active and most functional group can be reduced over these catalysts under mild conditions [56]. Especially palladium is one of the more important metals in the catalyst family. It is the best catalyst for hydrogenation of olefins as well as for the hydrogenolysis of C-C, C-O, C-S and C-N bonds. Sulfur resistance varies with the nature of the noble metal. Guo and Song demonstrated that for naphthalene hydrogenation in the presence of benzothiophene, supported Pt is less resistant to sulfur poisoning as compared to Pd for a given zeolite [26]. Although Pt is more active than Pd for a feedstock with low sulfur concentration, Pt is more susceptible to poisoning and deactivation as feedstock sulfur concentration increased. It was also reported that Ru and Ir catalysts were not very active compared to the other metals in platinum group from the result of for naphthalene hydrogenation over MCM-41 supported Pt, Pd, Rh, Ru and Ir catalyst test [57]

***Size of metal particle***

It was reported that the small Pd particle (10 atoms and less) has a greater electron affinity and more electron-deficient than bulk Pd, since they act as good electron acceptors/poor electron donors [51]. This electron accepting/donating ability of metal particles has been used to explain the sulfur resistance of noble metal catalysts supported on zeolites. Computational studies performed by using extended Hückel calculation suggested that Pd clusters up to 10 atoms have different electronic properties compared to that of bulk palladium [58]. It was reported that the work function of a 10-atom Pd aggregate cluster is 8.1 eV compared to 4.5 eV for bulk Pd obtained from experiment, suggesting that small Pd clusters are electron- deficient and can be better electron acceptors as compared to bulk Pd metal. The experimental study of small Pd

particles by X-Ray Photoelectron Spectroscopic (XPS) also substantiates the calculations. Karpinski et al. reported that core electron binding energies of supported Pd clusters decrease with an increase of cluster size less than 4 nm, but the particles with 4-5 nm have the same binding energies as bulk Pd [51]. A graph plotted for electron binding energy (Pd $3d_{5/2}$ shell) versus particle size in Figure 2-7 shows that as Pd particle size decreases the electron deficiency of the metal particle increases.

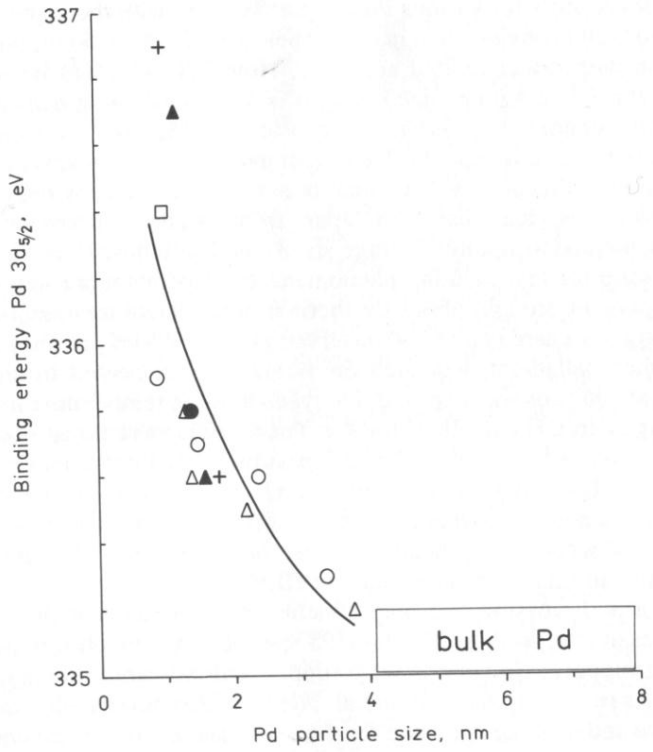


Figure **2-7**: Electron binding energies of Pd 3d5/2 as a function of metal particle size supported on various Pd supports: Δ Pd/SiO2; ▲,+ Pd/C; o Pd/Al2O3; □ Pd/Y-zeolite [51]

***Bimetallic catalyst***

The other approach for improved sulfur resistance of noble-metal catalysts is bi-or multi-metallic catalyst. It has been proposed to improve the sulfur resistance of supported noble metal by adding another metal that either enhance metal support interactions or remove electron density from noble metal. As the electron deficiency of the noble-metal is related to sulfur resistance of the catalyst, it was proposed that utilization of electrophilic metal species would reduce electron density of the noble-metal in a bimetallic catalyst and improve sulfur resistance. Several bimetallic Pt catalysts (Co-Pt, Mo-Pt, Ni-Pt, Re-Pt, Ag-Pt and Pd-Pt) were tested and it was found that the addition of Pd to Pt evidently improved the sulfur resistance of the catalyst whereas other bimetallic combinations did not show enhancement [24]. Hu et al. also adopted several transition metals (Cr, W, La, Mn, Mo, Ag) to Pd catalysts for toluene hydrogenation [59]. It was found that Pd-Cr and Pd-W catalysts exhibited higher catalytic activity than the Pd monometallic catalyst and the enhancement was mainly attributed to the electron deficiency of Pd interacted with $CrO_x$.

Yasuda et al. have also shown improved catalytic activity of Pd-Pt/USY bimetallic catalysts on tetralin hydrogenation in the presence of dibenzothiophene as sulfur, and determined the optimum Pt:Pd molar ratio of 4:1 for high sulfur resistance with maintaining high hydrogenation activity [15]. Pd-Pt catalyst was also compared with a mixture of Pd and Pt catalyst with the same Pd/Pt ratio and metal content, but no synergistic effect was observed. Although hydrogenation activity is improved by a bimetallic catalyst, it is still unclear whether bimetallic noble-metals have improved sulfur resistance. Fujikawa also exhibited that Pt-Pd/$SiO_2$-$Al_2O_3$ catalyst has much higher activity for aromatic hydrogenation compared to either monometallic Pt or Pd catalysts and also suggested that the optimum ratio of Pd : Pt is 4:1. However, they claimed the Pt-Pd bimetallic system is composed of the “Pd dipersed on Pt particle” structure, which significantly enhances the intrinsic catalytic activity for aromatic

hydrogenation. Niquille-Röthlisberger et al. introduced Pd-Pt bimetallic catalyst to hydrodesulfurization of DBT and 4,6-DMDBT [60]. It was displayed that Pd-Pt catalyst favors hydrogenation pathway in hydrodesulfurization and is faster for removal of 4,6-DMDBT than DBT and compensated for the loss of catalytic activity by sulfur poisoning occurred in desulfurization.

However, the major problem related to these approaches is that the metal active sites are still exposed to and poisoned by organosulfur compound remaining in the fuel feed. Thus, by selecting appropriate support parameters, a noble-metal catalyst can be designed with improved sulfur resistance. A high surface area support, with moderate acidity, is desirable to give highly dispersed, electron deficient metal particles, which exhibit a weaker bonding interaction with electron acceptors such as sulfur compounds.

## 2-4. Studies on naphthalene hydrogenation

In this research work, naphthalene and tetralin are main model aromatic compounds for diaromatics hydrogenation. Since naphthalene hydrogenation is a stepwise process, it should be well-acquainted with the hydrogenation reaction network as well as thermodynamic of hydrogenation in order to understand this research work.

### 2.4.1. Reaction network for naphthalene and tetralin hydrogenation

It has been understood that naphthalene hydrogenation proceeds stepwise, first ring saturation, followed by second ring saturation and conformational isomerization. Several different reaction pathways have been proposed, since this series of processes are complicated by the intermediate products, octalins. [20, 61-65]. However, all of them do not deviate from the major steps as depicted in Figure 2-8: (1) hydrogenation of naphthalene to tetralin, (2) hydrogenation of tetralin to decalins and (3) conformational isomerization of cis- and trans-decalin. For cis-decalin production, there is only a single pathway, direct tetralin hydrogenation to cis-decalin, i.e. *cis*-addition of hydrogen to tetralin. On the other hand, trans-decalin has two possible pathways, direct tetralin hydrogenation and cis-decalin isomerization, whereas another view was proposed that partially hydrogenated intermediates such as 1,9-octalin is the sole precursor to trans-decalin [65]. Furthermore, it has been demonstrated that conformational isomerization of cis-decalin to trans-decalin can occur over a catalyst on both acid and metal active sites [64].

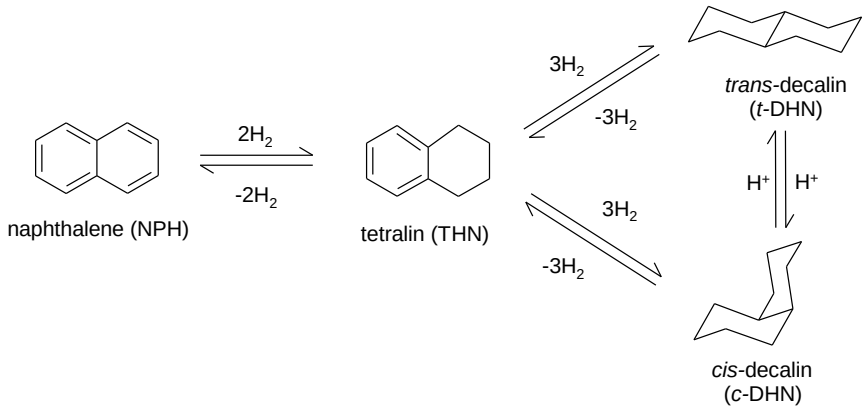


Figure **2-8**: Naphthalene hydrogenation network

### 2.4.2. Thermodynamic Equilibrium of naphthalene hydrogenation

Hydrogenation of aromatics including naphthalene is an exothermic reaction with the typical range 63-71 kJ/mole $H_2$ of heat of reaction [2]. The hydrogenation of an aromatic can be expressed as:

$$A + nH_2 \rightleftharpoons AH$$

where A and *AH* represent aromatics (naphthalene or tetralin) and partially or fully saturated aromatic (tetralin, decalin), respectively.

The equilibrium concentration of the aromatic species can be expressed as shown below,

$$\frac{Y_A}{Y_A + Y_{AH}} = \frac{1}{1 + K_a \times P_{H_2}^n}$$

where $Y_A$, $K_a$ and $P_{H_2}$ are the mole fractions of species, the equilibrium constant, and the partial pressure of hydrogen, respectively [2]. From the equation, it can be expected that high hydrogen pressure or high equilibrium constant $K_a$ decreases the aromatic contents in the system. Since $K_a$ increases with lowering the temperature, aromatic hydrogenation favors low temperatures and high hydrogen pressure [1].

The equilibrium of naphthalene hydrogenation studied by Frye and coworkers were recalculated in this chapter [66, 67]. Figure 2-9 shows the relationship between equilibrium constant and temperature for naphthalene (NPH) hydrogenation, tetralin (THN) hydrogenation and decalin (DHN) isomerization.

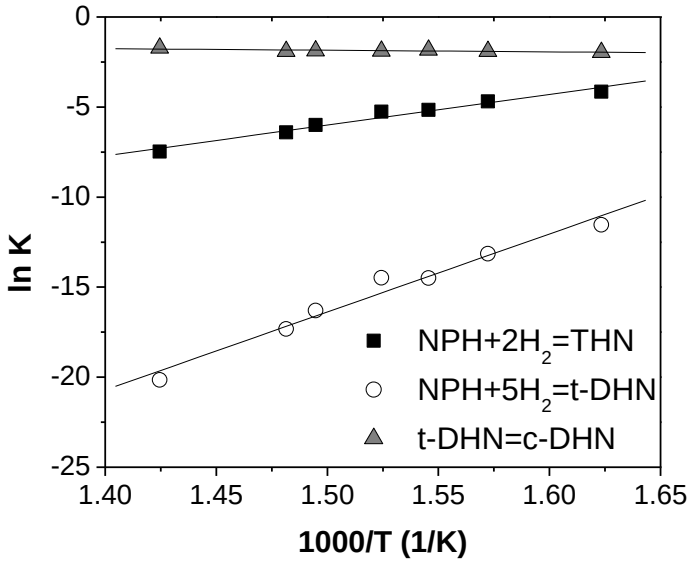


Figure **2-9**: Equilibrium constants for hydrogenation of naphthalene and tetralin as a function of temperature. Data adapted from [67]

It shows that the each equilibrium constant of naphthalene hydrogenation decreases as temperature increases, suggesting that the concentration of naphthalene at equilibrium increases with increasing temperature. For naphthalene to tetralin hydrogenation, naphthalene to trans-decalin hydrogenation and cis- to trans- decalin isomerization, the linear fits are expressed as below.

NPH to THN : $\ln K = 17055.73/T - 31.59$

NPH to trans-DHN : $\ln K = 43328.32/T - 81.37$

Cis-THN to trans-DHN : $\ln K = -888.54/T - 0.51$

Based on the calculated values from Frye's data, further calculation was performed for thermodynamic equilibrium of aromatic and cyclic compounds as a function of temperature and pressure. Hydrogen pressure was corrected as fugacity, $F_{H_2} = P_{H_2}(1 + 0.00033P_{H_2})$ for the non-ideality of hydrogen pressure.

The equilibrium for hydrogenation of naphthalene to tetralin as a function of temperature and hydrogen pressure is shown in Figure 2-10. The results depict that naphthalene hydrogenation favors lower temperature as well as higher hydrogen pressures, leading the equilibrium towards the hydrogenated species, tetralin. Furthermore, complete conversion of naphthalene to tetralin above 350°C is impossible due to its limitation of thermodynamic equilibrium. It is also evident that extremely high hydrogen pressure above 1200 psig is necessary for more than 95 % conversion of naphthalene hydrogenation to tetralin under typical hydrotreating temperatures range (350-400°C).

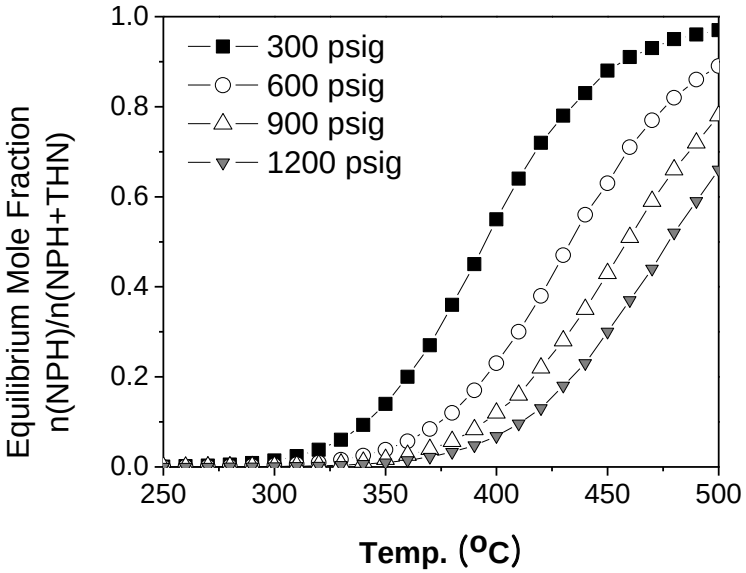


Figure **2-10**: Equilibrium of first ring hydrogenation of naphthalene to tetralin as a function of temperature and $H_2$ pressure (calculation based on data from [67])

Likewise, equilibria of tetralin hydrogenation to both cis- and trans-decalin (Figure 2-11 and 2-12) show the same trend as naphthalene hydrogenation to tetralin, but are more severely influenced by temperature. At 400 °C and 600 psig of hydrogen pressure, conversion of tetralin to *cis*- and *trans*-decalin is limited to 20 and 60 mole %, respectively, where conversion of naphthalene to tetralin is around 90%. These are in a good agreement with the fact that the second ring of diaromatics is more difficult to be hydrogenated than the first ring.

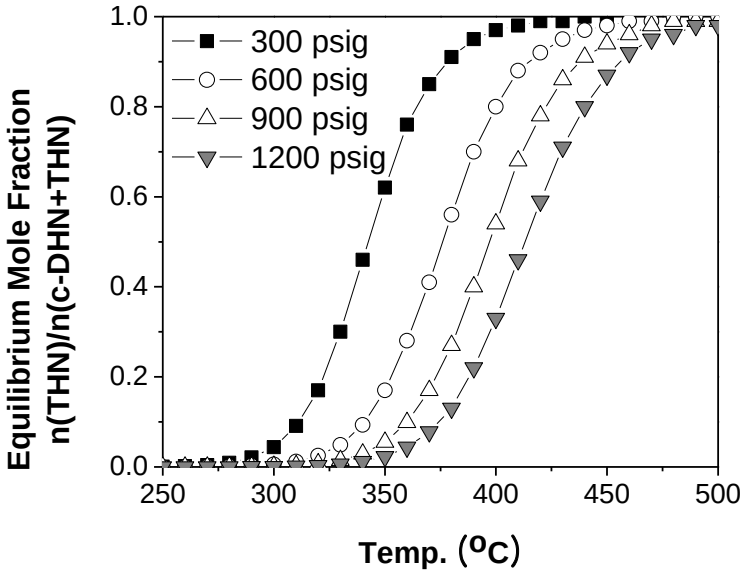


Figure **2-11**: Equilibrium concentration hydrogenation of tetralin to cis-decalin as a function of temperature and hydrogen pressure. (calculation based on data from [67])

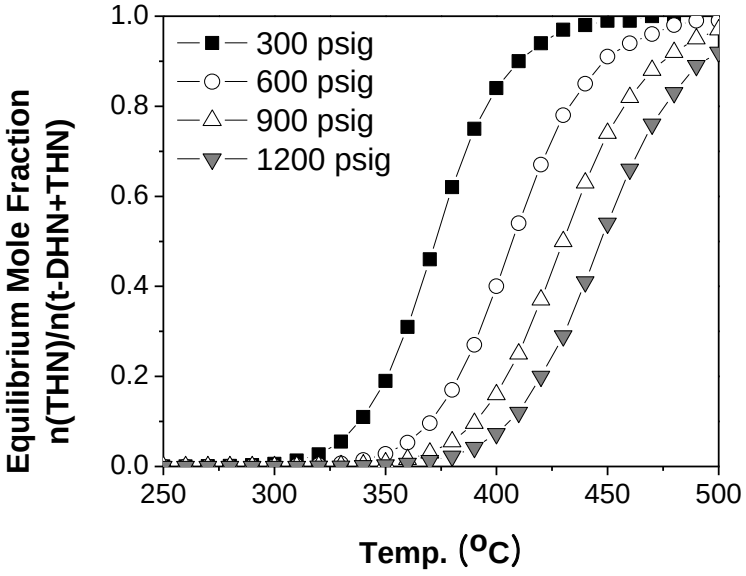


Figure **2-12**: Equilibrium concentration hydrogenation of tetralin to trans-decalin as a function of temperature and hydrogen pressure. (calculation based on data from [67])

The isomerization of decalin isomer (cis- and trans-decalin) can be expressed below:

$$cis-decalin \rightleftharpoons trans-decalin$$

The equilibrium constant of decalin isomer, $K_a$, are obtained by mole fraction of trans- and cis- decalin.

$$K_a = \frac{Y_{trans-decalin}}{Y_{cis-decalin}}$$

It was also calculated based on the calculated values from Frye's data and could be expressed as a function of temperature.

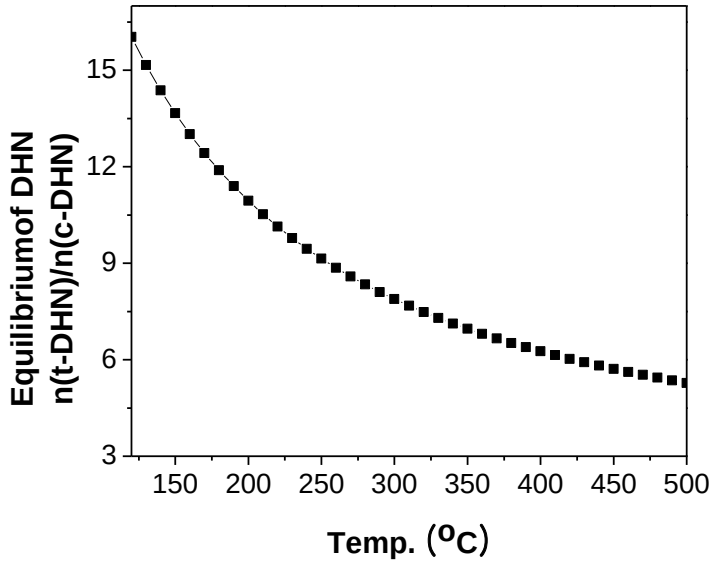


Figure **2-13**: Equilibrium of isomerization of cis- and trans-decalin as a function of temperature (calculation based on data from [67])

There is another way to determine the equilibrium composition of cis and trans-decalin, i.e. calculation of equilibrium constant from Gibbs energy. Since the equilibrium constant $K_a$ is also related to the difference of Gibbs energy, $\Delta G^o$, it also can be expressed as below:

$$\ln K_a = \frac{-\Delta G^o}{RT}$$

The general expression for the equilibrium constant of trans- and cis-decalin as a function of temperature was obtained from Lai et al. and expressed as below:

$$R \ln K_a = \frac{15370}{T} + 14.83 \ln T - 0.0365T + 1.885 \times 10^{-5} T^2 - 4.49 \times 10^{-9} T^3 - 85.2$$

where R and T are the gas constant (8.314 $Jmol^{-1}K^{-1}$) and the temperature, respectively. The calculated equilibrium constant, and composition for a binary mixture system of cis-decalin and trans-decalin based on the equation are listed in Table 2-2.

Since the equilibrium composition is important to establish the theoretical upper limit of the catalytic conversion, it is calculated using both methods and compared together. There are significant differences of the equilibrium constants in comparison between Figure 2-13 calculated from Frye's data and Table 2-2 from Lai's. It can be mainly due to the exponential function of equation derived from Lai, which is highly dependent on the thermodynamic parameters used. Furthermore, the trans-/cis-decalin ratio data calculated from Frye's are also very sensitive to denominator, i.e. mole fraction of cis-decalin. However, in any case, both theoretical calculation results show that the equilibrium of cis-decalin conversion decreases with increasing temperature.

Therefore, for production of high concentration of trans-decalin, a lower reaction temperature is thermodynamically favorable.

Table **2-2**: Equilibrium constant and composition of trans- and cis-decalin.(calculation based on equation from [64])

| Temp. (K) | Eq. Const. K | Comp. (%) | |
|---|---|---|---|
| | | trans-decalin | cis-decalin |
| 473 | 20.50 | 95.35 | 4.65 |
| 498 | 17.32 | 94.54 | 5.46 |
| 523 | 14.87 | 93.70 | 6.30 |
| 548 | 12.94 | 92.83 | 7.17 |
| 573 | 11.41 | 91.94 | 8.06 |
| 598 | 10.16 | 91.04 | 8.96 |
| 623 | 9.13 | 90.13 | 9.87 |
| 648 | 8.27 | 89.22 | 10.78 |
| 673 | 7.55 | 88.31 | 11.69 |
| 698 | 6.94 | 87.41 | 12.59 |
| 723 | 6.42 | 86.52 | 13.48 |

## 2.5. Application of literature knowledge to this research

The literature reviews present several important issues and strategies that are helpful to understand sulfur-induced deactivation as well as to improve sulfur tolerance of noble metal catalysts for low temperature hydrogenation of aromatics. It discusses that support properties such as zeolite framework structure, pore size and acidity as well as the metal properties are important in governing sulfur-induced deactivation of the metal catalyst. Based on the literature review, it is hypothesized that a hybrid noble metal catalyst having two different small and large-sized pore systems will improve hydrogenation of aromatics containing sulfur and the sulfur tolerance of the supported metal. Detailed hypotheses are listed below:

(1) Aromatics and bulky sulfur compounds react on the active metal sites located inside a zeolite having large pore (>6 Å), but they have difficulty accessing to the metal inside the small pore (<5 Å).

(2) The metal inside the pore dissociates hydrogen molecules and dissociated hydrogen atoms spill over to the adjacent catalyst surface within the pores.

(3) Hydrogen spillover from the small pore can recover the sulfur-poisoned sites in the large pore.

In order to verify the hypotheses, a series of experimental approaches are performed as below:

(1) Effect of supports

Pd catalysts on mordenite, zeolite Y, zeolite A and amorphous silica-alumina are employed to study the effect of supports having different pore structures, pore size and surface area in the sulfur tolerance of the supported metal catalysts.

(2) Effect of metals

Group 10 metals (Ni, Pd and Pt) are adopted to evaluate the sulfur tolerance of the zeolite Y-supported monometallic catalysts. The catalytic activity of Pd-Pt bimetallic catalyst is also compared with those of other monometallic catalysts.

(3) Hybrid catalyst

The hybrid zeolite-supported Pd catalyst is prepared, based on the proposed catalyst design concept to enhance sulfur tolerance of the catalyst. The hybrid catalyst is composed of Pd supported on zeolite Y and A. The zeolite Y-supported Pd catalyst having large pores and the zeolite A-supported Pd catalyst possessing small pores are adopted for aromatic hydrogenation and hydrogen spillover, respectively.

(4) Surface metal passivation

Silica coating is applied to zeolite A-supported Pd catalyst in order to passivate the Pd clusters on the external surface, which makes possible to observe the role of metal in small-pore catalyst system.

(5) Pore size control of zeolite A support

Potassium ion exchange is adopted to control the pore opening size of zeolite A. The pore size-controlled zeolite A sufficiently restrict not only aromatic sulfur but also smaller sized byproduct species including hydrogen sulfide molecule (3.6 Å), while allowing only hydrogen molecules and atomic hydrogen to diffuse in and out of the cages.

# Chapter 3

# Effect of support

## 3.1. Introduction

As previously mentioned in the literature review, selection of the appropriate support is crucial in the design of a noble-metal catalyst with high sulfur tolerance. In this chapter, the Pd metal catalysts on various supports of different pore size, pore structure and acidity are prepared in order to understand the effect of support on sulfur tolerance of the supported metal catalyst for hydrogenation of tetralin. Mordenite having two-dimensional pore configuration, amorphous silica-alumina, small porous zeolite A, large porous zeolite Y and potassium ion-exchanged zeolite Y are employed as support materials.

## 3.2. Experimental

### 3.2.1. Catalyst Preparation

In this study, Zeolite A (Advera 401N, Zeolyst International), zeolite Y (CBV 730, Zeolyst International), Mordenite (CBV 30A, Zeolyst International) and silica-alumina (Sigma-Aldrich) were adopted for the supports of the catalysts and were denoted as A, Y, M and $SiO_2$-$Al_2O_3$, respectively. Therefore, Pd/A, Pd/Y, Pd/M and Pd/ $SiO_2$-$Al_2O_3$ denoted Pd catalyst supported on them, respectively. The potassium ion-exchanged zeolite Y support and Pd catalyst supported on it were expressed as KY and Pd/KY, respectively.

The zeolite supports were calcined in air flow (60 mL/min) at 450 $^oC$ for 4 hr with a heating rate of 1.5 $^oC$ /min before catalyst preparation. Zeolite A in proton form was developed from sodium form of zeolite A by ion exchange with 0.4M $NH_4Cl$, washed with deionized water, dried in an oven at 100 $^oC$ and then calcined at 450 $^oC$. The zeolite KY support was prepared by ion exchange of zeolite Y support with an 0.4M aqueous solution of potassium chloride (KCl, Aldrich, 99.0%). Then, it was washed with deionized water, dried in an oven at 100 $^oC$ and then calcined at 450 $^oC$.

All supported Pd catalysts were prepared by incipient wetness impregnation (IWI) of aqueous solution of palladium chloride ($PdCl_2$, Aldrich, 99.999%) dissolved in dilute hydrochloric acid to a nominal metal concentration of 2 wt%. Since palladium chloride was immiscible in water, only sufficient quantity of dilute hydrochloric acid (2 of $HCl/PdCl_2$ molar ratio) was added to dissolve $PdCl_2$. After impregnation was complete, the catalysts were dried at 100 $^oC$ overnight and calcined in air flow (~60 ml/min) at 450 $^oC$ for 4 h at a heating rate of 1.5 $^oC$ /min.

### 3.2.2. Catalyst Characterization

The surface area and the pore volume of the zeolite-supported Pd catalysts were measured by Quantachrome Autosorb 1 instrument. Micromeritics Autochem 2910 TPD/TPR equipped with a TCD detector was applied for temperature programmed reduction (TPR), Temperature programmed desorption of ammonia ($NH_3$-TPD) and pulse chemisorption of hydrogen. The Pd dispersion of the catalysts was measured by hydrogen chemisorption.

For temperature programmed desorption (TPD), the samples were heated to 450$^oC$ with a heating rate of 10$^oC$/min and maintained for 1hr under helium followed by cooling to 110$^oC$. When the temperature reached to 110$^oC$, 10/% $NH_3$/He mixture gas was introduced by pulse injection until the TCD signal equilibrated. When there was no difference of the TCD signal after subsequent pulses passed through the sample, the $NH_3$ adsorption was stopped. The sample was purged for 2 h with pure helium to remove the weakly adsorbed ammonia and waited until the TCD baseline was stable. The sample was heated again from 110$^oC$ to 900$^oC$ at the ramp of 10$^oC$/min and desorption process was again recorded by the TCD and MS.

X-ray diffraction (XRD) spectra were obtained by using a Scintag X2 powder diffractometer to determine whether the support structure is decomposed by hydrochloric acid during catalyst preparation.

### 3.2.3. Catalyst Evaluation

Continuous fixed-bed flow reactor testing was conducted at 225 $^{o}$C under 600 psi of $H_2$ pressure. The catalyst was loaded and reduced in-situ under a hydrogen flow of 100 ml/min and 100 psig of $H_2$ pressure at 225 $^{o}$C prior to each experiment. After reduction, the reactor pressure and the hydrogen flow were set to 600 psig and 80 ml/min, respectively. Then the sulfur free model fuel was firstly injected into the reactor by HPLC pump for 90 min in order to stabilize the reactor system. Therefore, 90 min after the introduction of feedstock was designated as time-on-stream (TOS) equal to zero. Sulfur free feedstock was fed until 3.5 h TOS, at which point the feed was changed to sulfur feed and continued until the experiment finished. The model fuel for aromatic hydrogenation were prepared by mixing 20% of tetralin (1, 2, 3, 4-tetrahydronaphthalene, Aldrich, 99%) as aromatics with 75% hexadecane (Aldrich, 99+%, anhydrous) as solvent and 5% tetradecane (Aldrich, 99+%) as internal standard. For sulfur feed stock, benzothiophene (BT, Aldrich, 99%) was added to model fuel feedstock. Liquid products were analyzed by GC-FID (SRI 8610) using XTI-5 capillary column for quantitative analysis and GC-MS (Shimazu GC-17A with QP-5000 MS) using Restek Rxi$^{TM}$-5ms for identification of the products.

## 3.3. Result and Discussion

### 3.3.1. Effect of support type

The specification of zeolite supports and the textural properties of the Pd catalysts on various supports were shown in Table 3-1. Dispersion data of the Pd/Y and Pd/M catalysts were distinctively high and Pd/Y catalyst had high BET surface area. Even though Pd/$SiO_2$-$Al_2O_3$ had higher BET surface area, its metal dispersion was lower than Pd/M. Pd/A showed the lowest metal dispersion.

Table **3-1**: Properties of zeolite supported Pd catalyst used in this study

| Catalyst | Support | $SiO_2/Al_2O_3$ mol ratio | Size of Pore opening (Å) | Surface Area ($m^2/g$) | Metal Dispersion (%) |
|---|---|---|---|---|---|
| Pd/Y | Zeolite Y | 30 | 7.4 | 590 | 42.3 |
| Pd/A | Zeolite A | 1 | 4 | 428 | 18.6 |
| Pd/M | Mordenite | 38 | 7.0X6.5, 5.7X2.6, 4.8X3.4 | 392 | 47.0 |
| Pd/ $SiO_2$-$Al_2O_3$ | Silica-alumina | 11 | 38 | 420 | 31.1 |

The TPR profiles for the catalysts were shown in Figure 3-1. The profiles of all catalysts display the one single peak with a maximum below 100 $^oC$. Since all the catalysts are easily reduced at low temperature, the comparison of TPR profile and the maximum peak temperature might not be accurate in providing notable differences. However, it is interesting to note that both Pd/Y and Pd/A showed the sharp peaks compared with other two catalysts, which may be

ascribed to their 3-dimensional framework, making easy access of hydrogen into the zeolite framework. On the other hand, the profile of Pd/M exhibits long tail at high temperature region, which may be due to its two dimensional pore structure making hydrogen diffusion difficult. The amorphous silica-alumina supported Pd catalyst shows the broad peak distribution between 50 and 150$^{o}$C.

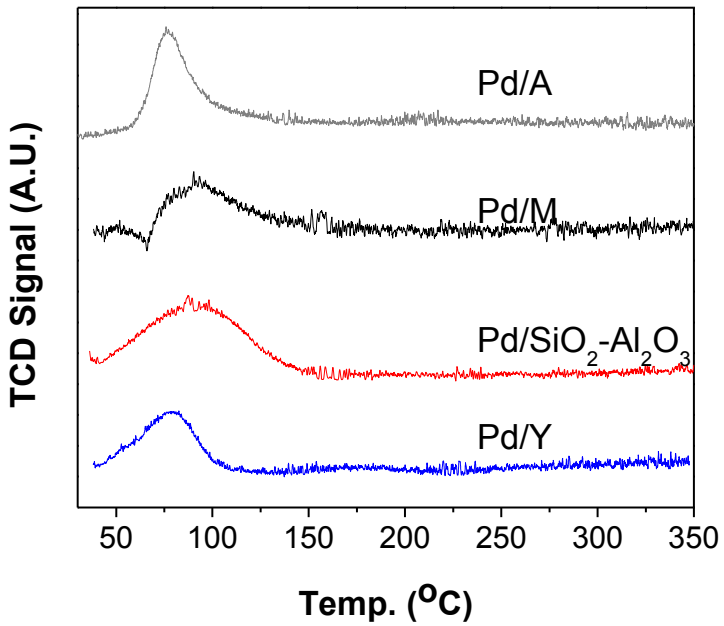


Figure **3-1**: TPR profile of Pd catalyst supported on various zeolite support and amorphous silica alumina

Figure 3-2~5 shows the X-ray diffraction patterns for the support materials and Pd catalysts supported on them. All the powder diffraction patterns of zeolite supports obtained correspond well with those reported by International Zeolite Association. Furthermore, comparison among the samples in each figure show that the diffraction patterns of the Pd catalysts are also identical with those of the corresponding zeolite frameworks, although the peak

intensities decreased due to the presence of the metal in the zeolite framework [68]. There is no decomposition detected on the geometry of the zeolite supports, implying that the zeolite frameworks were not decomposed by hydrochloric acid during the catalyst preparation step, at which diluted hydrochloric acid was added to dissolve Pd precursor in water. The intrinsic palladium peaks were not detected, which is likely that the metal is incorporated inside the zeolite framework. Furthermore, no peak of Pd was detected even on silica-alumina support, indicating that small Pd clusters is finely dispersed on the support material.

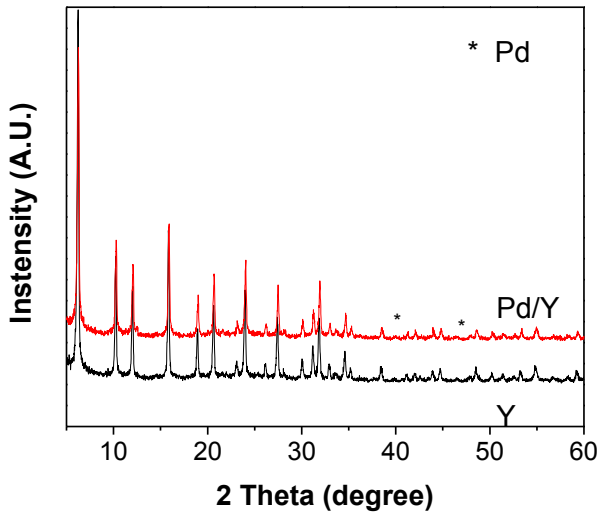


Figure **3-2**: XRD pattern of Zeolite Y and Pd/Y

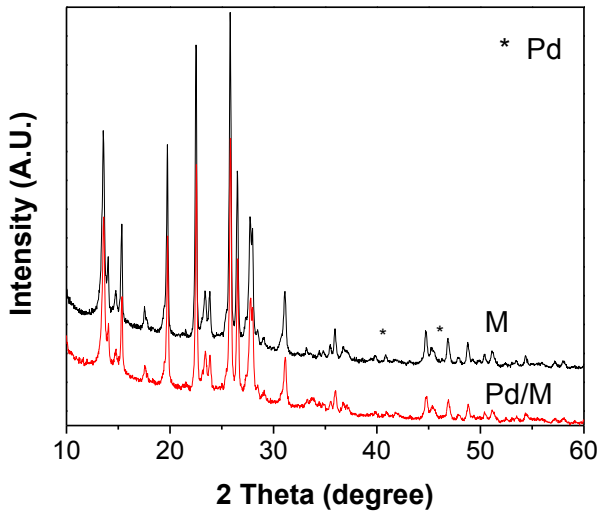


Figure **3-3**: XRD pattern of H-Mordenite and Pd/M

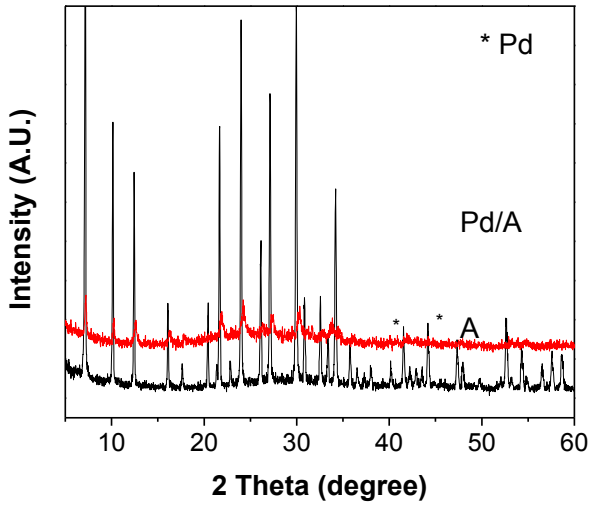


Figure **3-4**: XRD pattern of Zeolite A and Pd/A .

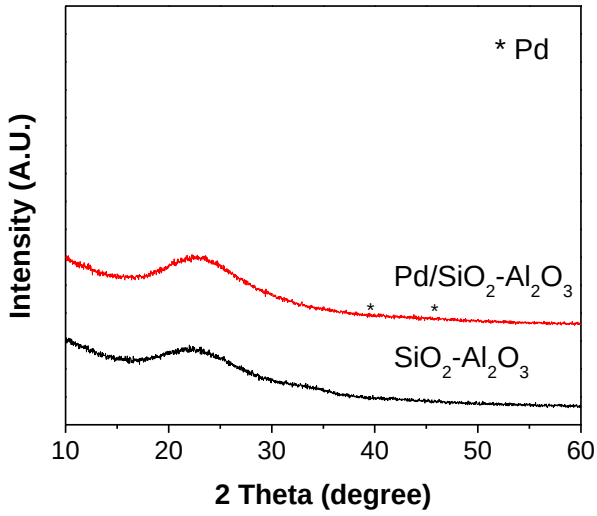


Figure **3-5**: XRD pattern of $SiO_2$-$Al_2O_3$ and Pd/$SiO_2$-$Al_2O_3$

Figure 3-6~9 represents the ammonia TPD profiles of the supports and Pd catalysts supported on them. When compared among the supports, there is distinctively huge TPD peak observed over 500$^{o}$C on zeolite supports, mordenite and zeolite A, revealing that ammonia molecules on the zeolite supports are strongly adsorbed. Interestingly, no significant peak at high temperature was observed over 500 $^{o}$C, but two consecutive peaks with maximum at 350-400 $^{o}$C were detected on the silica-alumina support. These peaks below 400 $^{o}$C are also observed only for Zeolite Y among the zeolite supports, indicating that there are more than two acidic sites with different strengths present only on zeolite Y and silica-alumina.

Compared to TPD peaks of the supports, those of all Pd catalysts are shifted to lower temperature, indicating interaction between the metal catalyst and ammonia is weaker than that between acid site and ammonia. Furthermore, the area of ammonia desorbed on the Pd catalysts is smaller than that of supports. Schmitz previously observed the same trend in his n-Butylamine TPD and suggested that the metal particles preferentially attach to the support at strong acid centers to neutralize them [61]. In the case of silica-alumina supported Pd catalyst, only TPD peak at intermediate temperature range was reduced, which can be deduced that the metal only affects the acid sites with intermediate strength, i.e. the strongest acid sites of the silica-alumina support.

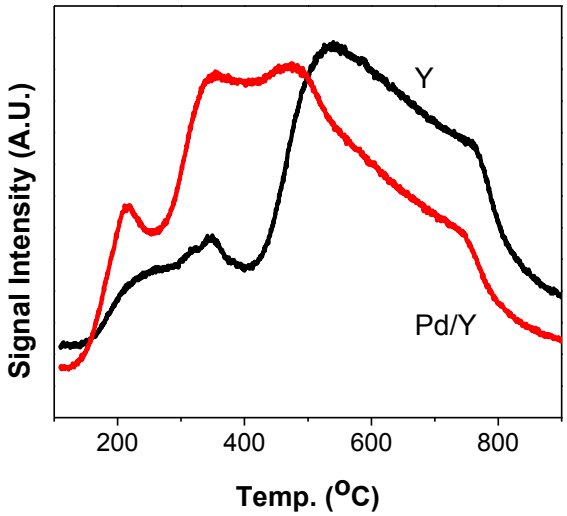


Figure **3-6**: Ammonia TPD profiles of Zeolite Y and Pd/Y

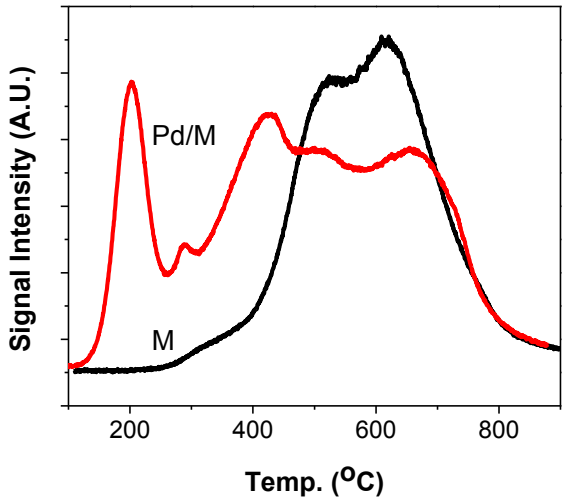


Figure **3-7**: Ammonia TPD profiles of mordenite and Pd/M

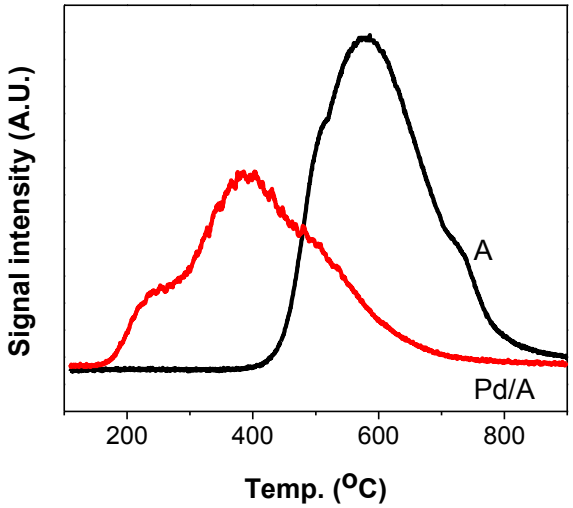


Figure **3-8**: Ammonia TPD profiles of Zeolite A and Pd/A .

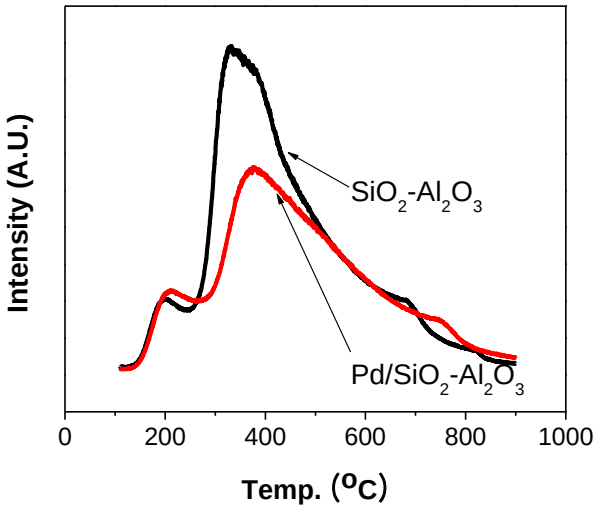


Figure **3-9**: Ammonia TPD profiles of $SiO_2$-$Al_2O_3$ and Pd/$SiO_2$-$Al_2O_3$

Hydrogenation of tetralin in the presence of benzothiophene was conducted to observe the effect of support on sulfur tolerance. For aromatic hydrogenation in this study, tetralin was chosen as a model aromatic compound, because saturation of the second aromatic ring is more difficult and rate-limiting in the hydrogenation process [1, 2]. Furthermore, tetralin as received was essentially free from sulfur contamination and required no further purification. Preliminary tetralin hydrogenation test over Pd catalyst was conducted for 20 h with sulfur-free feed. There was no deactivation of the catalyst observed, ensuring that the sulfur poisoning by benzothiophene is the main reason for catalyst deactivation in this study. Figure 3-10 shows the comparison of the tetralin conversion over Pd catalyst on various supports. Tetralin conversion over all Pd catalysts tested decreased with the addition of 100 ppmw sulfur concentration. It is clear that benzothiophene significantly hinders the catalytic activity and the accumulated sulfur amount results in decrease of tetralin conversion. Tetralin conversion of Pd/A drastically decreased, the fastest among the catalysts tested. Pd/Y showed highest sulfur tolerance maintaining 100% tetralin conversion up to 7 h TOS. Both Pd/$SiO_2$-$Al_2O_3$ and Pd/M performed similarly but deactivation of the former was severer than the latter after 8 h TOS. Between zeolite supported catalysts with similar $SiO_2/Al_2O_3$ ratios, Pd/Y ($SiO_2/Al_2O_3$=30) was observed to have superior sulfur tolerance to Pd/M ($SiO_2/Al_2O_3$=38).

An evident trend was found among surface area, metal dispersion and catalyst performance. Pd/Y catalyst having high surface area and metal dispersion maintained the highest level of tetralin conversion in the presence of sulfur. Pd/M catalyst with low surface area was not comparable to Pd/Y on tetralin conversion albeit it had distinctively high metal dispersion. Likewise, Pd/$SiO_2$-$Al_2O_3$ having lower surface area and metal dispersion than Pd/Y showed lower sulfur tolerance on tetralin conversion comparing to Pd/Y. The ratio of sulfur to surface Pd metal atom (S/Pd) at the decreasing point of tetralin conversion is calculated with the accumulated sulfur amount in the fuel divided by surface metal atom obtained from metal dispersion.

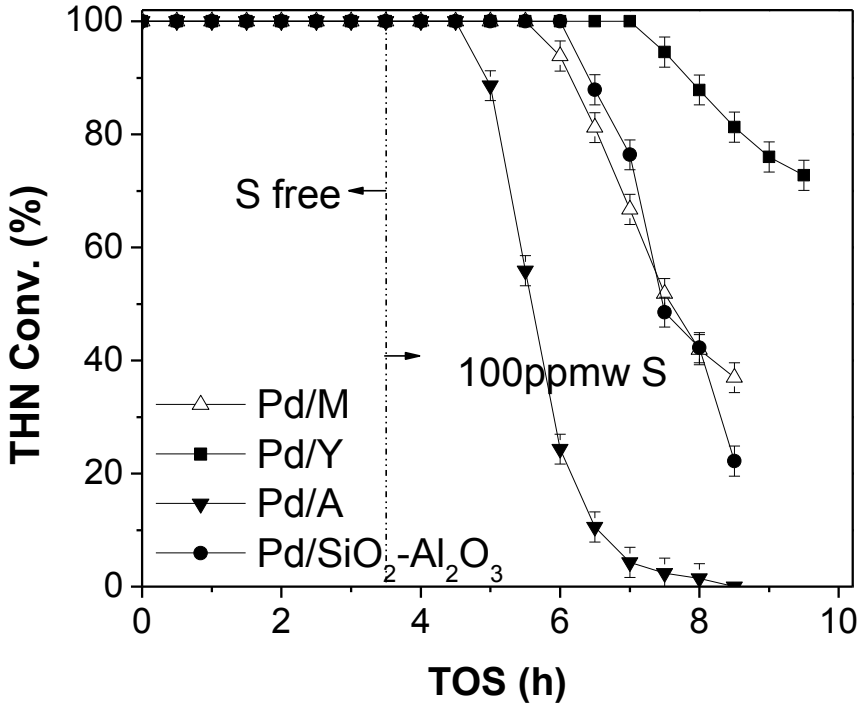


Figure 3-10: Tetralin conversion over various zeolite-supported Pd catalysts in the presence of 100ppmw sulfur as BT

For Pd/Y, Pd/M and Pd/ $SiO_2$-$Al_2O_3$ catalyst, S/Pd ratios were 1.02, 0.55 and 1.03, respectively. Even Pd/M catalyst shows the similar decreasing trend of tetralin conversion with Pd/$SiO_2$-$Al_2O_3$, it was found that Pd/M catalyst is less sulfur tolerant than Pd/ $SiO_2$-$Al_2O_3$. Since the mordenite support has various pore size, the metal clusters might be placed not only in the large pores but also in the medium or small pores, where the bulky tetralin molecules are difficult to be penetrated. On the other hand, S/Pd ratio of Pd/ $SiO_2$-$Al_2O_3$ is comparable to that of Pd/Y, but low surface area of $SiO_2$-$Al_2O_3$ might negatively affect the fast decrease of tetralin conversion.

It was interesting to note that Pd/A catalyst showed 100% tetralin conversion in the absence of sulfur, but dramatic decrease after introduction of sulfur. It is evident that the metal particles are located not only inside the small pores of zeolite but also on the support surface. It

seems that metal clusters on the external surface of Pd/A acts as the active sites for tetralin hydrogenation, but can be easily and immediately poisoned by benzothiophene. Low metal dispersion data of Pd/A also substantiates this explanation. It is likely that small pore opening of zeolite A causes diffusional difficulty for penetration of the Pd precursor into zeolite structure even if metal can be introduced into very small pores during calcination step [53, 69].

### 3.3.2. Effect of acidity

Figure 3-11 depicts the comparison of ammonia TPD between zeolite Y and KY. Seen from the result on zeolite KY, the ammonia desorption peak over 500$^{o}$C was smaller than that of zeolite Y and the peak detected at around 350$^{o}$C was disappeared, which is likely that potassium ion exchange significantly attenuates the acidity of zeolite Y support.

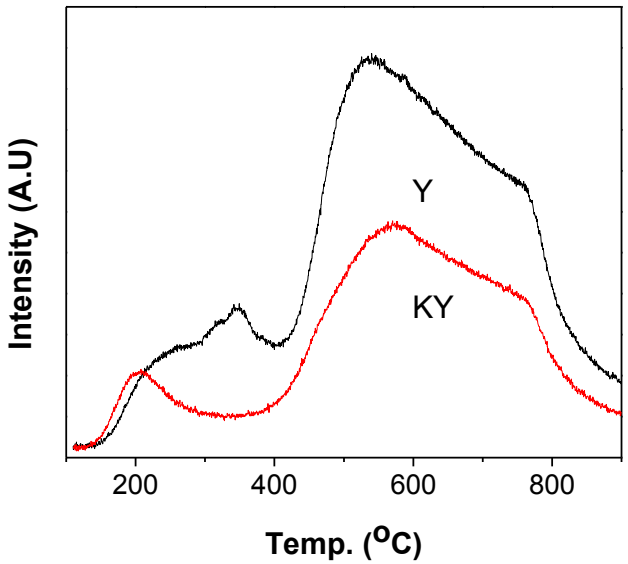


Figure **3-11**: Ammonia TPD profiles of zeolite Y and KY

Table 3-2 presents the surface area and metal dispersion of the Pd/Y, Pd/KY catalysts. The metal dispersion of the Pd/KY is higher than Pd/Y catalyst, implying that K addition by ion exchange improves the metal dispersion of palladium catalyst. It is also well agreed on that addition of basic promoter such as alkali and alkaline earth metal to the catalyst improves the dispersion of the metal [70].

Table 3-2: Surface area and metal dispersion of supported Pd catalysts

| Catalyst | BET Surface Area ($m^2/g$) | Metal Dispersion (%) |
|---|---|---|
| Pd/Y | 590 | 42.3 |
| Pd/KY | 615 | 48 |

The TPR profiles of the catalysts were shown in Figure 3-12. From the profile of Pd/Y, Pd metal started to reduce from around room temperature and reached to maximum at around $70^oC$, but on the Pd/KY catalyst, a sharp peak was displayed between 50 and $75^oC$ with the maximum at $62.5^oC$, which is likely that metal becomes more electron rich status by potassium addition, thus easier to be reduced.

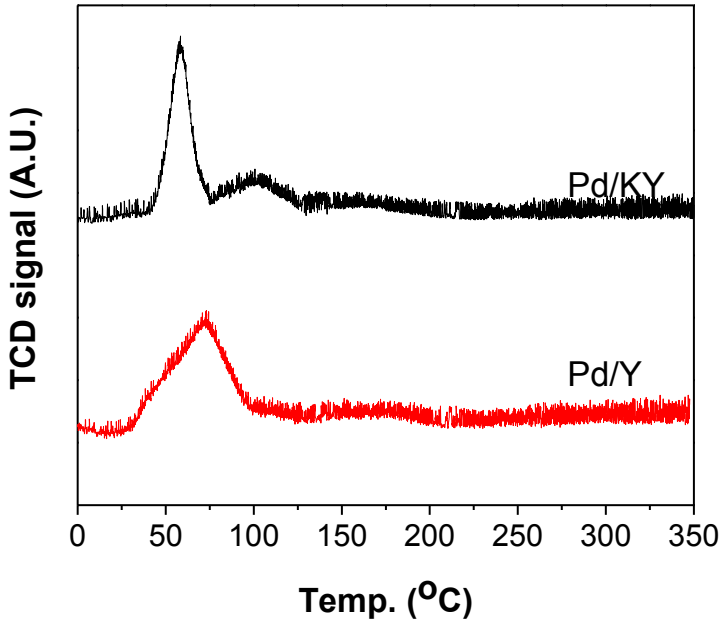


Figure 3-**12**: TPR profile of Pd catalyst supported on zeolite Y or KY support.

Tetralin hydrogenation test was also conducted for comparison of sulfur tolerance between Pd/Y and Pd/KY catalyst on tetralin hydrogenation. Figure 3-13 displays the result of tetralin conversion over the Pd/Y and Pd/KY in the presence of 100 ppmw sulfur as benzothiophene. Tetralin conversion over Pd/KY catalyst was drastically decreased right after introduction of sulfur, while that of Pd/Y displays gradual decrease. At 14 h TOS, conversion of tetralin over Pd/KY was less than 20%, mostly losing its catalytic activity, compared to around 60% over Pd/Y. It was already shown that potassium ion exchange of zeolite Y attenuated the acidity of the support, but hard to neutralize the acidic sites of zeolite Y. However, it is evident that its supported catalyst (Pd/KY) is much less sulfur tolerant than acidic zeolite Y supported Pd catalyst (Pd/Y).

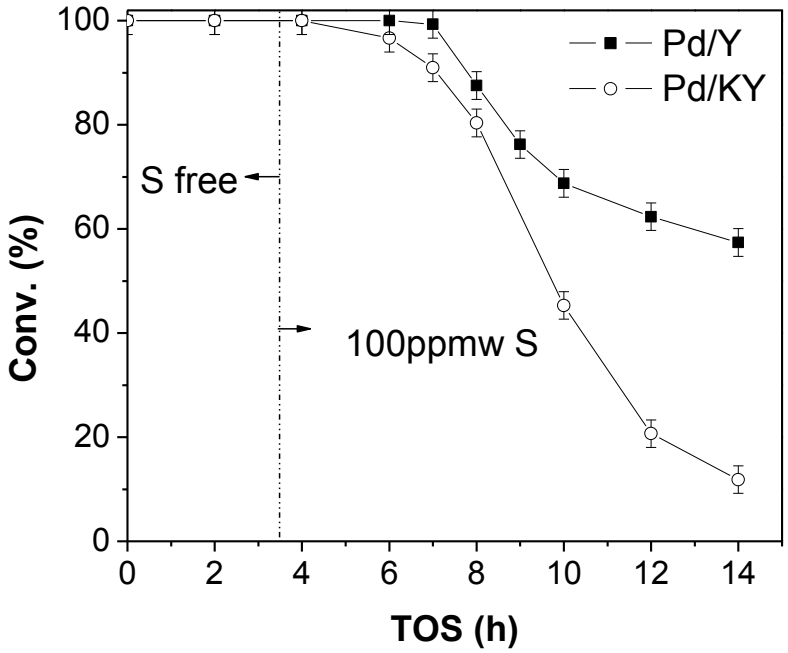


Figure **3-13**: Tetralin conversion over zeolite Y-supported Pd catalysts (Pd/Y and Pd/KY) in the presence of 100ppmw sulfur as BT

It should be noticed that significant sulfur tolerance of the Pd/Y catalyst maintaining high catalytic activity on tetralin hydrogenation is mainly ascribed to not only zeolite Y support material but also support acidity, which may cause strong metal-support interaction making Pd metal clusters on the support more electron-deficient, therefore, more sulfur-tolerant.

## 3.4. Conclusion

The study performed in this chapter demonstrates that the support type, pore structure, pore opening size and surface acidity are important factors for the sulfur tolerance of the aromatics hydrogenation catalysts. Zeolite Y- supported Pd catalyst showed excellent sulfur tolerance compared with other supports tested, which is likely due to its high surface area and 3-D zeolite framework. Furthermore, acidity of zeolite support also results in significant improvement on sulfur tolerance of the metal catalyst. The acidic zeolite support may cause strong metal-support interaction, and thus makes the metal clusters on the support more sulfur tolerant.

**Chapter 4**

# Enhanced Sulfur Tolerance of Hybrid Zeolite-Supported Pd Catalyst for Low-Temperature Hydrogenation of Diaromatics

Abstract

A hybrid zeolite-supported Pd catalyst was prepared for improving sulfur tolerance based on a proposed catalyst design concept for low-temperature aromatic hydrogenation of distillate fuels [C.S. Song, Chemtech, 29 (1999) 26-30]. The hybrid catalyst consists of Pd supported on Y and A zeolites. Pd/A shows no catalytic activity for hydrogenation of tetralin but adding Pd/A to Pd/Y significantly enhanced sulfur tolerance of the catalyst for both naphthalene and tetralin hydrogenation in the presence of 100 ppmw sulfur as benzothiophene. This may be mainly attributed to the small pore system (Pd/A) in the hybrid catalyst, serving size-selective exclusion of bulky benzothiophene as well as hydrogen spillover from metal inside small pore in Pd/A to recover the poisoned metal sites in large pores in Pd/Y.

Keywords: sulfur tolerance, naphthalene, tetralin, hydrogenation, hybrid catalyst, shape selectivity, hydrogen spillover

## 4.1. Introduction

As high aromatic content in distillate fuels lowers the fuel quality and contributes to the formation of environmentally harmful emissions in exhaust gases from combustion engines, reducing aromatic content has been a target for the recent transportation fuel regulation [1, 2]. Noble metal catalysts are candidates for deep hydrogenation owing to their high catalytic activity at low temperature, but a serious problem is the rapid deactivation when they are exposed to sulfur even at trace level [5]. Previously, a sulfur-tolerant catalyst design concept was proposed by our group, which mainly focused on noble metal catalyst supported on shape-selective zeolite for aromatic hydrogenation in the presence of sulfur [4, 29]. According to the proposed concept, the catalysts are supported on zeolite material possessing bimodal pore size distributions. The large pore systems (>6 Å) allow hydrogenation of multi-ring aromatics and hydrodesulfurization of organosulfur compounds, while bulky aromatics and organic sulfur are selectively excluded from the small pore systems (<5 Å). $H_2$ molecules can enter both large and small pores, be dissociated on metal sites and be transported between both pore systems by hydrogen spillover. When metal in the large pore systems becomes deactivated by adsorbed sulfur molecules, spillover hydrogen from the small pores can recover the poisoned metal sites.

Related to this proposed concept several research groups have conducted research on development and application of zeolite-supported catalyst for aromatics hydrogenation with hydrogen spillover [6, 71-75], but it has not been clarified whether the small pore system participates in sulfur tolerance of the catalyst. The objectives of this study are to clarify the effect of adding a small-pore catalyst on the sulfur tolerance of a large-pore catalyst where the small-pore catalyst is not active for hydrogenation of two-ring aromatics. The hybrid catalyst was

prepared by mixing two different zeolite-supported Pd catalysts having different pore-opening sizes, Pd on Zeolite Y (7.4 Å) and Pd on zeolite A (4.1 Å), in order to have bimodal pore size distribution. For further investigation of the role of metal in small-microporous zeolite system, Pd clusters on the external surface of Zeolite A-supported Pd catalysts were passivated by chemical vapor deposition (CVD) of tetraethylorthosilicate (TEOS). Naphthalene and tetralin hydrogenation were conducted by varying concentration of benzothiophene as aromatic sulfur compound.

## 4.2. Experimental

In this study, Zeolite A (Zeolyst International, Advera 401N) and zeolite Y (Zeolyst International, CBV720) were used as supports for hybrid Pd catalysts. Zeolite A was pretreated by ion exchange with 0.4M $NH_4Cl$, followed by drying overnight at 100 $^oC$ and calcining at 450 $^oC$. Both supported Pd catalysts were prepared by the incipient wetness impregnation (IWI) of aqueous solution of palladium chloride (Aldrich, 99.999%) dissolved in dilute hydrochloric acid to metal concentration of 2 wt%, consecutive drying at 100 $^oC$ overnight and calcining in air flow (60 ml/min) at 450 $^oC$ for 4 h at a heating rate of 1.5 $^oC$ /min. In order to passivate Pd metal on the external surface of zeolite support, chemical vapor deposition (CVD) with tetraethylorthosilicate (TEOS) on Pd/A was accomplished by the procedure detailed in an earlier study [76]. The hybrid catalyst was prepared by physical mixing of Pd/Y with Pd/A for batch reactor test or with silica-coated Pd/A for flow reactor test at the weight ratio of 2:1. The surface area and the pore volume of the zeolite-supported Pd catalysts were measured by Quantachrome Autosorb 1 instrument. The metal dispersion of the catalysts was measured by hydrogen chemisorption using Micromeritics Autochem 2910 TPD/TPR equipped with a TCD detector.

Batch reactor testing was carried out in a 25ml horizontal tubing bomb reactor. Naphthalene, the model aromatic compound, was firstly purified by successive recrystallization and adsorption over active Raney nickel to remove unwanted heteroaromatics [77]. Naphthalene feedstock was prepared by mixing 10 wt% of naphthalene as aromatics, 85 wt% of hexadecane (Aldrich, 99+%, anhydrous) as solvent and 5 wt% of tetradecane (Aldrich, 99+%) as internal standard, then benzothiophene (Aldrich, 99%) was added for sulfur feed. 5 g of feedstock was charged to the reactor with 0.1 g of catalyst and the reactor was triply purged with hydrogen,

pressurized to 1000 psig, then placed and vertically agitated with a rate of 240 strokes/min in a fluidized sand bath at 200 $^{o}$C. Liquid products were separated from the spent catalyst by filtration and the used catalysts were washed by acetone onto a filter. The liquid products were analyzed by GC-FID (SRI 8610) using XTI-5 capillary column for quantitative analysis and GC-MS (Shimadzu GC-17A with QP-5000 MS) using Restek Rxi$^{TM}$-5ms for identification of the products.

Continuous fixed-bed flow reactor tests were conducted under 600 psig of $H_2$ pressure with two kinds of model fuel prepared by mixing aromatic compound and linear hydrocarbons: 10% naphthalene or 20% tetralin (1, 2, 3, 4-tetrahydronaphthalene, Aldrich, 99%) as aromatic compound, hexadecane as solvent and 5 wt% tetradecane as internal standard. For sulfur-containing feedstock, benzothiophene equivalent to 100 ppmw sulfur were added to the model fuels. The sulfur-free feedstock was firstly fed for specific times and then was changed to 100 ppmw sulfur feed and continued until the experiment finished.

### 4.3. Result and discussion

Table 4-1 shows the surface area and metal dispersion of Y and A zeolite supported Pd catalysts. Figure 4-1 presents naphthalene conversion in the presence of sulfur as benzothiophene. Pd/Y shows the highest naphthalene conversion on the test with 56 ppmw sulfur concentration. The high catalytic activity of Pd/Y can be mainly attributed to its high metal dispersion, 42% as listed in Table 4-1. However, the conversion drastically decreased as sulfur concentration increased to S/Pd atomic ratio > 1 over the Pd catalyst with the large pore openings of the zeolite Y. Although well-dispersed Pd metal active sites inside the zeolite might be less affected by sulfur at low sulfur concentration, they were seriously poisoned by a large amount of benzothiophene entering through the aperture of zeolite Y. On the other hand, Pd/A+Pd/Y hybrid catalyst surpassed Pd/Y at high sulfur concentrations (S/Pd atomic ratio > 1), presenting significantly higher naphthalene conversion even at S/Pd atomic ratio > 4, but little less than Pd/Y at low sulfur concentration. It should be also noticed that the mixture of zeolite Y (without Pd) and Pd/A did not show any conversion even at low sulfur concentration (56 ppmw). It was previously reported that the support without metal did not have significant catalytic activity for hydrogenation [6, 78], suggesting that Pd metal on zeolite Y support are the main active sites for naphthalene hydrogenation in this reaction condition. Furthermore, little or no catalytic activity was observed on the Pd/A catalyst even at low sulfur concentrations. It seems that the metal sites on A-type zeolite are excluded from contacting with bulky naphthalene since they were located mainly inside the small pore channel of zeolite A. Although some metal sites were present on the external surface of zeolite framework particles, they were immediately deactivated upon exposure to benzothiophene. As the Pd/A catalyst did not have any significant catalytic activity for

naphthalene hydrogenation, the higher sulfur tolerance of the Pd/A+Pd/Y hybrid catalyst can be mainly attributed to synergistic interaction between Pd/A and Pd/Y catalysts. The products from all batch reactor tests were mainly tetralin. It is likely that most of sites responsible for further hydrogenation of tetralin to decalins were either poisoned by added benzothiophene, or was not available for tetralin due to competitive adsorption of naphthalene. These results are consistent with an earlier study[14] with several Pd/Y catalysts and indicate that tetralin hydrogenation is more difficult and more sensitive to sulfur poisoning. Subsequently, flow reactor tests were conducted for detailed examination on sulfur tolerance of the hybrid Pd catalyst.

Table **4-1**: Surface area and metal dispersion of supported Pd catalysts

| Catalyst | BET Surface Area ($m^2/g$) | Metallic Surface Area | | Metal Dispersion (%) |
|---|---|---|---|---|
| | | ($m^2$/g Sample) | ($m^2$/g Metal) | |
| Pd/Y | 590 | 3.7 | 185 | 42.3 |
| Pd/A | 428 | 1.7 | 83 | 18.6 |
| $SiO_2$-Pd/A | 298 | 1.5 | 75 | 16.8 |

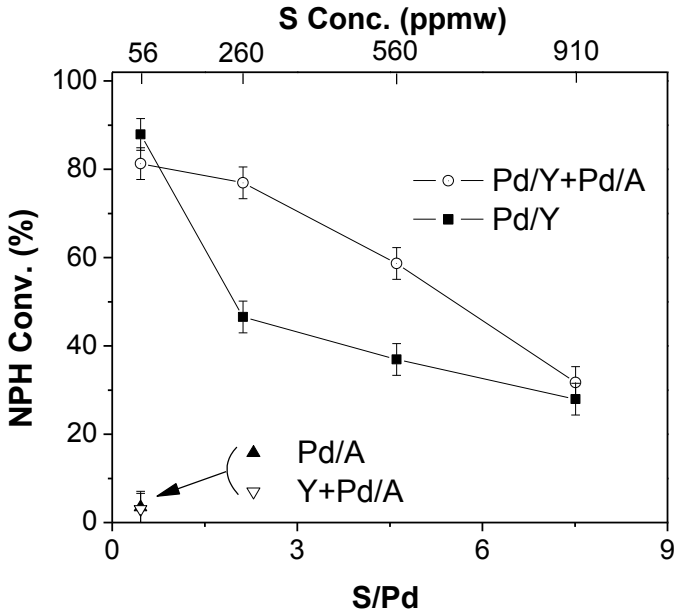


Figure **4-1**: Naphthalene conversions over various Pd catalysts at different sulfur concentrations as benzothiophene

For further investigation into the role of metal particles inside the small-pore zeolite, chemical vapor deposition (CVD) with tetraethylorthosilicate (TEOS) and consecutive condensation were performed on Pd/A catalyst to passivate Pd metal clusters on the external surface of zeolite particles. The Pd metal dispersion of the silica-coated Pd/A catalyst ($SiO_2$-Pd/A) in Table 1 is 16.8%, 1.8% less than that of uncoated Pd/A, thus confirming that the portion of the passivated metal surface area on the external surface is much smaller than the metal surface area inside the zeolite A, and silica coating was well-performed without hindering the entrance of hydrogen molecule through the pore opening of zeolite A.

Figure 4-2 presents the results for tetralin hydrogenation over single and hybrid Pd catalysts. Tetralin, the first ring-hydrogenated naphthalene (1,2,3,4-tetrahydronaphthalene), was chosen as a model aromatic compound because hydrogenation of tetralin (received in sulfur-free

form) is simpler and more sensitive to sulfur poisoning than naphthalene hydrogenation. The preliminary test of tetralin hydrogenation was conducted over the Pd/Y catalyst, but no deactivation of the catalyst was observed for 20 h with sulfur-free feed, ensuring that the sulfur poisoning is the main reason for catalyst deactivation with benzothiophene-containing feed. It should be noted that trans- and cis-decalin were the only products found from liquid product; neither ring opening reaction nor dehydrogenation of tetralin to naphthalene was observed under the conditions employed.

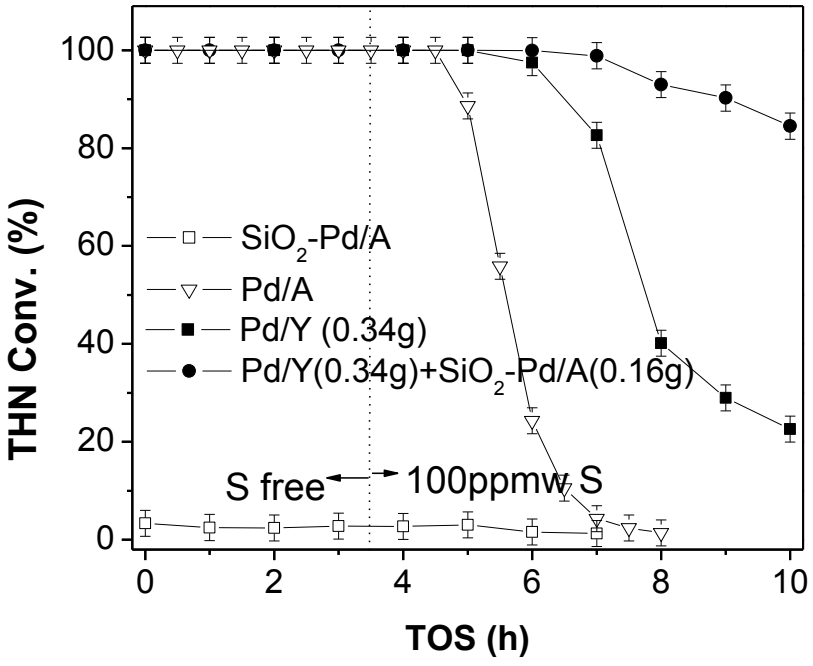


Figure **4-2**: Tetralin conversion over Pd/A, silica coated Pd/A, Pd/Y and hybrid catalyst in the absence and presence of 100ppmw sulfur as BT

As shown in Figure 4-2, tetralin conversion over uncoated Pd/A catalysts drastically decreased after introduction of 100 ppmw sulfur feed. It seems that metal clusters on the external surface of Pd/A as the active sites for tetralin hydrogenation were easily and immediately poisoned by introducing benzothiophene. Upon silica coating, $SiO_2$-Pd/A did not show any significant catalytic activity even on the sulfur-free fuel feed, indicating that the Pd metal particles on the external surface of zeolite A were successfully passivated by silica coating, and that the Pd sites inside zeolite A are not accessible for tetralin hydrogenation. Tetralin conversion with Pd/Y was 100% for the sulfur-free feed, but decreased significantly upon switch to 100 ppmw sulfur feed, and down to as low as 20% in 10 h TOS.

In order to investigate the effect of addition of small pore system to the large pore system, the hybrid catalyst was prepared by mixing $SiO_2$-Pd/A (0.16 g) with the same amount of Pd/Y catalyst (0.34 g) that was used for the test of single Pd/Y (0.34g). Therefore, the amounts of Pd metal active sites for tetralin hydrogenation on both Pd/Y and $SiO_2$-Pd/A + Pd/Y catalysts were same considering that the $SiO_2$-Pd/A catalyst alone shows no catalytic activity for tetralin conversion. The results in Figure 4-2 clearly demonstrates that adding $SiO_2$-Pd/A increased the sulfur tolerance of the Pd/Y catalyst with 100 ppmw sulfur feed, maintaining high catalytic activity with over 80% tetralin conversion even after 10 h TOS. This represents a dramatic improvement of sulfur tolerance, with 4 times higher tetralin conversion at 10 h TOS (over 80% vs 20% observed on Pd/Y). It is clear that the Pd/Y catalyst could retain its catalytic activity in the presence of the silica-coated Pd/A although the latter alone shows no catalytic activity for tetralin conversion. This greatly enhanced sulfur tolerance of Pd/Y is likely made possible by hydrogen spillover from $SiO_2$-Pd/A to Pd/Y.

Figure 4-3 depicts the trans- and cis-decalin yields from hydrogenation of tetralin over Pd/Y and $SiO_2$-Pd/A + Pd/Y. In the absence of sulfur (at 0 and 2 h TOS), both catalysts showed consistently high yields of trans-decalin (> 90%) and low yields of cis-decalin (<10%), with

trans-decalin/cis-decalin ratio of around 10.3. Compared with the data from other studies [61, 64, 79] in the low temperature range of 200-225 $^{o}$C, it confirms that the reaction over both catalysts reached quasi-equilibrium state in the absence of sulfur.

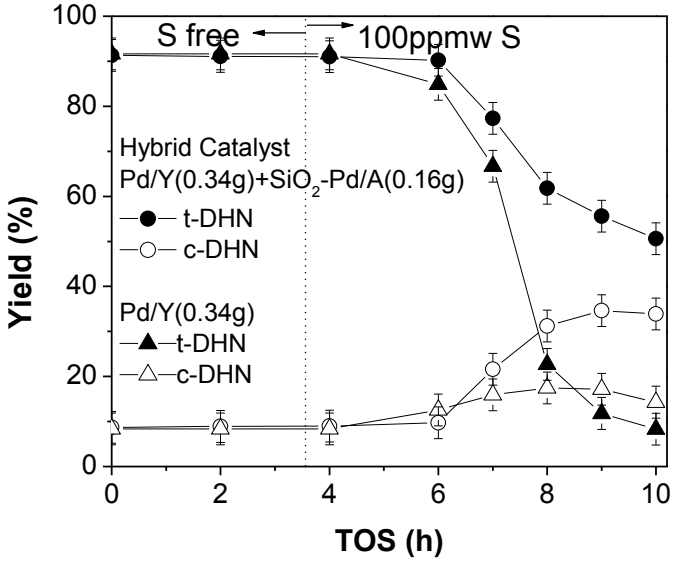


Figure **4-3**: Product yields on tetralin hydrogenation over Pd/Y and hybrid catalyst in the absence and presence of 100ppmw sulfur as BT

Introduction of sulfur feed profoundly influenced the selectivity of decalin. The decrease of trans-decalin and the simultaneous increase of cis-decalin were observed on tetralin hydrogenation as sulfur-induced deactivation proceeded. This tendency could be explained by "active site competition between tetralin and cis-decalin", as suggested by Huang et al. and Jongpatiwut et al. [19, 80]. They reported that cis- to trans- isomerization is hindered by the presence of tetralin when the tetralin conversion was relatively low, but it is accelerated at high

tetralin conversion. As discussed in this study, sulfur poisoning is the main reason of catalyst deactivation and the amount of active sites for hydrogenation depends on the degree of sulfur poisoning. When the catalyst is poisoned and the amount of active sites is reduced, it will lead to tetralin hydrogenation rather than cis-decalin isomerization due to the preferential adsorption of tetralin. In that case, it is plausible that the selectivity of decalin is changed in accordance with the degree of sulfur poisoning on the catalyst. Therefore, it should be noticed that the hybrid catalyst displayed slower decrease of trans-decalin yield and higher cis-decalin yield compared with the Pd/Y catalyst, because it is also another supportive evidence of good sulfur tolerance on the hybrid catalyst with the aid of $SiO_2$-Pd/A.

Figure 4-4 shows the results of naphthalene hydrogenation over both Pd/Y and $SiO_2$-Pd/A+Pd/Y hybrid catalysts with the same loading amount (0.5g) in the presence of 100 ppmw sulfur as benzothiophene. On both catalysts, naphthalene was completely converted to either tetralin or decalins for the duration of the 20 h TOS without sulfur and with 100 ppmw sulfur. In the absence of sulfur, most of the products are isomers of decalin, the completely hydrogenated products. Only a trace amount of tetralin was detected, but it gradually increased after sulfur was introduced. These results demonstrate that the total conversion of naphthalene is not influenced by sulfur, even at 100 ppmw, under the reaction condition employed, and that the first aromatic ring is easier to be hydrogenated than the second ring [1, 2].

Therefore, the level of catalyst deactivation induced by sulfur poisoning could be determined by tetralin yield, the intermediate product from naphthalene hydrogenation to decalin, rather than naphthalene conversion. The lower tetralin yields were observed on the hybrid catalyst compared to Pd/Y in the presence of sulfur, suggesting that the former maintained higher catalytic activity than the latter.

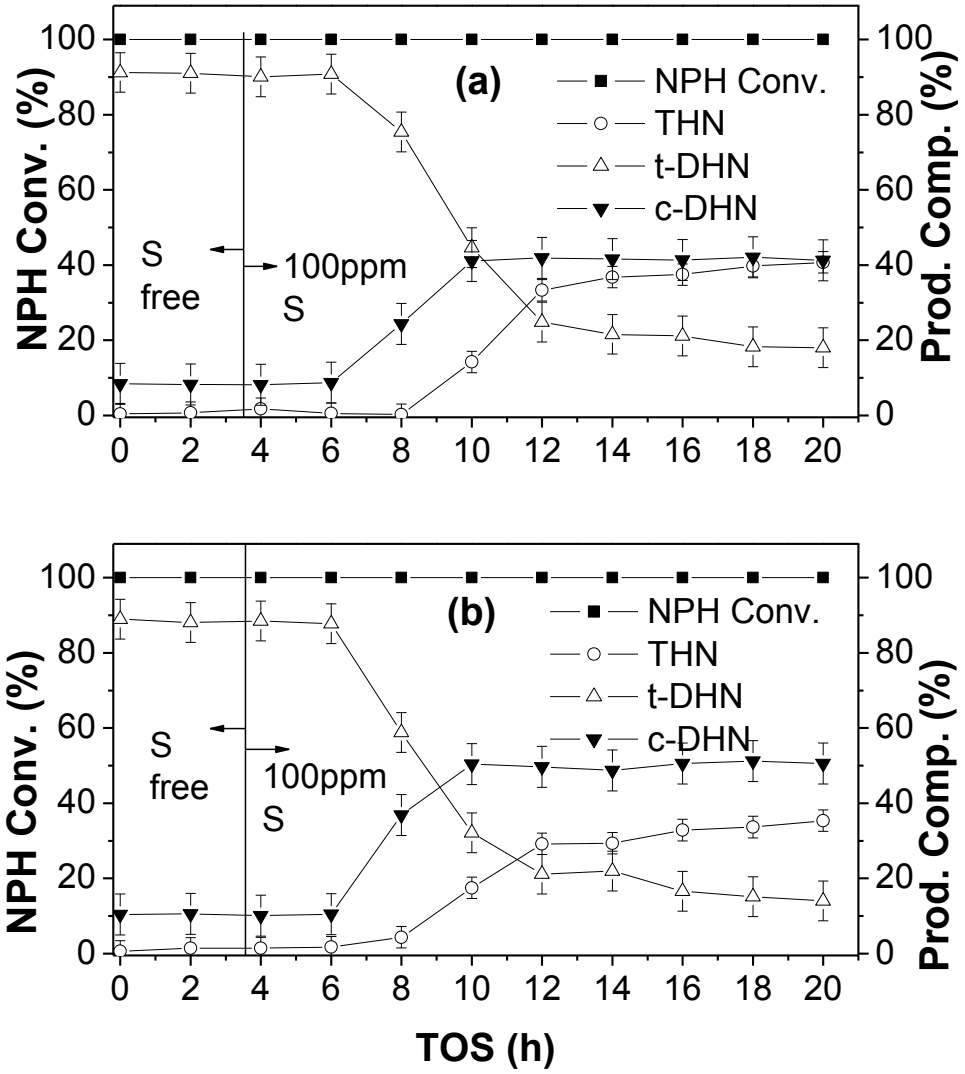


Figure **4-4**: Conversion and product yields of naphthalene hydrogenation over (a) Pd/Y and (b) Pd/Y+$SiO_2$-Pd/A hybrid catalyst in the presence of 100ppw sulfur as BT

The cis- and trans- decalin yields in Figure 4-4 showed the same trends as observed on tetralin hydrogenation in Figure 4-2. In the absence of sulfur in the fuel feed, both yields of cis-

and trans-decalin maintained consistent, demonstrating that the reaction reached quasi-equilibrium state. As TOS increased after introduction of sulfur feed, trans-decalin yield gradually reduced, but cis-decalin yield initially increased but reached and maintained a certain level until the test finished. The cis-decalin yield over the hybrid catalyst was approximately 10% higher than that over Pd/Y. However the reason is unclear whether the hybrid catalyst has either high activity toward cis-decalin production with the aid of hydrogen spillover. It is also possible that certain active sites for the cis-decalin isomerization to trans-decalin are seriously hindered by sulfur poisoning. This should be further studied in future. Anyway, even both catalysts showed decrease of catalytic activities as the reaction proceeded in the presence of sulfur, the hybrid catalyst maintained higher catalytic activity displaying lower tetralin yield and higher cis-decalin yield compared with Pd/Y. Furthermore, trans-decalin yield over the hybrid catalyst showed milder decrease. Based on the result, it was clarified that the sulfur-tolerant hybrid catalyst outperforms Pd/Y on naphthalene hydrogenation in the presence of benzothiophene.

## 4.4. Conclusion

The hybrid catalyst consisting of Pd/A+Pd/Y mixture showed enhanced sulfur tolerance, which is mainly attributed to the small pore system, Pd/A catalyst. It seems that Pd/A plays a role for shape selective exclusion of bulky benzothiophene as well as hydrogen spillover from metal inside small pore system to prohibit the metal sites in large pore system from sulfur-induced deactivation. Overall, the hybrid catalyst based on our design concept of sulfur-tolerant catalyst is applicable for low-temperature diaromatics hydrogenation in presence of benzothiophene, due to the reactant shape selectivity and hydrogen spillover.

**Chapter 5**

# Sulfur-tolerant Hybrid Zeolite-Supported Pd Catalyst based on Shape-selective Exclusion and Hydrogen Spillover for Low-temperature Hydrogenation of Aromatics

Abstract

A hybrid zeolite-supported Pd catalyst was prepared for improving sulfur tolerance, based on a new catalyst design concept proposed for low temperature hydrogenation of aromatics in distillate fuel [C.S. Song, Chemtech, 29 (1999) 26-30]. The hybrid catalyst consists of Pd supported on Y and A zeolites and surface metal passivation and potassium ion exchange were employed to zeolite A-supported Pd catalyst for precise investigation of the role of small pore system in hybrid catalyst. The hybrid catalyst significantly enhanced sulfur tolerance of the catalyst for tetralin hydrogenation as well as isomerization of cis-decalin in the presence of benzothiophene. This may be mainly attributed to the small pore system (Pd on zeolite A) in the hybrid catalyst. It is suggested that the small pore system in the hybrid catalyst which is not directly active for tetralin hydrogenation serves size-selective exclusion of sulfur compounds as well as hydrogen spillover from metal inside small pore to prohibit from poisoning on the metal sites in large pores in Pd/Y.

Keywords: shape selectivity, hydrogen spillover, sulfur tolerance, hydrogenation, hydrodesulfurization, hybrid catalyst

## 5.1. Introduction

Environmental regulations in many countries have been setting more and more stringent standards on fuel specifications in accordance with increasing awareness towards the health risks related to the liquid transportation fuel. Thus, the refineries are facing major challenges to meet the fuel specification along with the required reduction of aromatic contents, and currently, deep desulfurization and aromatic hydrogenation of distillate fuels are receiving considerable attention.

The conventional hydrotreating processes predominantly utilize Co-Mo and Ni-Mo sulfide catalysts operating at relatively high temperature (>300 $^{o}$C). However, since deep aromatic hydrogenation favors lower temperature, these catalysts are not suitable to overcome thermodynamic limitation of aromatic hydrogenation [2]. Recently, the noble metal catalysts have been considered as excellent candidates for deep hydrogenation owing to its high catalytic activity at low temperature, but they have one main serious problem, rapid deactivation when they are exposed to sulfur compounds existing in industrial fuel feedstock [4, 5, 44]. For these reasons, considerable research has been devoted to development of sulfur-resistant noble metal catalysts in many ways such as metal alloy and acidity of zeolite support [9, 10, 24, 25, 53, 54, 81]. With a different point of view in this research, our group has been focusing on the pore configuration of zeolite support in developing sulfur-tolerant noble metal catalyst. The earlier exploratory work showed that the zeolite structure can promote sulfur tolerance by shape selective exclusion, from which the new design of noble metal catalysts for hydrogenation was proposed [4, 29].

The concept invokes distinct shaped zeolite as support material for noble metal catalysts and utilizes shape selective exclusion of sulfur compound and hydrogen spillover. According to

the concept, noble metals are supported on zeolite material possessing bimodal pore size distributions. The large pore system (> 6Å) allows hydrogenation of polyaromatics and hydrodesulfurization of aromatic sulfur compounds, while bulky aromatics and organic sulfur compounds such as thiophenic molecules are selectively excluded from the small pore system (< 5Å). $H_2$ molecules can enter both large and small pores, be dissociated on metal sites and be transported between both pore systems by hydrogen spillover. When metal in the large pore systems becomes inactivated by adsorbed sulfur molecules, spillover hydrogen from the small pores can recover the poisoned metal sites by elimination of organic sulfur compound.

Several research groups have conducted research on development and application of zeolite-supported catalysts related to this proposed concept [6, 71-75]. Zhang et al. and Zhou et al. prepared the MCM-41 overgrown on Y composite zeolite as a bimodal porous support for noble metal catalyst and improved sulfur tolerance of the catalyst on hydrogenation of polyaromatic compounds and hydrodesulfurization of dibenzothiophene, respectively [71, 72]. Ismagilov et al. adopted ZSM-5 and montmorillonite as supports for bimodal pore distribution and showed the high catalytic efficiency on ultra deep desulphurization of LCO (light cycle oil) as well as hydrodesulfurization of thiophene and hydrogenation of benzene [74]. However, those researchers did not seriously consider sulfur poisoning of the metal clusters inside the small porous system, which could be induced by the product from decomposition of thiophenic compound such as $H_2S$. The research by Yang et al. and Chen et al. were devoted to the size-controlled microporous structure to exclude sulfur poisoning induced by $H_2S$ and the effect of hydrogen spillover on naphthalene hydrogenation over zeolite Y [6, 75]. Nevertheless, it is still unclear whether the small pore system participates in increasing sulfur tolerance of the catalyst and hydrogen spillover can recover the sulfur-poisoned metal active sites.

The present study focused on the sulfur-tolerant, hybrid zeolite-supported noble metal catalyst with shape selective exclusion and hydrogen spillover for low temperature tetralin

hydrogenation in the presence of benzothiophene. The main objectives in this study are to clarify the role of hydrogen spillover in improving sulfur tolerance of the catalyst and to investigate the influence of hybrid zeolites and supported metals on the hydrogenation activity and sulfur resistance of the catalysts. For bimodal pore configuration, the hybrid zeolite-supported catalyst was prepared by mixing two different zeolite-supported Pd catalysts possessing different pore sizes, Y and A zeolites. For precise investigation of role of microporous system, chemical vapor deposition (CVD) of tetraethylorthosilicate (TEOS) and ion exchange were adopted on zeolite A-supported Pd catalyst for surface metal passivation and pore size control, respectively. Tetralin hydrogenation as well as cis-decalin isomerization was conducted by varying concentration of benzothiophene as aromatic sulfur.

## 5.2. Experimental

### 5.2.1. Catalyst Preparation

Zeolite A (Zeolyst International, Advera 401N) and zeolite Y (Zeolyst International, CBV720) were used as zeolite supports for hybrid Pd catalysts. The zeolite supports were calcined in air flow (60 mL/min) at 450 $^{o}$C for 4 h with a heating rate of 1.5 $^{o}$C /min before catalyst preparation. The zeolite A supports in proton and potassium form were developed from sodium form of zeolite A by ion-exchange with an 0.4M aqueous solution of ammonium chloride ($NH_4Cl$, Aldrich, 99.5%) and potassium chloride (KCl, Aldrich, 99.0%) at 80 $^{o}$C under stirring, respectively. Then, it was washed with deionized water, dried in an oven at 100 $^{o}$C and then calcined at 450 $^{o}$C. The obtained samples were denoted as A and KA, respectively. The supported Pd catalysts (Pd/Y, Pd/A and Pd/KA) were prepared by the incipient wetness impregnation (IWI) of aqueous solution of palladium chloride ($PdCl_2$, Aldrich, 99.999%) dissolved in dilute hydrochloric acid to a nominal metal concentration of 2 wt%. After impregnation was complete, the catalysts were dried at 100 $^{o}$C overnight and calcined in air flow (~60 ml/min) at 450 $^{o}$C for 4 h at a heating rate of 1.5 $^{o}$C /min.

Chemical vapor deposition (CVD) with tetraethyl orthosilicate (TEOS) on zeolite A-supported Pd catalyst was performed in a flow-type CVD reactor system to passivate Pd clusters on the external surface of Pd/A or Pd/KA catalysts. Figure 5-1 shows the schematic diagram of surface metal passivation by CVD of TEOS. The procedure of CVD in this study followed Reddy's [76]: Either Pd/A or Pd/KA catalyst was loaded into the quartz tube reactor and purged

under 20ml/min $N_2$ flow at 450 $^oC$ for 1 h. The temperature was brought down to 200 $^oC$ and subsequently TEOS was fed at the rate of 0.05 ml/min for 1 h using a liquid syringe pump. Then condensation was performed with air flow (20 ml/hr), heating to 450 $^oC$ with a temperature ramp of 15 $^oC$ /min and maintaining at 450 $^oC$ for 2 h.

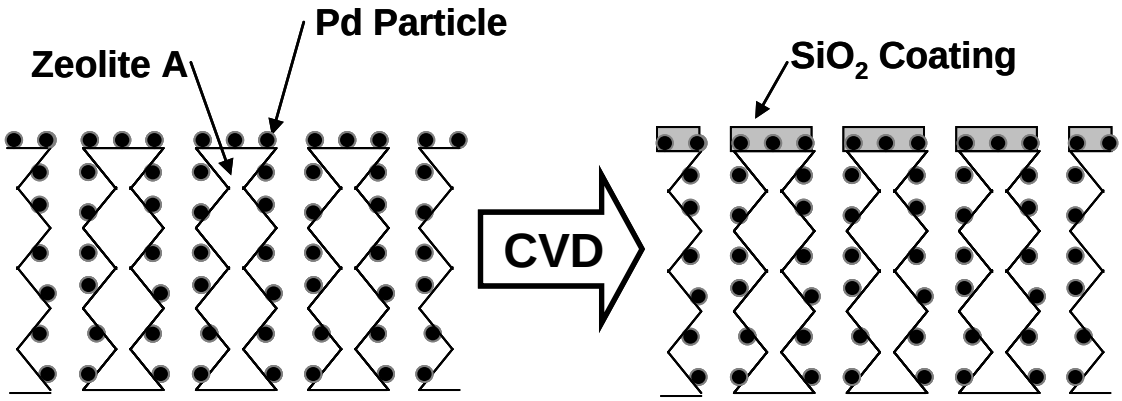


Figure **5-1**: Schematic diagram of surface metal passivation by CVD of TEOS on zeolite A-supported Pd catalyst

Both hybrid catalysts were prepared by physical mixing of Pd/Y with silica coated Pd/A or Pd/KA ($SiO_2$-Pd/A or $SiO_2$-Pd/KA) at the weight ratio of 2:1, denoting $SiO_2$-Pd/A+Pd/Y or $SiO_2$-Pd/KA+Pd/Y, respectively. For example, 0.5 g of $SiO_2$-Pd/A+Pd/Y hybrid catalyst was prepared by mixing 0.34 g of Pd/Y with 0.16 g of $SiO_2$-Pd/A. The other types of hybrid catalysts were prepared by mixing zeolite Y support with $SiO_2$-Pd/A+Y or $SiO_2$-Pd/KA+Y in order to investigate the effect of support (zeolite Y).

### 5.2.2. Catalyst Characterization

The surface area and pore volume of the zeolite-supported Pd catalysts were measured by Quantachrome Autosorb 1 instrument. The Pd dispersion of the catalysts was measured by hydrogen chemisorption using Micromeritics Autochem 2910 TPD/TPR equipped with a TCD detector. Powder X-ray diffraction (XRD) patterns of the calcined catalysts were obtained by a Scintag (Thermo Scientific) PAD V Powder Diffractometer, using Cu-Kα radiation (λ = 0.154 nm). In order to determine the structure change, the diffraction patterns were analyzed using MDI JADE 8.0 software and the standard JCPDS files. Transmittance electron microscopy (TEM) images were obtained using a JEOL EM-2010F electron microscope with a field-emission source operated at 200 kV.

Temperature programmed desorption (TPD) studies of ammonia were conducted on zeolite-supported Pd catalyst samples using the Micromeritics Autochem 2910 analyzer. The samples were heated to 450 $^{o}$C with a heating rate of 10$^{o}$C/min and maintained for 1 h under helium followed by cooling to 110 $^{o}$C. When the temperature reached to 110 $^{o}$C, 10/% $NH_3$/He mixture gas was introduced by pulse injection until the TCD signal equilibrated. When there was no difference of the TCD signal after subsequent pulses passed through the sample, the $NH_3$ adsorption was stopped. The sample was purged for 2 h with helium to remove the weakly adsorbed ammonia and held until the TCD baseline was stable. The sample was heated again from 110$^{o}$C to 900$^{o}$C at the ramp of 10$^{o}$C/min and desorption process was again recorded by the TCD and MS.

Hydrogen spillover was measured by hydrogen consumption at 200 $^{o}$C. $WO_3$, widely adopted for the measurement of hydrogen spillover, was employed as a sorbent for spilt-over hydrogen from small-pore catalyst [82-85]. $WO_3$ and the Pd catalyst sample were mixed together then placed in a U-shaped Pyrex tube reactor surrounded by a split furnace equipped in Micromeritics 2910 analyzer. The reactor was heated to 200 $^{o}$C with a heating rate of 10$^{o}$C/min and maintained for 30 min under argon flow. When the system reached stable condition, 5% $H_2$/Ar mixture gas was introduced into the reactor at the rate of 10 ml/min and the outlet hydrogen rate was monitored by Mass Spectrometer (Dycor). The hydrogen uptake rate was first calculated by subtracting the outlet hydrogen rate from the inlet hydrogen rate and then the extent of sorbed hydrogen was obtained via integration of the uptake rate curve.

### 5.2.3. Catalyst Evaluation

Continuous fixed-bed flow reactor testing was conducted at 225$^{o}$C under 600 psi of $H_2$ pressure. The catalyst was loaded and reduced in-situ under a hydrogen flow of 100 ml/min and 100 psig of $H_2$ pressure at 225$^{o}$C prior to each experiment. Hydrogenation of tetralin was carried out at 600 psi and 225 $^{o}$C, with a WHSV of 7.7 hr$^{-1}$ and volumetric hydrogen to liquid ratio of 1000. The sulfur free model fuel was first injected into the reactor by HPLC pump for 90 minutes in order to stabilize the reactor system. Therefore, 90 min after the introduction of feedstock was designated as time-on-stream (TOS) equal to zero. Sulfur free feedstock was fed until a certain hour, at which point the feed was changed to sulfur feed and continued until the experiment finished. Two kinds of model fuels, one for tetralin hydrogenation and the other for cis-decalin isomerization, were prepared. 20 wt% of either tetralin (1, 2, 3, 4-tetrahydronaphthalene, Aldrich, 99%) for hydrogenation or cis-decalin (cis-decahydronaphthalene, Aldrich, 99%) for cis-decalin

isomerization was mixed with 75% hexadecane (Aldrich, 99+%, anhydrous) as solvent and 5% tetradecane (Aldrich, 99+%) as internal standard. For sulfur feed stock, benzothiophene (BT, Aldrich, 99%) was added to these model fuels. Liquid products were analyzed by GC-FID(SRI 8610) using XTI-5 capillary column for quantitative analysis and GC-MS (Shimazu GC-17A with QP-5000 MS) using Restek Rxi$^{TM}$-5 ms for identification of the products.

## 5.3. Result and Discussion

### 5.3.1. Characterization of catalyst

Surface area, metal surface area and dispersion derived from $N_2$ adsorption-desorption and hydrogen pulse chemisorption were organized in Table 5-1. The measurement of surface area on Pd/KA via $N_2$ adsorption-desorption was not available due to smaller pore opening of zeolite KA support (3Å) [6] than the probe molecule, $N_2$ (kinetic diameter: 3.64Å) [86]. The high metal dispersion (42%) for zeolite Y supported Pd catalyst (Pd/Y) is ascribed to the higher surface area and bigger pore openings. The low metal dispersions of both zeolite A-supported Pd catalysts (Pd/A and Pd/KA) could be mainly due to the relatively smaller pore openings of zeolite A support. The slightly higher metal dispersion of Pd/KA compared to Pd/A implies that addition of potassium acts as basic promoter to improve the metal dispersion of the catalyst [70].

HRTEM images of Pd/A, Pd/KA and Pd/Y catalysts were adopted, thus allowing precise investigation of the size and location of metal particles by tilting the sample holder under the electron beam. As seen from Figure 5-2, the Pd particles of Pd/Y were uniformly dispersed, mainly located inside the zeolite pore. Their average particle size determined was around 1.5 nm, in good agreement with the size of spherical zeolite Y supercage (minimum free diameter: 13 Å, from [87] and 16-20 Å, from the measurement referred from library of Material Studio 5.0). The TEM images of both zeolite A supported Pd catalysts revealed that there were two distinguished metal particle distributions coexisted. The sizes of Pd particles within the range between 1.0-1.5 nm are almost same as or slightly bigger than the size of α-cage of the zeolite A (minimum free

diameter: 11.4 Å [87] and 13.5 Å from the library of Material Studio 5.0). By tilting of the sample holder under the electron beam, it was confirmed that the well-dispersed small Pd particles below 1.5 nm (black dots) were placed inside of zeolite cavities. As suggested by Matsui and Gallezot, noble metals can be placed in the zeolite cavities with some local destruction of zeolite framework [88, 89]. However, the big metal particles were also placed outside of the zeolite supports, even it was reported that metal atoms can introduce into very small pores during calcination [53, 69], which is likely that some Pd precursors agglomerated on the external surface of the zeolite support developed to bigger Pd particles. The image of Pd/KA showed that the metals were well-dispersed, in good agreement with the metal dispersion data.

Table **5-1**: Surface area and metal dispersion of supported Pd catalysts

| Catalyst | BET Surface Area ($m^2/g$) | Metallic Surface Area | | Metal Dispersion (%) |
|---|---|---|---|---|
| | | ($m^2/g$ Sample) | ($m^2/g$ Metal) | |
| Pd/Y | 590 | 3.7 | 185 | 42.3 |
| Pd/A | 428 | 1.7 | 83 | 18.6 |
| Pd/KA | 0.5 | 1.9 | 95 | 21.3 |
| $SiO_2$-Pd/A | 298 | 1.5 | 75 | 16.8 |
| $SiO_2$-Pd/KA | - | 1.6 | 81 | 18.1 |

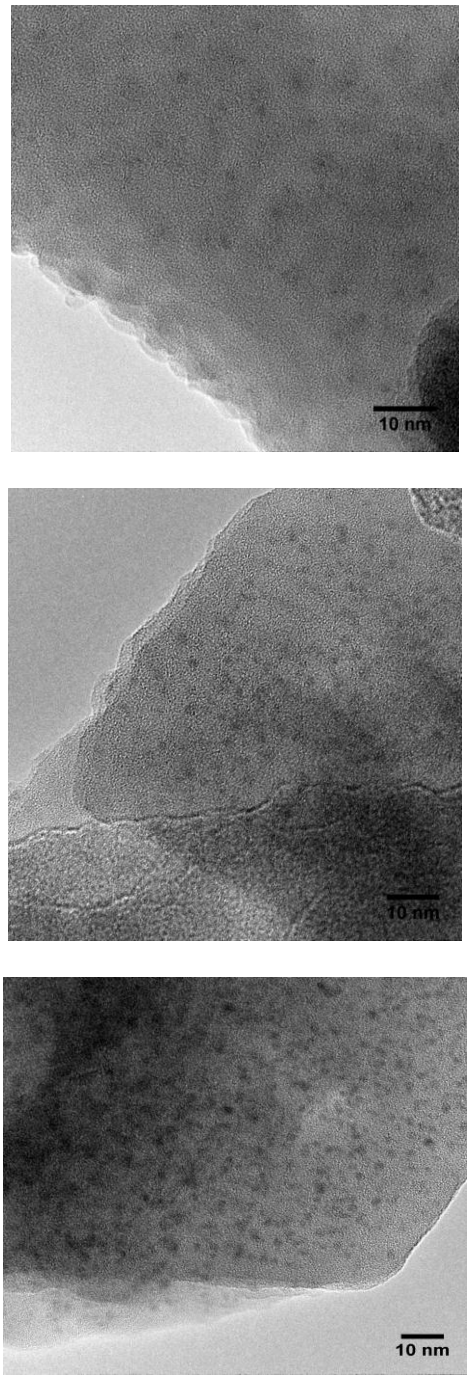


Figure **5-2**: TEM images of Pd/A (top), Pd/KA (middle) and Pd/Y(bottom)

In Figure 5-3, ammonia desorption from Pd/A showed a major peak at about 400$^{o}$C and a minor peak at 220$^{o}$C, while the opposite trend was observed on Pd/KA peaks, the weak intensity at 400$^{o}$C and the strong one at 220$^{o}$C. It implies that the adsorption strength of ammonia on Pd/KA is weaker than that on Pd/A, which might be mainly due to the electro-positivity of potassium.

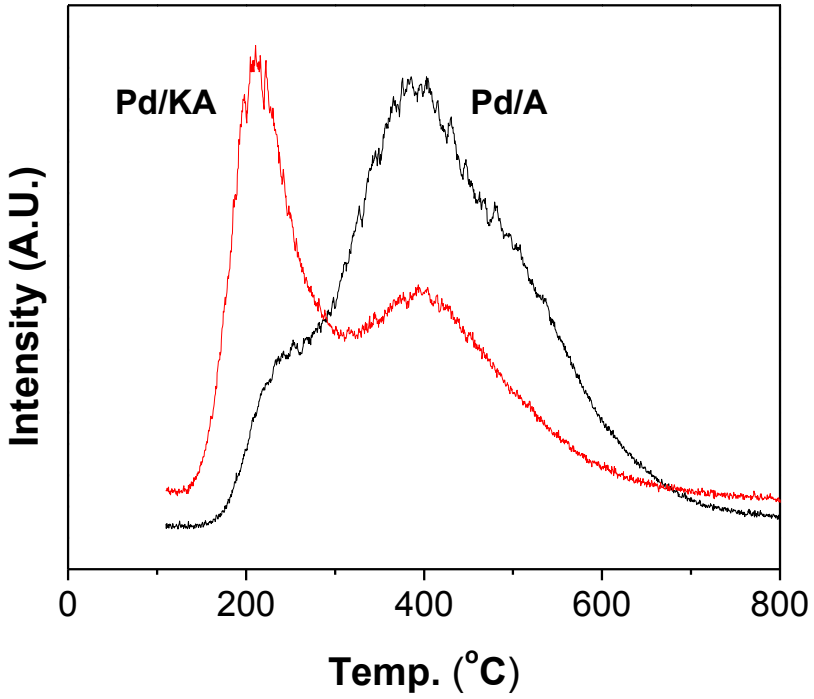


Figure **5-3**: Ammonia TPD profiles of the Pd/A and Pd/KA catalysts

### 5.3.2. Surface metal passivation of zeolite A-supported Pd catalyst

For further investigation into the role of metal inside the small-microporous zeolite system, chemical vapor deposition (CVD) with tetraethyl orthosilicate (TEOS) and consecutive condensation were performed to passivate Pd metals on the external surface of zeolite A-supported Pd catalyst. As seen from Table 5-1, the metal dispersion of silica coated Pd catalyst ($SiO_2$-Pd/A and $SiO_2$-Pd/KA) measured by hydrogen chemisorption decreased by roughly 2-3% compared to Pd/A or Pd/KA catalyst. It suggests that most metal atoms exposed to hydrogen were placed inside the pore of zeolite A and the silica coating was well performed without hindering hydrogen molecule from entering through the zeolite pore opening.

The X-ray diffraction patterns for zeolite supports, Pd catalysts and silica-coated Pd catalysts were compared in Figure 5-4. The patterns of both zeolite A (A and KA) corresponded well with that of zeolite A in the standard JCPDS file, suggesting that there was no significant geometric decomposition of zeolite framework which might be caused by ion exchange. Diffraction patterns for the Pd catalysts and their silica-coated catalysts were also identical with the corresponding zeolite frameworks, although the peak intensities decreased due to the presence of the metal in the zeolite framework [90]. The intrinsic palladium peaks were not detected, which is likely that the metal clusters are mainly incorporated inside the zeolite pore structure.

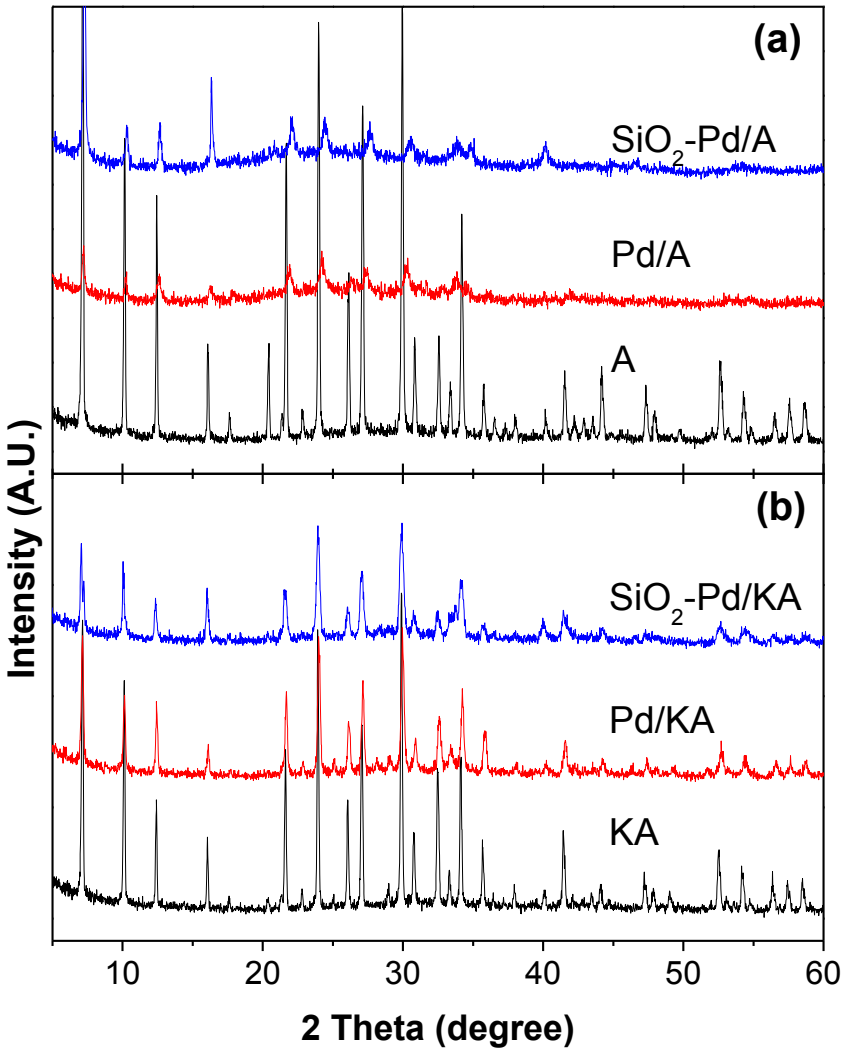


Figure **5-4**: XRD pattern of (a) Zeolite A, Pd/A and $SiO_2$-Pd/A (b) Zeolite KA, Pd/KA and $SiO_2$-Pd/KA

Quantification of hydrogen spillover was attempted to inspect the effect of the support on hydrogen spillover over Pd catalyst. Figure 5-5 (a) shows a schematic diagram of hydrogen sorption by secondary spillover from small- pore-catalyst to $WO_3$. No hydrogen uptake was observed on $WO_3$ without the Pd catalyst for 1 h, confirming that the Pd metal plays a main activator for hydrogen spillover. Likewise, the catalyst alone without $WO_3$ was also tested, but no significant hydrogen consumption was detected on the catalyst, which is likely that the amount of catalyst used is too small (0.05 g). Figure 5-5 (b) shows the rate of hydrogen spillover and the amount of hydrogen uptake on $WO_3$ mixed with small-pore catalyst. Both mixtures reached the maximum value at around 30 min, and the overall hydrogen uptake on $SiO_2$-Pd/KA is 1.4 times higher than that on $SiO_2$-Pd/A. Similar result was shown from the highest hydrogen uptake rate deduced from the increasing slope, that over $SiO_2$-Pd/KA catalyst is approximately 1.5 times higher than that over $SiO_2$-Pd/A. This may be attributed to the higher metal dispersion of $SiO_2$-Pd/KA than $SiO_2$-Pd/A. It is also possible that addition of potassium ion used for pore size control also affects catalytic property of Pd metal such as changing the electron density of Pd metal [70]. The result demonstrates that silica coating on Pd catalyst was well performed without blocking the pore opening, maintaining the catalytic activity of Pd metals inside the pore of zeolite A.

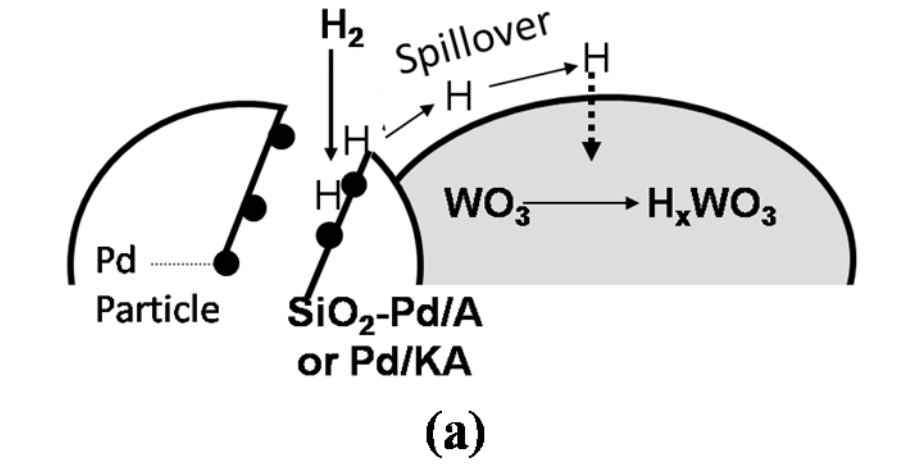


(a)

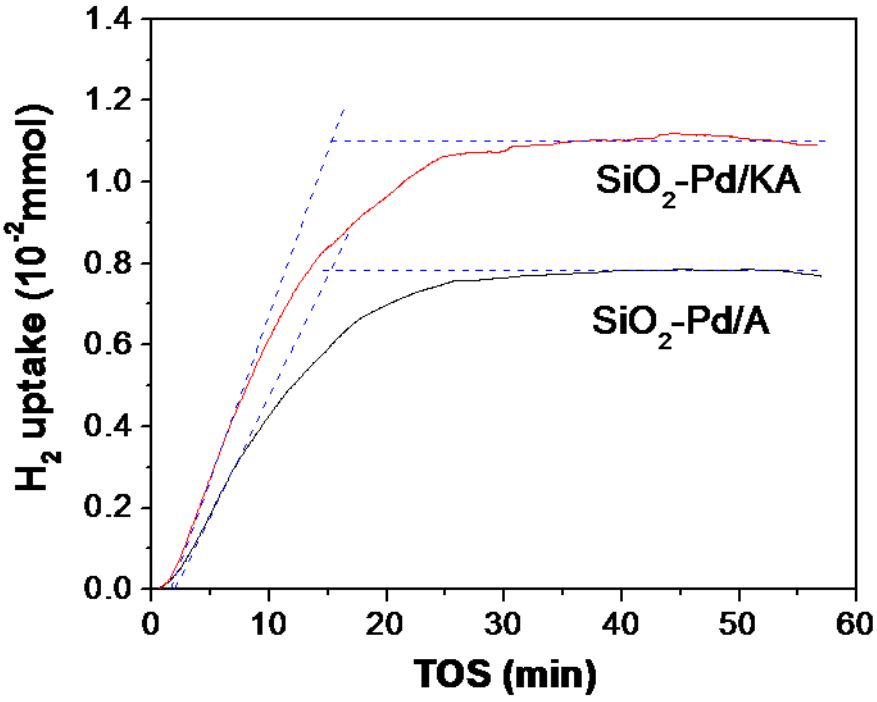


(b)

Figure **5-5**: (a) Schematic diagram of hydrogen spillover test between Pd catalyst and $WO_3$ (b) extent of hydrogen uptake on $WO_3$ by hydrogen spillover

The flow reactor test was adopted for investigation of sulfur tolerance of catalyst on tetralin hydrogenation. It should be noted that decalin (1,2,3,4,5,6,7,8,9,10-decahydronaphthalene) was the only product found from GC analysis data. Table 5-2 displays the comparison of tetralin conversion among four catalysts, Pd/A, Pd/KA, $SiO_2$-Pd/A and $SiO_2$-Pd/KA in the absence and presence of 100 ppmw sulfur. The conversions over both Pd/A and Pd/KA catalysts were drastically decreased after introduction of sulfur even though Pd/KA maintained catalytic activity longer than Pd/A did. Meanwhile, no significant catalytic activity was observed on both silica-coated Pd catalysts ($SiO_2$-Pd/A and $SiO_2$-Pd/KA), suggesting that Pd metals on the external surface of zeolite A are the main active sites on the zeolite A supported Pd catalyst for tetralin hydrogenation, but are susceptible to be poisoned by benzothiophene.

Table **5-2**: Tetralin conversion (%) over zeolite A supported Pd catalysts in the absence (at 3 h TOS) and presence of 100 ppmw sulfur as BT (after 5 h TOS)

| TOS (h) | 3 | 5 | 7 | 9 |
|---|---|---|---|---|
| Pd/KA | 100.0 | 99.9 | 22.6 | 1.6 |
| Pd/A | 100.0 | 88.6 | 4.3 | 1.3 |
| $SiO_2$-Pd/KA | 2.8 | 3.0 | 1.3 | - |
| $SiO_2$-Pd/A | 1.0 | 2.0 | 1.2 | - |

### 5.3.3. Tetralin hydrogenation over hybrid catalyst

Figure 5-6 shows tetralin conversion over Pd/Y and two hybrid catalysts, $SiO_2$-Pd/A mixed with Pd/Y (Pd/Y+$SiO_2$-Pd/A) and $SiO_2$-Pd/KA mixed with Pd/Y (Pd/Y+$SiO_2$-Pd/KA), in the presence of 100 ppmw sulfur. In order to investigate the effect of addition of small pore catalyst, the same amount of Pd/Y (0.34 g) that was used for the hybrid catalyst was also compared. Tetralin conversions over both hybrid catalysts were higher than those over Pd/Y catalysts. Especially, $SiO_2$-Pd/KA+Pd/Y hybrid catalyst maintained high catalytic activity with over 90% conversions until 14 h TOS, while $SiO_2$-Pd/KA alone was almost inactive for hydrogenation. This represents a significant enhancement of sulfur tolerance attributed to small pore catalyst. However, when the fuel containing 30 ppmw sulfur was introduced, no distinguishable difference among catalysts was observed. As seen from Figure 5-7, all catalysts maintained over 90% of conversion for 45 h, indicating that low sulfur concentration in the model fuel does not seriously affect the activity of the catalysts tested.

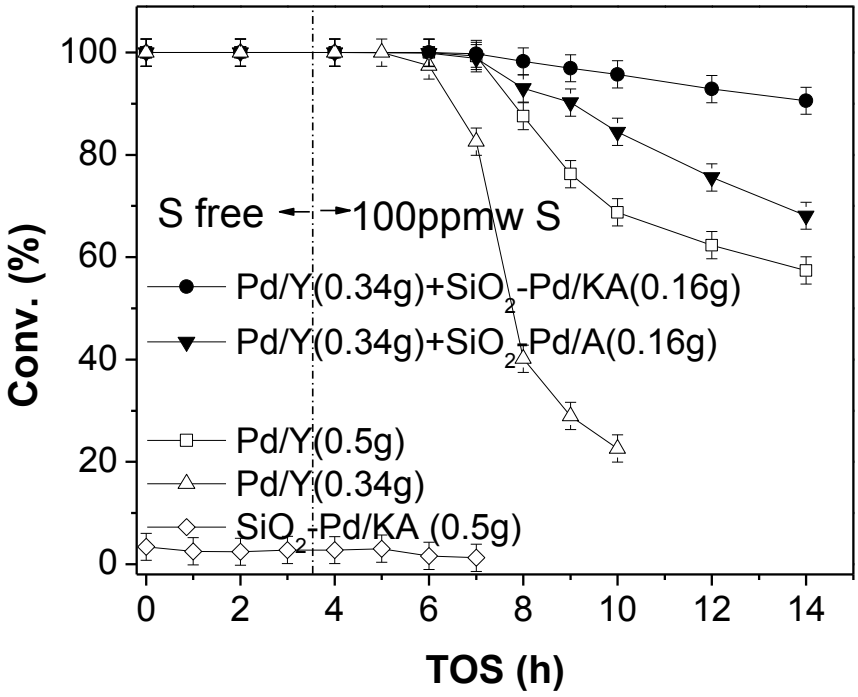


Figure **5-6**: Tetralin conversion on tetralin hydrogenation in the absence and presence of 100 ppmw sulfur as BT

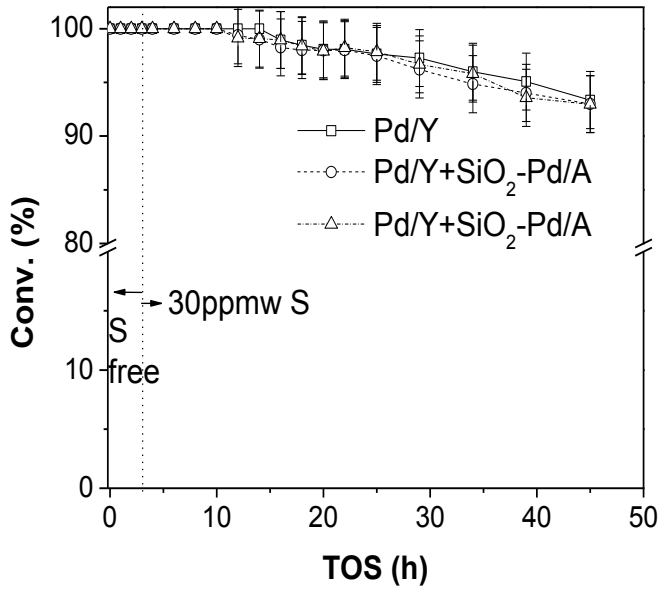


Figure **5-7**: Comparison of conversion on tetralin hydrogenation over the same amount (0.5 g) of catalyst in the absence and presence of 30 ppmw sulfur as BT

The result of sulfur concentrations in the liquid products in Figure 5-8 was also comparable to the conversion result. After the introduction of benzothiophene-containing feed, the sulfur concentration increased steadily on all catalysts, indicating that the catalytic activity for hydrodesulfurization also decreased as well. Both hybrid catalysts showed the lower sulfur concentration than Pd/Y, and $SiO_2$-Pd/KA+Pd/Y maintained low sulfur concentration below 10 ppm even after 14 h TOS. From both results of tetralin conversion and sulfur concentration of liquid products, it was confirmed that the hybrid catalysts have the higher sulfur tolerance than Pd/Y and $SiO_2$-Pd/KA+Pd/Y outperforms $SiO_2$-Pd/A+Pd/Y.

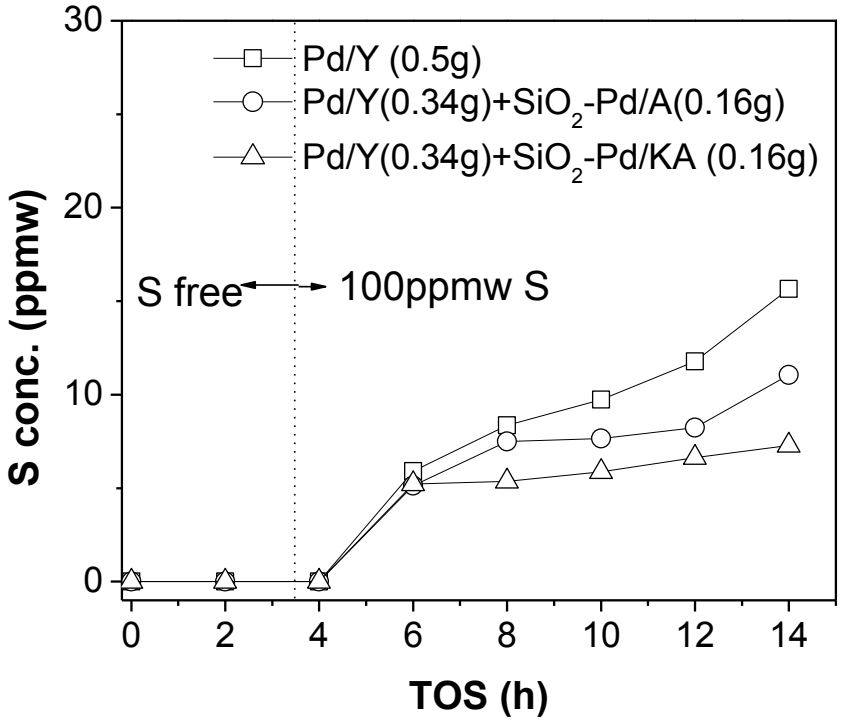


Figure **5-8**: Sulfur concentration of liquid product on tetralin hydrogenation in the absence and presence of 100 ppmw sulfur as BT

Figure 5-9 represents the selectivity of trans- and cis-decalin and their yields on tetralin hydrogenation over Pd/Y and the hybrid catalysts in the presence of 100 ppm sulfur. All catalysts showed consistently high yields of trans-decalin (>90%) and low yields of cis-decalin (<10%) with trans-decalin/cis-decalin ratio of around 10.3. Compared with the data from other studies in the low temperature ranges of 200-225 $^{o}$C [61, 64, 79], it is confirmed that the reaction over all catalysts reached quasi-equilibrium state in the absence of sulfur. Introduction of benzothiophene profoundly influenced the selectivity of decalin. After the feedstock was switched to sulfur-containing feed, the trans-decalin/cis-decalin ratio drastically decreased, demonstrating that not

only tetralin conversion but also selectivity of decalin is affected markedly with sulfur and the latter is more sulfur-sensitive than the former. This trend was clearly observed from the comparison of the trans- and cis-decalin yields over three catalysts. As seen from Figure 5-9 (b), the decrease of trans-decalin and simultaneous increase of cis-decalin yield were observed as sulfur-induced deactivation proceeded. It seems that both hybrid catalysts prefer cis-decalin production, compared to Pd/Y. Especially, $SiO_2$-Pd/KA+Pd/Y hybrid catalyst showed distinct differences among the catalysts, milder decrease of trans-decalin yield and highest cis-decalin yield than the other catalysts.

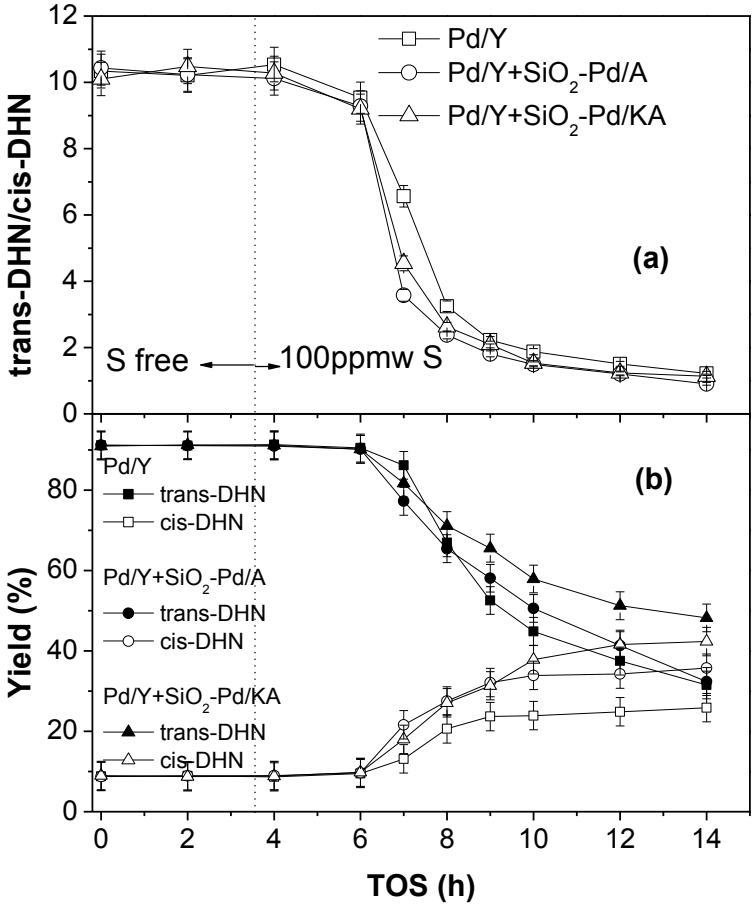


Figure **5-9**: Comparison of (a) trans-decalin/cis-decalin ratio and (b) product yields on tetralin hydrogenation over the same amount (0.5 g) of catalyst in the absence and presence of 100 ppmw sulfur as BT

The reaction model of tetralin hydrogenation was adopted to determine the reaction kinetics and explain the drastic change of decalin selectivity [20, 61-63]. The model shown in Figure 5-10 consists of both series and parallel reactions, where there is a single reaction pathway

for cis-decalin production, direct tetralin hydrogenation to cis-decalin. Another possible pathway, isomerization from trans- to cis-decalin, is negligible compared to the reverse isomerization [64, 80]. For trans-decalin production, there are two reaction pathways, direct tetralin hydrogenation and cis-decalin isomerization. Even it was suggested that trans-decalin may be formed through addition of hydrogen to olefinic intermediate (possibly 1,9-octalin), it was not considered in this study since olefinic intermediate was not observed in the products from our study [64, 65].

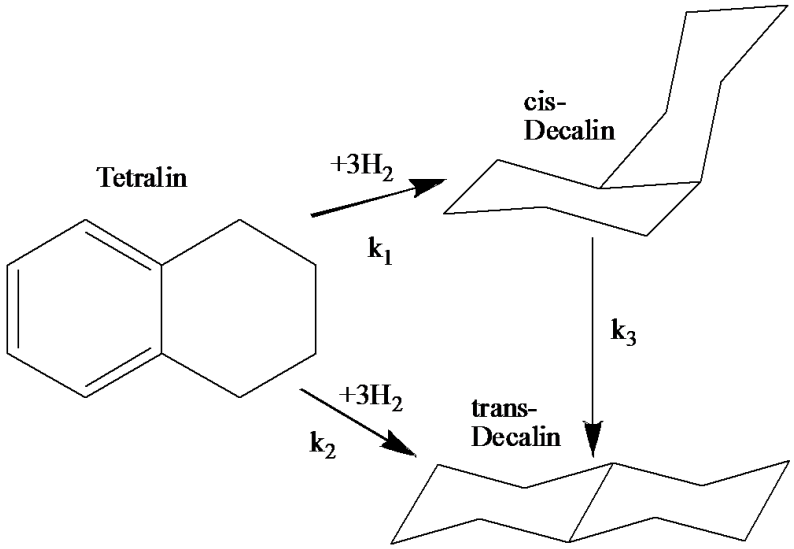


Figure **5-10**: Reaction pathway of Tetralin Hydrogenation

Based on the reaction model and simple power law equation, the rate constants, $k_1$, $k_2$ and $k_3$, were calculated and plotted in Figure 5-11. All three rate constants for $SiO_2$-Pd/KA+Pd/Y hybrid catalyst are the highest among the catalysts. Although $k_2$ and $k_3$ of Pd/Y were also

comparable to those of $SiO_2$-Pd/KA+Pd/Y at 7 h TOS, but rapid declines were observed in 1 h, while the hybrid catalyst exhibited slower decrease.

It was interesting to note that the rate constant for tetralin hydrogenation to cis-decalin, $k_1$, was least susceptible to sulfur poisoning compared with the others. The rate constant of tetralin hydrogenation to trans-decalin, $k_2$, displayed the highest value among three rate constants at 8 h TOS, but decreased rapidly as TOS increased. The most sensitive one to sulfur is $k_3$ for cis-decalin isomerization, converging to zero as sulfur introduced. Therefore, the increasing trend of cis-decalin yield with increase of TOS shown in Figure 5-9 is mainly attributed to the significant decrease of both activities to trans-decalin suppressed by sulfur-induced catalyst deactivation.

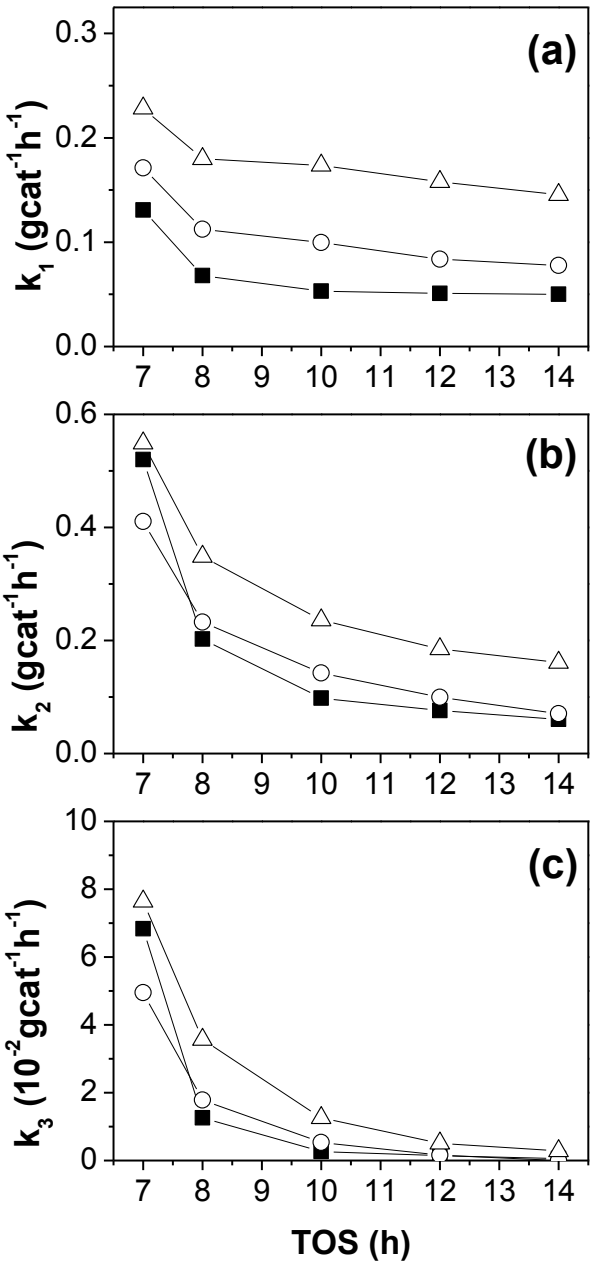


Figure **5-11**: Change of rate constants as a function of time on hydrogenation of tetralin in the presence of 100 ppmw sulfur as BT (a) tetralin hydrogenation to cis-decalin (b) tetralin hydrogenation to trans-decalin (c) cis-decalin isomerization to trans-decalin (−■− : Pd/Y, −○− : Pd/Y+$SiO_2$-Pd/A and −△− : Pd/Y+$SiO_2$-Pd/KA)

This tendency could be explained by "active site competition" between tetralin and cis-decalin, as proposed by Huang et al and Jongpatiwut et al. [19, 80]. They reported that adsorption of cis-decalin onto the metal active sites for isomerization is inhibited by tetralin present in the fuel. Since sulfur poisoning is the main reason of catalyst deactivation in this study, the amount of active sites for hydrogenation depends on the degree of sulfur poisoning. Therefore, decrease of the amount of active sites will lead to tetralin hydrogenation rather than cis-decalin isomerization due to the adsorption affinity of tetralin. However, it is still unclear whether this "active site competition" can affect $k_2$, which is also sulfur sensitive. Weitkamp suggested that $\Delta^{1,9}$-octalin is the only intermediates for tetralin hydrogenation to trans-decalin [65]. Tetralin is first hydrogenated to the olefinic intermediate, $\Delta^{1,9}$-octalin for trans-decalin formation. Next, $\Delta^{1,9}$-octalin changes the position by flipping over or desorption and consecutive re-adsorption on the active site, then hydrogenated to trans-decalin. If the decreasing trend of $k_2$ is mainly due to the decrease of total active sites by sulfur poisoning, the rate constant $k_1$ will increase or at least $\Delta^{1,9}$-octalin will be detected from the product. However, $k_1$ results also showed mild decrease and the olefinic intermediate such as octalin was not observed in our study. It is mostly likely that there are specific active sites for tetralin hydrogenation or cis-decalin isomerization to trans-decalin, which could be more susceptible to be deactivated by sulfur poisoning than the other active sites for cis-decalin production.

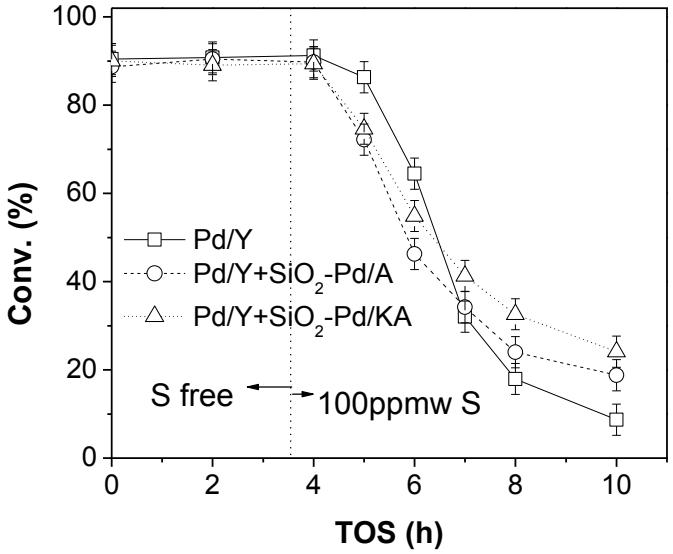


Figure **5-12**: Comparison of conversion on cis-decalin isomerization over the same amount (0.5 g) of catalyst in the absence and presence of 100 ppmw sulfur as BT

Sulfur tolerance of the hybrid catalysts was further investigated on cis-decalin isomerization. From Figure 5-12, cis-decalin isomerization over all the catalysts drastically decreased as sulfur feed was introduced, which was severer compared with tetralin hydrogenation results. In the case of both hybrid catalysts, conversions of cis-decalin were lower than Pd/Y before 7 h TOS, which is mainly ascribed to the less amount of active sites for hydrogenation, but overturned after 7 h TOS. The turnover frequencies for isomerization of cis-decalin as a function of S/Pd are compared in Figure 5-13, where S/Pd is defined as the molar amount of sulfur treated for the duration of reaction per surface Pd metal. At around 0.5 of S/Pd, the turnover frequencies (TOF) of all catalysts are approximately 2. As S/Pd increases, TOF of both hybrid catalysts gradually decreased whereas rapid decline was observed on Pd/Y. $SiO_2$-Pd/KA+Pd/Y hybrid

catalyst shows slightly higher turnover frequency than that over $SiO_2$-Pd/A+Y, which might be due to the higher hydrogen spillover activity of $SiO_2$-Pd/KA.

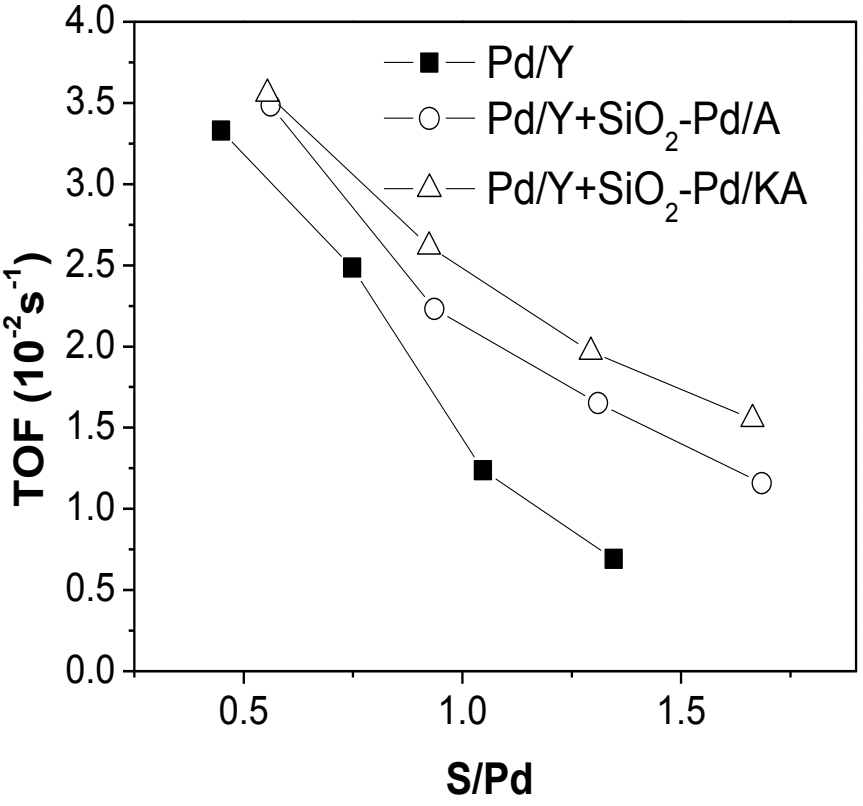


Figure **5-13**: **Comparison of TOF on cis-decalin isomerization in the presence of 100 ppmw sulfur as BT**

The effect of small-pore catalyst onto zeolite Y support was examined with different type of hybrid catalysts, $SiO_2$-Pd/A or $SiO_2$-Pd/KA mixed with zeolite Y without Pd metal loading. For exact comparison of catalytic activity, the same amount of silica coated catalysts (0.16 g) is used for the reaction over both hybrid catalysts and the pure silica coated catalysts without mixing zeolite Y. From Figure 5-14, no discernable tetralin conversion was observed over all the

catalysts, suggesting that tetralin is difficult to be hydrogenated over the Y zeolite support. Although several groups reported that naphthalene can be hydrogenated by spillover hydrogen [1, 2, 6, 75], but saturation of second ring, tetralin, is more difficult comparing to first ring of naphthalene and the reaction condition adopted in this study might be too mild to overcome this barrier. Interestingly, the result of outlet sulfur concentration of liquid product shows significant decrease of sulfur concentration over the hybrid catalysts. In the case of Y zeolite itself, there was no sulfur concentration change detected except 4 h TOS, right after sulfur introduction, which might be due to physical adsorption of benzothiophene on zeolite Y. On both silica coated Pd catalysts, a few ppm drop of sulfur concentration is detected. It is likely that the silica surface on the catalyst participates in hydrodesulfurization of benzothiophene. On both hybrid catalysts, mixture of the silica- coated Pd catalyst with Y zeolite, sulfur level of liquid product drastically decreased. Furthermore, $SiO_2$-Pd/KA+Y mixture shows less sulfur concentration than $SiO_2$-Pd/A+Y. It demonstrates that zeolite Y possibly acts as active sites for hydrodesulfurization of benzothiophene with the aid of hydrogen spillover and the active sites for the hydrodesulfurization could be both metal and support of the catalyst, unlike that those for tetralin hydrogenation is only metal sites. Similar results were reported from Sugioka et al. that Pt/$SiO_2$ mixed with various zeolite supports showed higher catalytic activity for hydrodesulfurization of thiophene than those of pure components (Pt/$SiO_2$ or zeolite supports) [91-93].

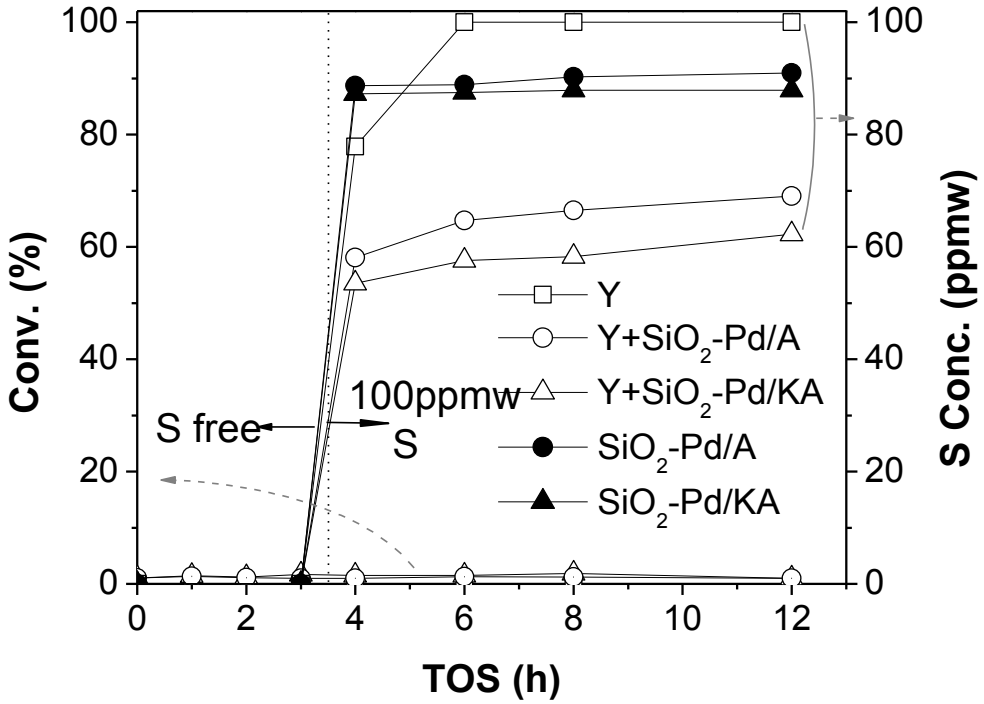


Figure **5-14**: Tetralin Conversion and Sulfur concentration of outlet liquid product on tetralin hydrogenation in the absence and presence of 100 ppmw sulfur as BT

In order to evaluate the sulfur resistance to high sulfur concentration and recovery of catalytic activity on the deactivated catalyst, the model fuel containing 400 ppmw sulfur with tetralin was firstly introduced to the reactor system and switched to sulfur free fuel after 5 h TOS. From Figure 5-15, no significant sulfur tolerance was observed on the hybrid catalysts during injection of high sulfur concentration feed. At 5 h TOS, all the catalysts tested showed 0% tetralin conversion except 0.5 g of Pd/Y with 7.5% and both hybrid catalysts totally lost their catalytic activity of tetralin conversion by continuous high sulfur flow. It implies that 400 ppmw sulfur concentration exceeds the capacity limit of sulfur resistance on the hybrid catalyst.

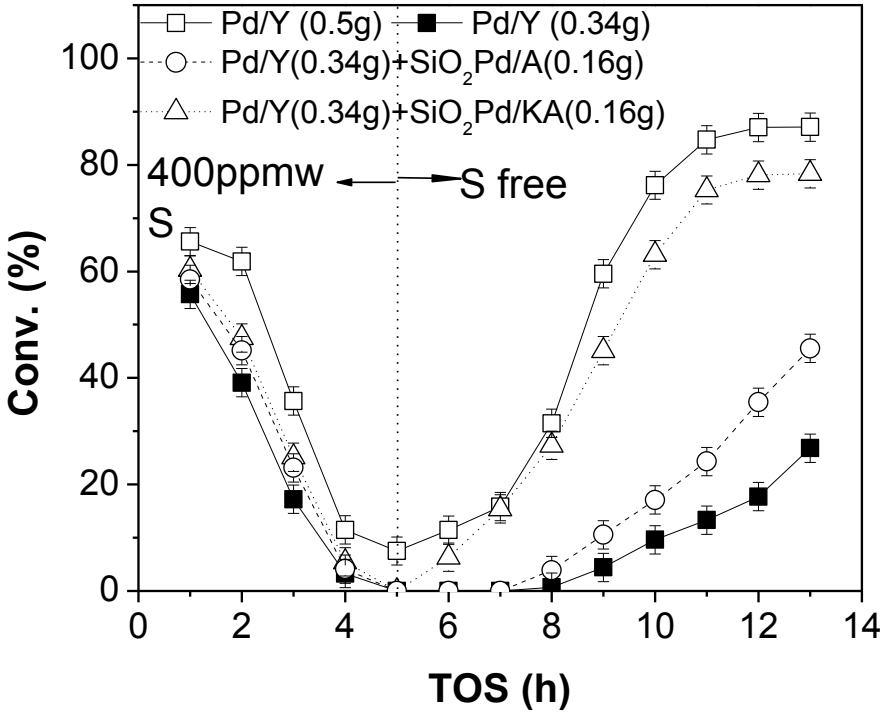


Figure **5-15**: **Comparison of conversion on tetralin hydrogenation in the presence and absence of 400ppmw sulfur as BT**

A noticeable result on recovery of catalytic activity was observed after 5 h TOS when the sulfur-containing model fuel was switched to sulfur free one. Even the same Pd/Y catalysts tested with different loading amount (0.5 g-the same amount as total catalyst loaded or 0.34 g- same amount as Pd/Y catalyst loaded in the hybrid catalyst), the different recovery rates of the catalysts are observed, the dramatic increase of tetralin conversion over 0.50 g of Pd/Y compared with 0.34 g of Pd/Y catalyst. It can be deduced that the available metal active sites which is not poisoned in 0.5 g of Pd/Y help the adjacent deactivated metal sites recover, while 0.34 g of Pd/Y, where the

majority of metal sites poisoned by sulfur takes more time to recover the catalytic activity on tetralin hydrogenation. Interestingly, $SiO_2$-Pd/KA+Pd/Y hybrid catalyst showed superior recovery rate, indicating that $SiO_2$-Pd/KA considerably contributes to recovery of the sulfur-poisoned Pd/Y. It may be due to the high catalytic activity of hydrogen spillover on Pd/KA as well as the smaller pore opening of Pd/KA modified by K ion exchange. Previously mentioned, the pore opening of zeolite KA (theoretically 3Å) did not permit the entrance of $N_2$ (3.64 Å), which size was comparable to $H_2S$ (3.6 Å). Yang et al. already showed from the hydrogen chemisorption tests that the metal particles in silica coated zeolite KA are well-protected from exposure of $H_2S$ [6]. Therefore, the possible products from benzothiophene decomposition including $H_2S$, organosulfur and hydrocarbon species, might be prevented from entering the pore of zeolite KA, thus the metal particles inside the small pore could keep intact and maintain its role, hydrogen spillover.

## 5.4. Conclusion

The experimental results performed in this study demonstrate that the hybrid zeolite-supported Pd catalyst showed a significant improvement on sulfur tolerance. Both hybrid catalysts, $SiO_2$-Pd/KA+Pd/Y and $SiO_2$-Pd/A+Pd/Y show higher catalytic activities than the homogeneous Pd/Y catalyst for tetralin hydrogenation as well as cis-decalin isomerization in the presence of benzothiophene. In particular, the former displayed more enhanced sulfur tolerance than the latter, which might be primarily due to higher catalytic activity for hydrogen spillover on $SiO_2$-Pd/KA. Although both small-pore catalysts ($SiO_2$-Pd/A or $SiO_2$-Pd/KA) alone participate in tetralin hydrogenation, it was found that they aided benzothiophene decomposition on zeolite Y support. $SiO_2$-Pd/KA+Pd/Y hybrid catalyst also shows good recoverability when it was poisoned by sulfur, which may be mainly ascribed to the small-pore system. Therefore, the hybrid catalyst based on our design concept is applicable for aromatics hydrogenation in the presence of benzothiophene, due to the selective exclusion of sulfur and hydrogen spillover.

# Chapter 6

# Effect of metal

## 6.1. Introduction

In this chapter, the effects of metals for sulfur tolerant metal catalyst are studied. The metals in group 10, two noble metals, Pd and Pt, and a base metal, Ni, are selected as potential elements for hydrogenation and evaluated for tetralin hydrogenation in the presence of benzothiophene. Pd-Pt bimetallic catalyst with 4 of Pd to 1 of Pt molar ratio [15] [94] are also compared with the monometallic catalysts in order to investigate the effect of bimetal on improving sulfur tolerance. Lastly, Pd-Pt bimetallic catalyst is applied to the large pore system in the hybrid catalyst and tested on tetralin hydrogenation as an extension study of the catalyst design concept proposed.

## 6.2. Experimental

### 6.2.1. Catalyst Preparation

Zeolite Y (Zeolyst International, CBV720) was adopted as zeolite supports in this study. The zeolite Y support was calcined in air flow (60 mL/min) at 450 $^{o}$C for 4 h with a heating rate of 1.5 $^{o}$C /min before catalyst preparation. All metal catalysts (Ni/Y, Pd/Y, Pt/Y and Pd-Pt/Y) were prepared by the incipient wetness impregnation (IWI) of aqueous solution of metal precursors to a nominal metal concentration of 2 wt%. Both metal precursor solution, nickel (II) chloride ($NiCl_2$, Aldrich, 99.9999%) and chloroplatinic acid ($H_2PtCl_6$, Aldrich, 99.995%) were dissolved in deionized water. Palladium chloride ($PdCl_2$, Aldrich, 99.999%) was dissolved in dilute hydrochloric acid. The zeolite Y supported Pd-Pt bimetallic catalysts (Pd-Pt/Y) was prepared by co-impregnation of both metal precursors, $PdCl_2$ and $H_2PtCl_6$. The ratio of Pd to Pt adopted for Pd-Pt bimetallic catalyst was 4:1 as molar ratio. After impregnation was complete, the catalysts were dried at 100 $^{o}$C overnight and calcined in air flow (~60 ml/min) at 450 $^{o}$C for 4 h at a heating rate of 1.5 $^{o}$C /min.

The silica-coated Pd catalyst supported on zeolite KA ($SiO_2$-Pd/KA) is also used as the small-pore catalyst for the hybrid catalyst. The preparations of the $SiO_2$-Pd/KA catalyst and its hybrid catalyst followed the same method, as described in the previous chapters.

### 6.2.2. Catalyst characterization and evaluation

The surface area, metal dispersion, X-ray diffraction (XRD), temperature programmed reduction (TPR) and temperature programmed desorption of ammonia ($NH_3$-TPD) were

conducted using the same equipment at the same condition as described in the previous chapters. In preparation of reduced samples, Ni/Y (others at 225 $^{o}$C) was reduced in-situ at 400 $^{o}$C for 60 min based on TPR result.

Diffuse reflectance infrared spectra of CO adsorbed catalyst sample were measured by using Nicolet Nexus 470 Infrared (IR) spectrometer. The sample was loaded into DRIFT cell and reduced in situ with UHP (ultra high purity) hydrogen at 225$^{o}$C for 30 min. After reduction, IR spectrum of the reduced samples was collected for baseline. For CO adsorption, the 10% CO/He gas mixed with hydrogen at the volumetric flow ratio of 1:12 passed through the sample for 5 minutes, and then IR spectra were obtained.

Continuous fixed-bed flow reactor testing also followed same procedure as mentioned in previous chapters. The model fuel feedstock was prepared by mixing 20 wt% of tetralin (1, 2, 3, 4-tetrahydronaphthalene, Aldrich, 99%) with 75% hexadecane (Aldrich, 99+%, anhydrous) as solvent and 5% tetradecane (Aldrich, 99+%) as internal standard. For sulfur feed stock, benzothiophene (BT, Aldrich, 99%) was added to these model fuels.

## 6.3. Result and discussion

### 6.3.1. Zeolite Y supported Pd, Pt , Ni monometallic and Pd-Pt bimetallic Catalysts

Table 6-1 presents the surface area and metal dispersion of the monometallic Ni/Y, Pd/Y, Pt/Y and bimetallic Pd-Pt/Y catalysts. The dispersion of the Pt/Y is the highest among the monometallic catalysts tested. The metal dispersion of Ni/Y shows the lowest dispersion among the catalysts. Since Ni/Y catalyst needs high temperature to be reduced, it might be sintered and agglomerated during calcination (450$^{o}$C) step in preparation of catalyst or the pre-reduction step (400$^{o}$C) before performing chemisorption. It is apparent that the Pd-Pt bimetallic catalyst exhibits higher metal dispersion compared to other monometallic catalysts. Although the major metal component of Pd-Pt catalyst is Pd (Pd:Pt =4:1), its metal dispersion is obviously higher than Pd catalyst. It is likely that addition of Pt metal increases metal dispersion in the Pd-Pt bimetallic system, dispersing the active Pd atoms without agglomeration.

Table **6-1**: Surface area and metal dispersion of supported metal catalysts

| Catalyst | BET Surf. Area ($m^2/g$) | Metal Dispersion (%) |
|---|---|---|
| Ni/Y | 428 | 5 |
| Pd/Y | 590 | 42 |
| Pt/Y | 604 | 49 |
| Pd-Pt/Y | 631 | 53 |

The TPR profiles for the catalysts are shown in Figure 6-1. Compared with other noble metal catalyst, Ni/Y displays the reduction peak at high temperature, around 370$^o$C. It suggests that Ni/Y catalyst should be pre-reduced at higher temperature than reaction temperature (225$^o$C) in order to observe the performance of the nickel "metallic" catalyst. The other noble metal, Pd and Pt catalysts showed the reduction peak at low temperature region below 150$^o$C. The profile of Pd/Y displays the sharp peak with a maximum at around 70$^o$C, but for the Pt/Y catalyst, a broad peak was appeared in the range between 0 and 150$^o$C.

In the case of Pd-Pt/Y in our study, there is only one sharp peak exhibited, rather than displaying two distinguished peaks. Generally, if two metals were loaded together but there was no interaction between them, two separate peaks would be displayed. However, only one single sharp peak of Pd-Pt/Y was also placed at between 50-100$^o$C, almost same temperature range where both monometallic Pd and Pt metal catalysts reduces. However, it is notable that the maximum point of the peak was shown at around 88$^o$C, shifted toward around 15$^o$C higher temperature than that of Pd/Y. There are two possible explanations in peak shift of Pd-Pt

bimetallic catalyst. One could be the effect of metal particle size. From the dispersion result in Table 6-1, Pd-Pt/Y has the highest metal dispersion, suggesting that Pt-Pd metal clusters are the smallest among the catalysts. Since the small metal particles supported on acidic zeolite Y are more electron deficient [95], the Pd-Pt/Y catalyst might be more difficult to be reduced than the Pd/Y. The other possible explanation is the change of electron state of Pd metal by strong metal interaction between Pd and Pt, which also can make the surface metal more electron-deficient [24].

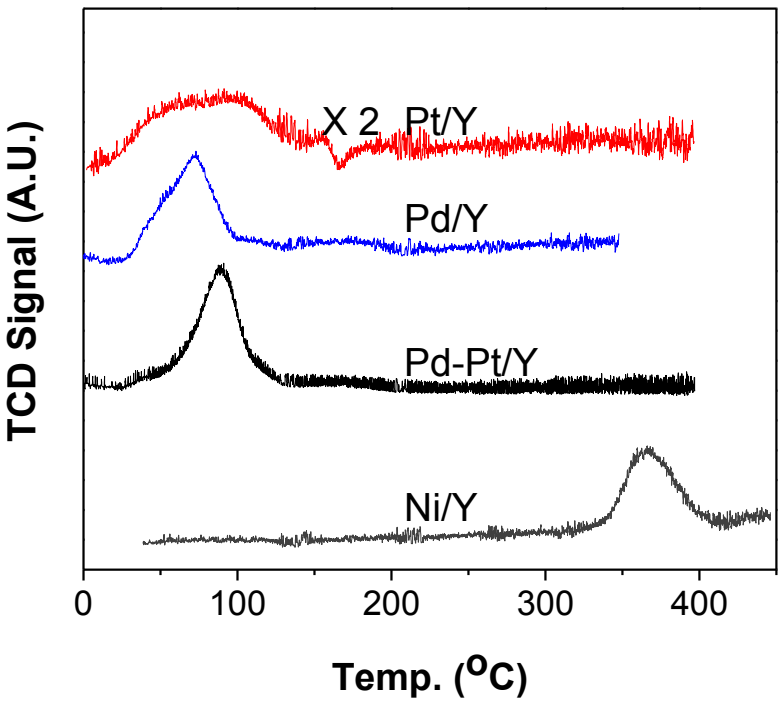


Figure **6-1**: TPR profiles of monometallic and bimetallic catalysts supported on zeolite Y

As shown in Figure 3-2 in chapter 3, XRD patterns of Pd/Y and zeolite Y were compared and found that both patterns are identical and no indicative metal peak was observed in the XRD pattern of noble Pd/Y catalyst. It implies that zeolite framework was intact without any deformation by diluted hydrochloric acid during catalyst preparation. Likewise, as displayed in Figure 6-2, even a trace of metal peak was not detected from the XRD pattern of metal catalyst supported on zeolite Y except Ni/Y. It implies that noble metal is well dispersed and possibly incorporated inside the pore without serious aggregation outside the zeolite framework. However, in the case of Ni/Y, the small peak of nickel as nickel oxide was detected, suggesting that the size of Ni cluster is big enough to be detected by X-ray diffraction. Since the possible lower limit of particle size that can be detected by XRD (lower detection limit : 2 nm) is bigger than the size of supercage of zeolite, the nickel clusters detected might be placed outside of the zeolite framework. It seems that nickel clusters were not properly anchored and stabilized on the acid sites, but were aggregated outside of the zeolite framework, possibly during calcination or reduction step.

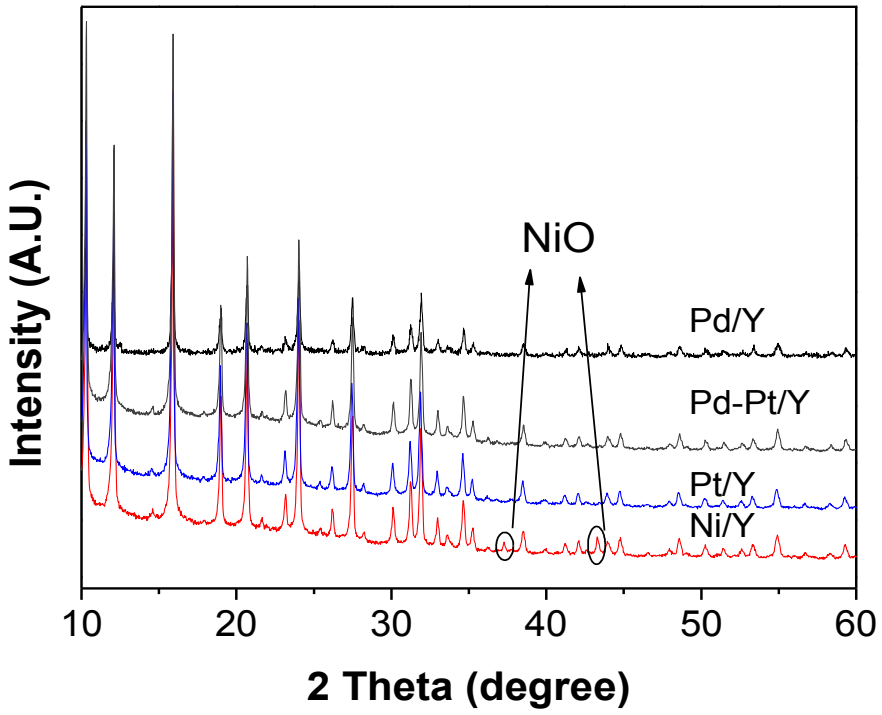


Figure **6-2**: XRD patterns of zeolite Y supported Pt, Pd, Ni and Pd-Pt catalysts

Figure 6-3 shows the comparison of the tetralin conversion over mono or bimetallic catalysts on zeolite Y supports in the presence of 100 ppmw of sulfur as BT. It should be noted that pre-reduction of Ni/Y was performed at 400$^{o}$C and cooled down to 225$^{o}$C for tetralin hydrogenation on the basis of TPR result.

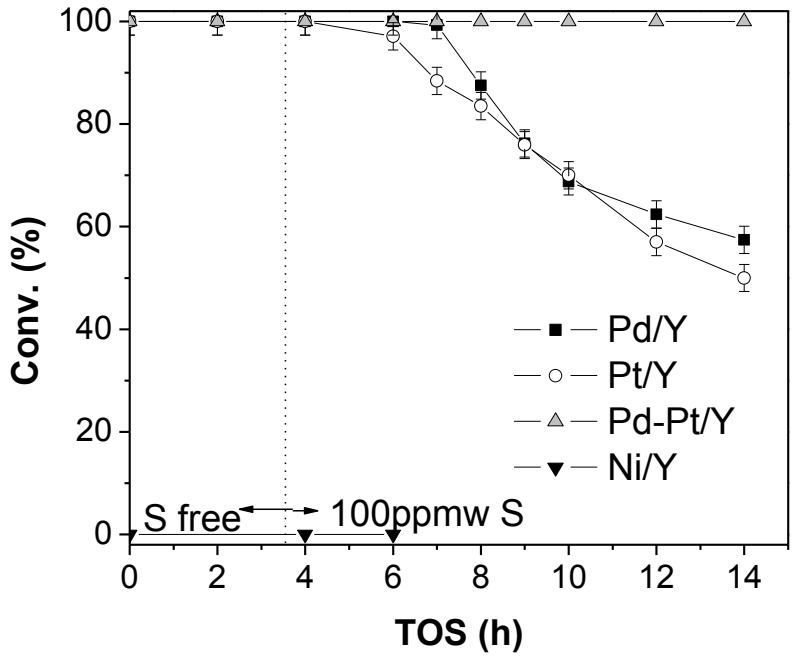


Figure **6-3**: Tetralin conversion over monometallic and bimetallic catalyst in the presence of 100ppmw sulfur as BT.

It reveals that Ni/Y catalyst did not have any catalytic activity on tetralin hydrogenation even in the absence of sulfur compound in the reaction condition adopted in this study. The high temperature pre-reduction at 400$^{o}$C, necessary for metal cluster to become active, might cause to

agglomeration of nickel particle. Since the nickel catalyst prepared in this study contains low metal contents (2 wt%), it might be difficult to avoid metal agglomeration and thus might not show any catalytic activity. It was previously reported that the active industrial nickel catalyst contains high metal contents over 20% and it needs modifier to decrease the metal content (<10%) of the nickel catalyst with better dispersion [96]. However, it is not the only problem of metal agglomeration. There is no report that the nickel metal catalyst is highly active at low temperature under 300$^{o}$C for naphthalene or tetralin hydrogenation. Rautanen et al. used the nickel metal catalyst at low temperature (160$^{o}$C) for naphthalene hydrogenation. However, naphthalene conversion was less than 1%, even though they used a commercial nickel catalyst supported on alumina with high metal content (16%) without adding sulfur compound.

On the other hand, two noble metal catalysts showed 100% of tetralin conversion at the introduction of sulfur-free feed. But, both catalysts showed gradual decrease as sulfur feed was introduced and TOS increased. Previously, in chapter 3, the sulfur tolerance of the metal catalyst was explained in accordance with metal dispersion. Thus, high metal dispersion and the small metal size is definitely one of the important factors in achieving high hydrogenation in the presence of sulfur, if the single Pt or Pd monometallic catalysts with different metal loading or supported on different supports are compared. However, this result shows that dispersion alone cannot be responsible for increased sulfur tolerance in comparison among the different metal catalysts, as the monometallic Pd catalyst outperformed the Pt catalyst, despite having lower dispersion than Pt/Y.

The ratio of sulfur to surface metal atom (S/Pd or S/Pt) at the decreasing point of tetralin conversion is calculated with the accumulated sulfur amount in feedstock divided by surface-exposed metal atom obtained from metal dispersion. For Pd/Y catalyst, S/Pd ratio is 1.02, which value is higher than 0.72 of S/Pt on Pt/Y catalyst. These calculated value is also consistent with the order of sulfidation affinity of bulk metal phase, Ni-S>>Pt-S>Pd-S [97]. Thus, it is apparent

that Pt metal is less sulfur-tolerant than Pd, which also substantiate the experimental results from others [25, 93] that Pt catalyst is active in aromatic hydrogenation, but is more susceptible to be poisoned by sulfur compounds. It is interesting to note that Pd-Pt /Y catalyst maintained 100% tetralin conversion for the duration of the experiment, albeit both Pd/Y and Pt/Y catalysts began to be deactivated due to sulfur poisoning. It indicates that the bimetallic combination provides an enhancement in sulfur resistance, as compared with the monometallic catalysts.

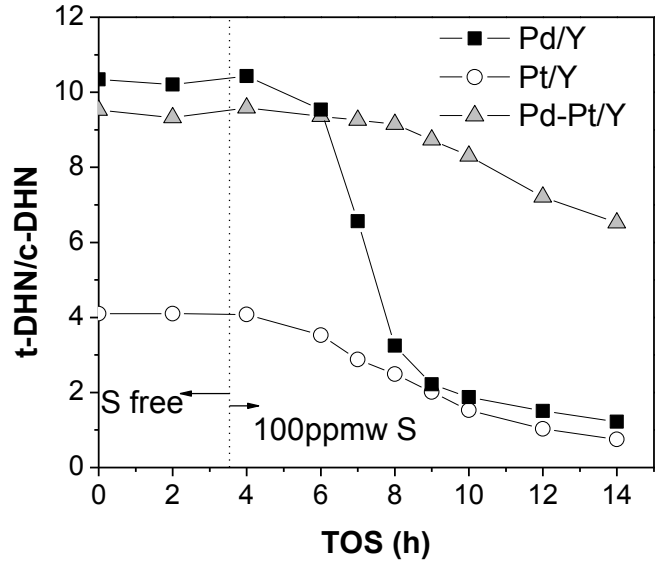


(a)

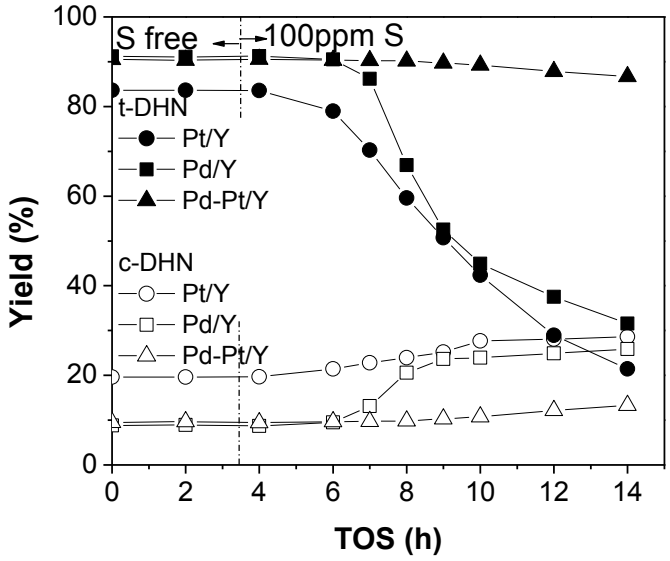


(b)

Figure **6**-**4**: (a) trans-decalin/cis-decalin ratio of decalin product and (b) Product yields of tetralin hydrogenation over Pd, Pt, Pd-Pt/Y catalysts in the presence of 100 ppmw sulfur as BT

The selectivity of trans- and cis-decalin was compared and expressed as the trans-decalin/cis-decalin ratio of decalin product from tetralin hydrogenation over Pt, Pd and Pd-Pt/Y catalysts in the presence of 100 ppmw sulfur. In Figure 6-4, all three catalysts showed the consistent yield of decalin, mainly selective towards trans-decalin in the absence of sulfur compounds in fuel feed. The trans-/cis-decalin ratio from Figure 6-4 (a) shows huge differences between Pd and Pt catalyst and Pd catalyst is more selective toward trans-decalin, meanwhile Pt catalyst is more selective toward cis-decalin. This result is also in good agreement with others, which seems that Pd is intrinsically more selective toward trans-decalin [61, 98, 99]. For exact comparison, trans- and cis-decalin yields from the tetralin conversion were also plotted in Figure 6-4 (b). When the yields are compared between Pd and Pt catalysts, the differences of both cis- and trans-decalin yields are around 10% in the absence of sulfur in the fuel feed.

Sulfur introduction changed the selectivity of decalin, toward cis-decalin on all Pd, Pt and Pd-Pt catalysts, same trend as the results in previous chapters. After switching to 100 ppmw sulfur feed and time-on-stream increased, the trans-decalin/cis-decalin ratio drastically decreased. It demonstrates that all the catalysts tested are selective toward trans- decalin in the absence of sulfur, and the selectivity of decalin is affected markedly with sulfur poisoning of these metal catalysts. In the case of Pd and Pt monometallic catalysts from Figure 6-4 (b), the drastic decrease of trans-decalin and simultaneous mild increase of cis-decalin were observed, as the reaction proceeds after sulfur introduction. As discussed in previous chapter, it can be deduced that the isomerization of cis-decalin to trans-decalin is suppressed by sulfur induced deactivation. Same trend was also observed from Jongpatiwut, where trans/cis decalin ratio over the Pd, Pt and Pd-Pt catalysts decreases as the tetralin conversion decreases even in the absence of sulfur [98]. Similar to the result of tetralin conversion, trans-/cis-decalin ratio and their yields also show that the Pd-Pt bimetallic catalyst is less sulfur-sensitive than the monometallic catalyst on the selectivity of

decalin. The trans-decalin/cis-decalin ratio maintaining around 10 gradually decreased, whereas that of the Pd or Pt monometallic catalyst showed the drastic decrease after sulfur introduction.

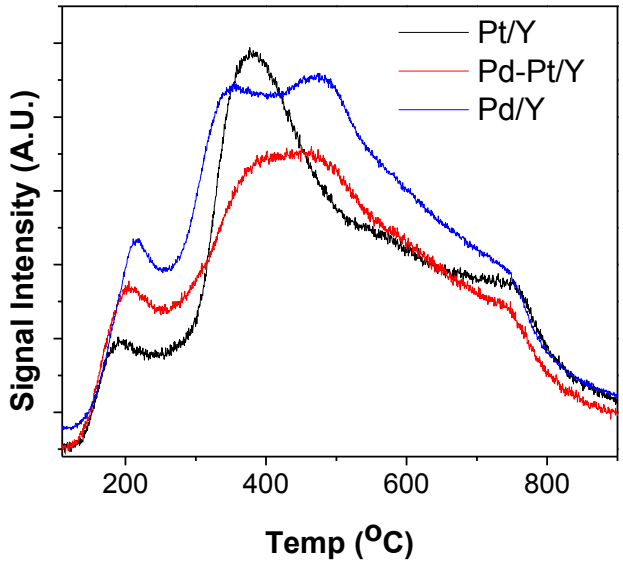


Figure **6-5**: Ammonia TPD profiles of the Pd, Pt monometallic and Pd-Pt bimetallic catalysts.

Figure 6-5 represents the ammonia TPD profiles of the supported Pd, Pt and Pd-Pt bimetallic catalysts. Overall, Pd-Pt/Y catalyst shows less amount of ammonia desorbed compared to other monometallic catalysts, which means the quantitative amount of adsorbed ammonia on the former is less than that on the latters, thus, less amount was detected during ammonia TPD. It may be ascribed to electron-deficiency of Pd-Pt metal.

In the temperature range between 100-300$^{o}$C, the first peaks appears on each catalyst tested and the amount of ammonia desorbed in this range decreases in the order Pd/Y > Pd-Pt/Y >Pt/Y. It implies that Pt/Y has less amount of weakly interacted ammonia on the catalyst surface

than other Pd containing catalyst. It is likely that ammonia adsorbed on Pd/Y and Pd-Pt/Y is slightly easier to be desorbed than that on Pt/Y catalyst.

In the range between 300-500$^{o}$C, the amount of ammonia decreases in the order Pt/Y > Pd/Y >Pd-Pt/Y. Pt/Y exhibit distinctively huge single peak while Pd/Y catalyst has two peaks overlapped. Pd-Pt/Y catalyst also shows a huge single peak with maximum around 430$^{o}$C. However, this peak is mostly like that two peaks are closely placed and overlapped each other, where the maximum of the first peak is placed at around 380$^{o}$C, almost same as that of Pt/Y, but slightly higher than that of Pd/Y, 360$^{o}$C. It is interesting to note that the peak for Pt/Y over 400$^{o}$C drastically decreased, while the other consecutive desorption peaks on both Pd-Pt/Y and Pd/Y appeared at around 480 $^{o}$C. It might be confused to conclude that more amount of ammonia is strongly adsorbed on Pd-Pt/Y and Pd/Y, but it should be noticed that Pt is very active for ammonia decomposition above 500$^{o}$C and it is reported that the reaction rate of ammonia decomposition on Pt is 10 times higher than that of Pd at around 500$^{o}$C [100]. Therefore, the peaks appeared above 500$^{o}$C are not reliable in determination of the ammonia desorption. Overall, it can be suggested that the Pd-Pt bimetallic catalyst has both characteristic of Pt and Pd catalyst, but the interaction between ammonia and catalyst is lower than each Pd and Pt monometallic catalyst mainly due to its more electron deficient character of Pd-Pt.

Adsorption of CO was employed to probe the nature of the metal surface and its electronic properties on noble metal catalysts. In Figure 6-6~9, the DRIFT spectra of the reduced catalyst before CO adsorption and after CO adsorption were shown as black and red lines, respectively. Figure 6-6 shows the DRIFT spectra of zeolite Y support and that of CO adsorbed one. There is no significant CO adsorption peak detected, but negligible peak placed at the range between 2300-2400 cm$^{-1}$ assigning to $CO_2$ was detected, which might be due to CO adsorption on the surface oxygen species of zeolite Y. However, IR spectra of each metal catalyst supported on zeolite Y shows different trend. At the spectra of Pt catalyst in Figure 6-7, two intense peaks are

shown in the range between 2340 and 2370 $cm^{-1}$ assigned to $CO_2$ adsorption (split OCO asymmetric stretching) and between 1900 and 2100 $cm^{-1}$ appointed to CO adsorption. The detection of $CO_2$ adsorption peak could be due to Boudouard reaction, caused by CO dissociation on Pt metal and consecutive CO oxidation with oxygen dissociated from CO. In Figure 6-8, IR spectrum for Pd/Y also exhibits the $CO_2$ peak at the same range, but it is not as intense as that of Pt/Y. Even the CO peak in the same range as Pt catalyst appeared, but the peak is not as sharp as Pt/Catalyst and intensity is much less than that. Additionally, different types of CO adsorption peak were observed in the range between 1750 and 2000 $cm^{-1}$. In the case of Pd-Pt catalyst from Figure 6-9, the intensity and position of $CO_2$ and CO peaks are analogous to that of Pd catalyst, rather than that of Pt catalyst.

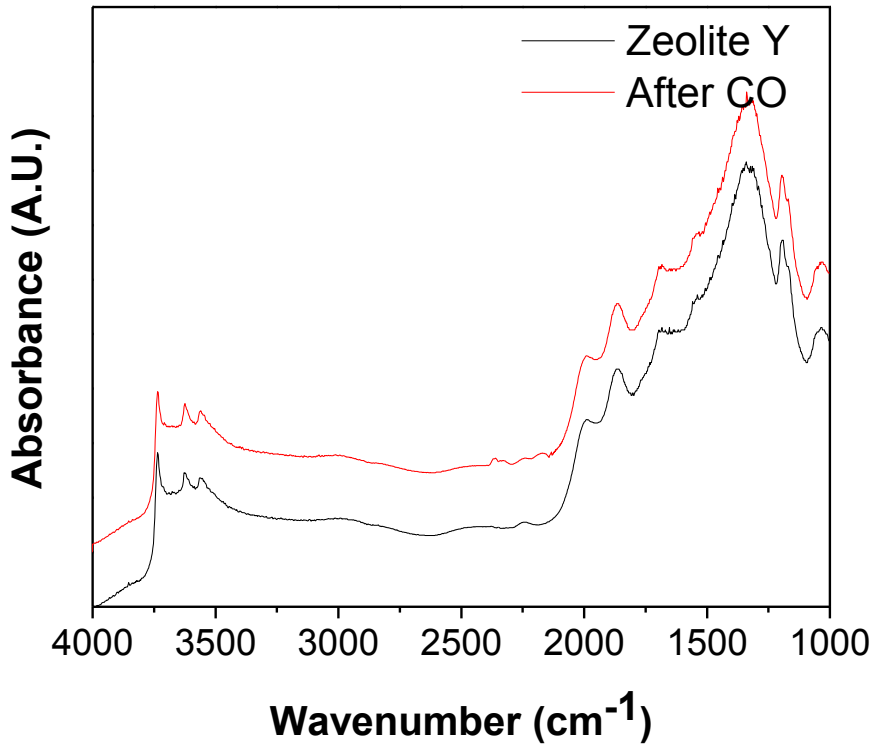


Figure **6-6**: DRIFT spectra of the zeolite Y before (black line) and after CO adsorption (red line)

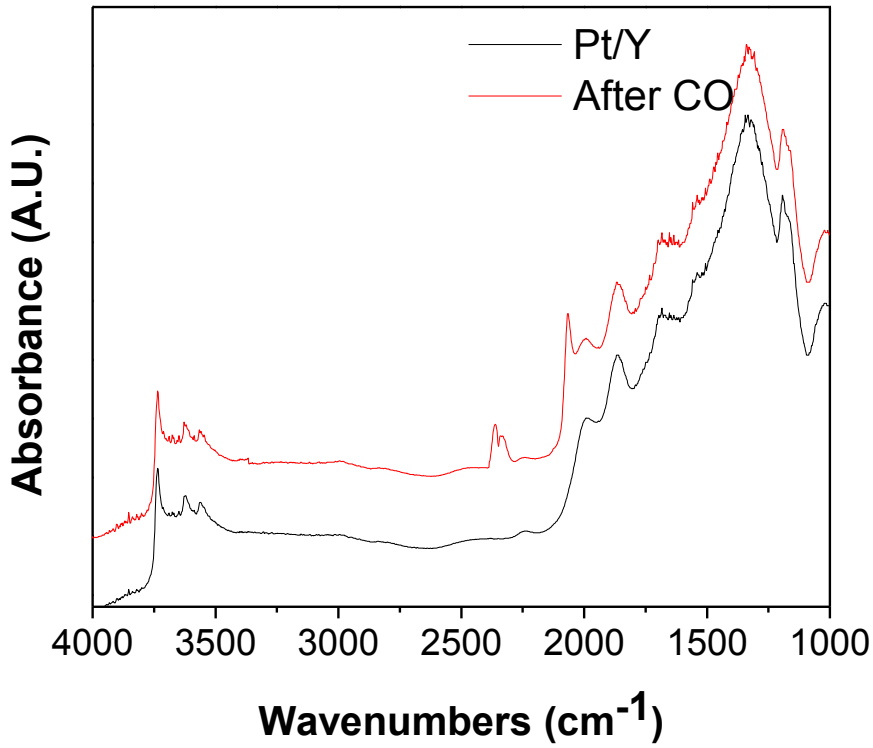


Figure **6-7**: DRIFT spectra of the Pt/Y before (black line) and after CO adsorption (red line)

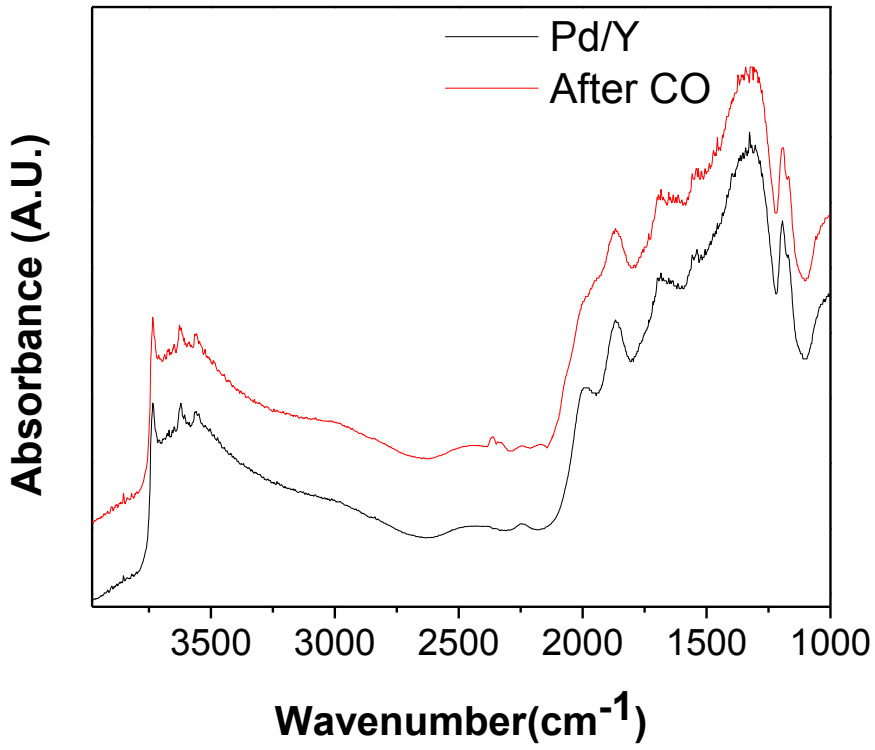


Figure **6-8**: DRIFT spectra of the Pd/Y before (black line) and after CO adsorption (red line)

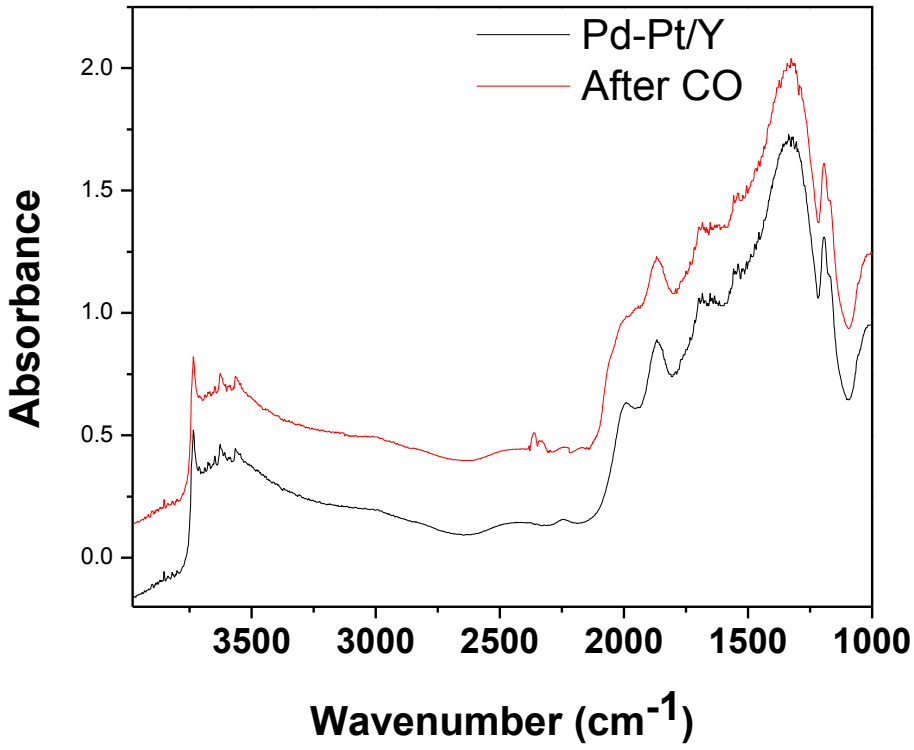


Figure **6-9**: DRIFT spectra of the Pd-Pt/Y before (black line) and after CO adsorption (red line)

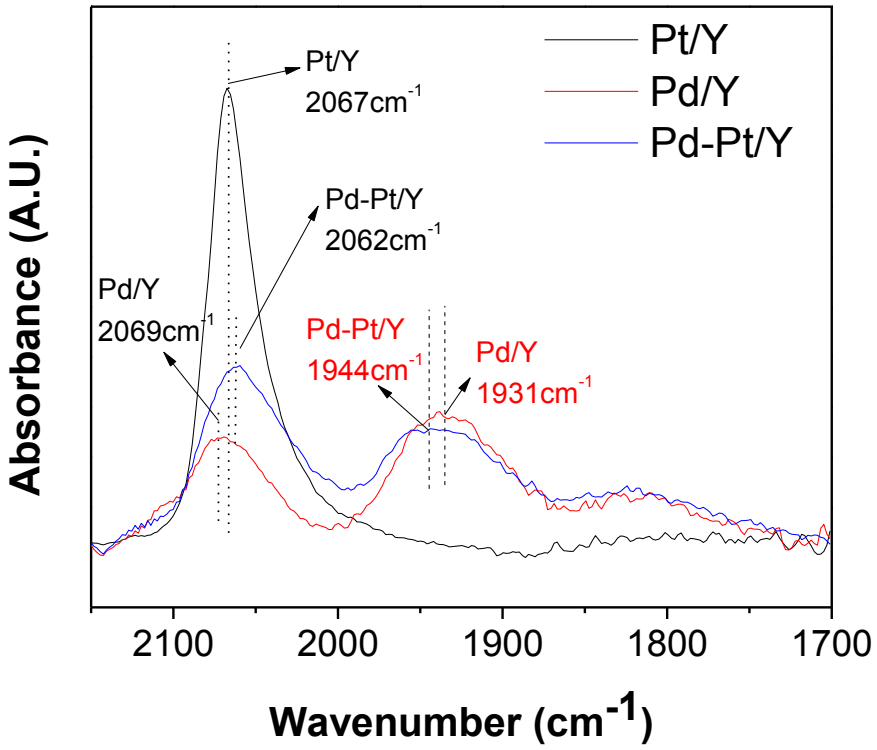


Figure **6-10**: Modified DRIFT spectra of CO adsorption on Pt, Pd and Pd-Pt/Y

For further analysis of these catalysts, the background-corrected IR spectra of CO adsorption on each catalyst (Pt, Pd and Pd-Pt catalysts) were compared in Figure 6-10. The spectrum on Pt catalyst consists of only one strong absorption band at 2067 $cm^{-1}$, which is the characteristic of linear CO adsorption on well-dispersed Pt catalyst. On both Pd and Pd-Pt catalysts, there are two separate CO bands observed; higher band around 2000~2100 $cm^{-1}$ and lower band around 1900~2000 $cm^{-1}$ assigned to linear and bridging CO adsorbed on the metal sites, respectively. It was found that the peak positions adsorbed on Pd-Pt bimetallic catalyst is different from those on single Pd or Pt catalyst. The IR spectrum of CO adsorbed on Pd-Pt catalyst is not just superposition of those on monometallic Pt and Pd catalyst even it is similar to

that on Pd catalyst. The peak assigned to the linear CO bands on Pd-Pt/Y is located at 2062 $cm^{-1}$, while the same peaks for Pd/Y and Pt/Y are placed at the higher wavenumbers, 2069 and 2067 $cm^{-1}$, respectively. It is likely that the frequency shift of linear CO bond is attributed to the increase of electron density due to the charge transfer between Pd and Pt. The slightly lower frequency shift of CO adsorption bands indicates some electronic modification of Pt due to the formation of Pd-Pt alloy [101] where electron density of Pd transfers to Pt having higher electron affinity [102].

Meanwhile, the bridging CO bands located at 1944 $cm^{-1}$ on Pd-Pt catalyst is slightly shifted to higher wavelength and broader than that on Pd catalyst (1931 $cm^{-1}$), which is another evidence of change of electron density of Pd metal and charge transfer between Pd and Pt. The same result was reported by Barbier et al that in Pd-Pt alloy catalyst, Pt atoms located in the proximity of the Pd modifies the intrinsic properties of the surface Pd [5]. Since the acidic zeolite support used for catalyst is the same, the change of the electronic properties of Pd confirms the metal-metal interaction between Pd and Pt. It is interesting to note that the absorbance of bridging CO on Pd-Pt bimetallic catalyst is almost the same as that on Pd monometallic catalyst. Taken into account that CO adsorbs onto the Pd surface as bridging configuration, it can be deduced that both Pd monometallic and Pd-Pt bimetallic catalysts have almost the same concentrations of Pd species related to bridging CO on the metal surfaces.

### 6.3.2. Application of Pd-Pt bimetallic Catalyst to hybrid catalyst system

Pd-Pt bimetallic catalyst was applied to hybrid catalyst system since the sulfur tolerance of Pd-Pt bimetallic catalyst is superior to that of other monometallic catalyst. The Pd-Pt/Y+$SiO_2$-Pd/KA hybrid catalyst system was prepared by mixing Pd-Pt/Y as large-pore microporous system with $SiO_2$-Pd/KA as small-pore microporous system and tested on tetralin hydrogenation in presence of benzothiophene. In order to investigate the catalyst deactivation of new hybrid catalyst by sulfur poisoning, sulfur concentration of the model fuel was set to 300 ppmw, since the single Pd-Pt/Y catalyst showed 100% conversion on tetralin hydrogenation in the presence of 100 ppmw sulfur in the previous test.

Tetralin conversion over homogeneous Pd-Pt/Y and two hybrid catalysts with different mixing ratio were compared in Figure 6-11. Although there was no significant improved sulfur tolerance observed on the hybrid catalysts with the same loading amount (total 0.5 g) as Pd-Pt/Y catalyst during the time period of reaction, it was found that addition of $SiO_2$-Pd/KA (0.25 g) to Pd-Pt/Y showed higher tetralin conversion than Pd-PT/Y catalyst after 10 h TOS, confirming that addition of small pore catalyst is more sulfur-tolerant than Pd-Pt/Y catalyst.

.

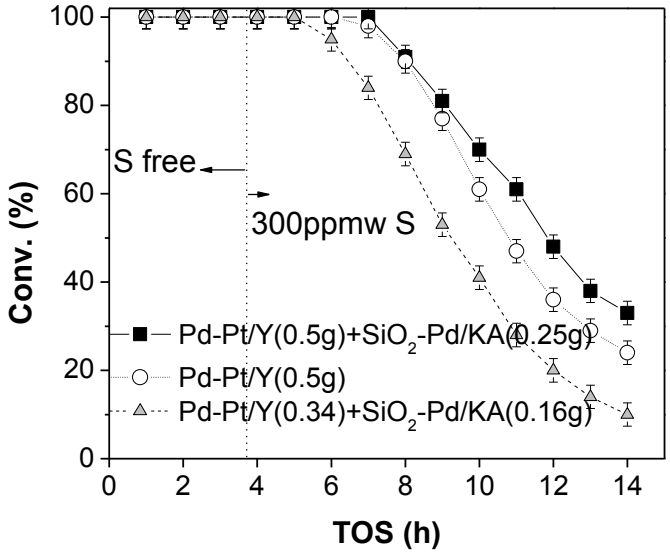


Figure **6-11**: Tetralin conversion over Pd-Pt/Y and hybrid catalysts in the presence of 300 ppmw sulfur as BT.

Calculation of the deactivation rate was attempted with the experimental result, based on the results of tetralin conversion over Pd-Pt/Y and addition of small pore to it. The activity of the catalyst at a certain time, a, is defined as below [103].

$$a = \frac{\text{rate at which the catalyst converts tetralin}}{\text{rate of reaction of tetralin with a fresh catalyst}} = \frac{-r_{THN}}{-r_{THN0}}$$

Both equations of reaction kinetics, tetralin hydrogenation and catalyst deactivation, were taken to be the first order.

$$-r_{THN} = k_{THN} C_{THN} \cdot a$$

$$-\frac{da}{dt} = k_d a$$

With these assumptions, the rate equations can be expressed as the following,

$$\ln\left(\ln\frac{C_{THN0}}{C_{THN}}\right) = \ln(k'\tau') - k_d t$$

Where $C_{THN0}$ and $C_{THN}$ are initial and reacted tetralin concentration, respectively, and $k_d$ denotes as the deactivation rate constant. The deactivation rate constants can be estimated by the slopes of the estimated fits of the result data, as in Figure 6-12.

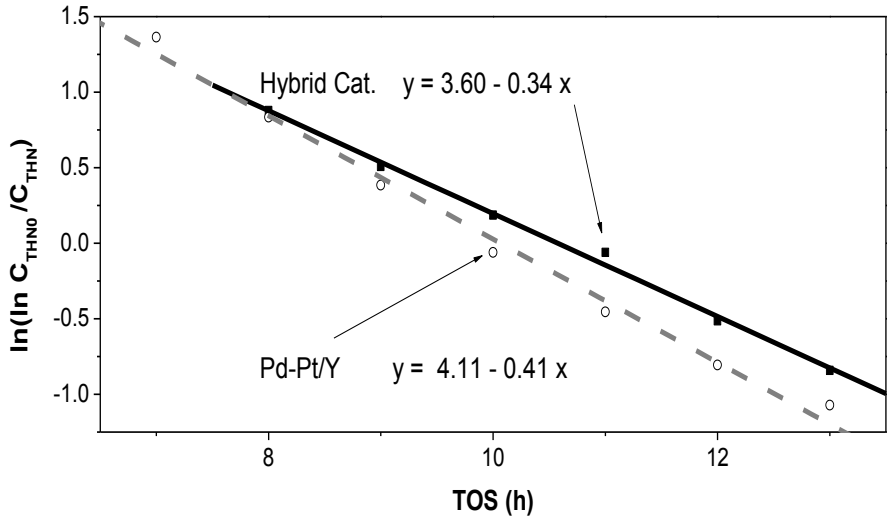


Figure **6-12**: Comparison of deactivation between Pd-Pt/Y and hybrid catalyst .

The equation obtained over Pd-Pt/Y is

$$\ln\left(\ln\frac{C_{THN0}}{C_{THN}}\right) = 4.11 - 0.41t$$

And for hybrid catalyst,

$$\ln\left(\ln\frac{C_{THN0}}{C_{THN}}\right) = 3.60 - 0.34t$$

Since the tetralin conversion over both catalysts in the absence of sulfur reached 100% and the left terms go infinity, it is not of interest to find the kinetic parameters from the intercept. Determined from the calculated fit, the rate constant of deactivation on hybrid catalyst ($k_d$) is 0.34, smaller than that of single Pd-Pt/Y catalyst, 0.41. From the comparison of the calculated value on deactivation, it can be speculated that the sulfur-induced deactivation of the Pd-Pt/Y catalyst can be alleviated by addition of small-pore catalyst, mainly with the aid of hydrogen spillover.

## 6.4. Conclusion

This study investigated the effect of metal on supported metal catalysts. It was found that the metal plays a crucial role in sulfur tolerance of the zeolite supported catalysts for tetralin hydrogenation in the presence of sulfur. Among group 10 metals tested (Ni, Pd and Pt) Pd is the most sulfur-tolerant monometallic catalyst, maintaining higher tetralin conversion than that of Pt. However, Pd-Pt bimetallic catalyst outperformed monometallic catalysts, maintaining 100% conversion even with continuous 100 ppmw sulfur feed for 14 h of run. High sulfur tolerance of Pd-Pt catalyst may be mainly due to more electron-deficient Pd metal with the aid of Pt having higher electronegativity, causing less metal-sulfur interaction. As a continuing study of the catalyst design concept proposed, the hybrid catalysts possessing Pd-Pt/Y as large porous system were performed and found that sulfur-induced deactivation of the Pd-Pt catalyst can be alleviated with the aid of small-pore catalyst.

# Chapter 7

# Conclusions

This study has sought to understand the role of supports and metals on the supported metal catalyst and prove the new design concept of the sulfur-tolerant noble metal catalyst based on shape selective exclusion of sulfur and hydrogen spillover for low temperature hydrogenation of aromatics in the presence of sulfur. Based on experiments of diaromatics hydrogenation at low temperature in the presence of sulfur, and also the supplemental characterization of the catalysts, the following conclusions were made:

Both supports and metals play significant roles on the sulfur tolerance of the supported metal catalysts. Configuration of the pore structure, pore size and acidity are the most important factors governing sulfur tolerance of the metal catalyst. Among the group 10 metals, Pd is the most sulfur-tolerant, but Pd-Pt bimetal which is more electron deficient and highly dispersed on the support exhibits greater sulfur tolerance than monometallic catalysts.

The new catalyst design concept is verified as promising from the study of the hybrid catalyst on diaromatics hydrogenation in the presence of aromatic sulfur. The addition of a small pore catalyst enhances the sulfur tolerance of large pore zeolite Y-supported metal catalyst. Shape selective exclusion of sulfur and hydrogen spillover from metal inside small pore catalyst can prevent sulfur-induced deactivation.

Hydrogen spillover makes the large-pore catalyst component more sulfur-tolerant. It can recover the sulfur-poisoned metal active sites in the large pore zeolite system.

# Chapter 8

## Recommendations for Future Work

Further study can be recommended with several issues.

1. Development of small pore catalyst with high catalytic activity

Several research groups suggested new preparation method for zeolite-supported metal catalyst with high metal dispersion, incorporation of metal precursor in zeolite synthesis step [6, 104], which method will be helpful in preparation of zeolite A supported metal catalyst with high metal dispersion. Utilization of Pt for small pore system (zeolite A supported catalyst in present study) is also recommended in improving hydrogen spillover.

2. Application of design concept to other catalytic reaction

This catalyst design concept of the metal catalyst possessing bimodal pore distribution may be useful for other reactions such as hydrodesulfurization and hydrogenolysis that utilize hydrogen.

## Appendix A

# Zeolite Supports used in this study

### Zeolite Y

Zeolite-Y is large-pore zeolite having a network of 3-dimensional intersecting channels where the pore-diameter is the same in each x,y,z-coordinate [86] The supercage of zeolite-Y is interconnected through 12-membered windows. Thus, the pore structure of zeolite-Y allows adsorption and diffusion of molecules of interest (hydrogen, hydrogen sulfide, naphthalene, tetralin and benzothiophene). Zeolite Y is widely used in solid acid catalysts, main components of fluid catalytic cracking and hydrocracking processes. The structure of zeolite-Y is depicted in Figure A-1.

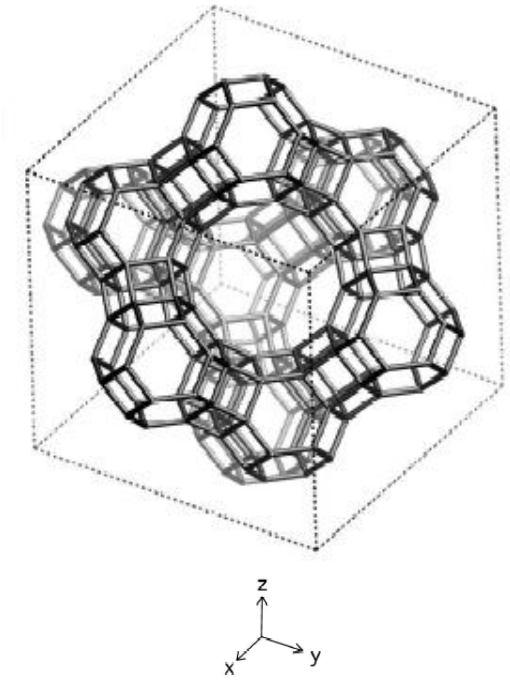


(a) Faujasite framework viewed along [1 1 1] adopted from [87]

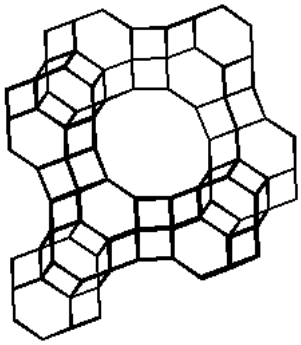

(b) Projection down [1 1 0] adopted from [105]

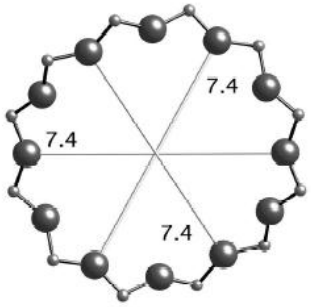


(c ) 12-membered pore opening viewed along [1 1 1].

Figure **A-1**: Crystalline structure of zeolite-Y. Dimension in Angstroms (Å).

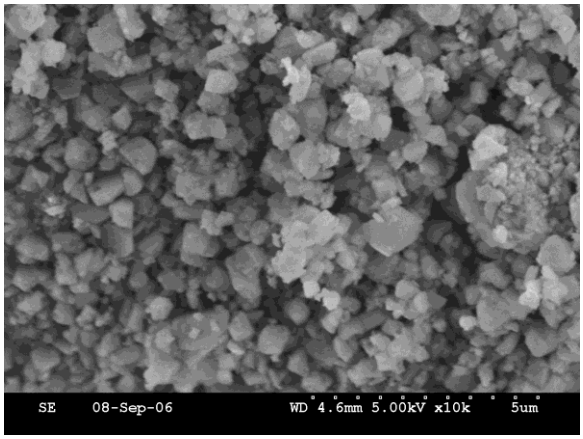


Figure **A-2**: SEM image of Zeolite Y obtained by a JEOL6700F FE-SEM at 5 kV. Samples were iridium sputter coated for 15 seconds/20mA

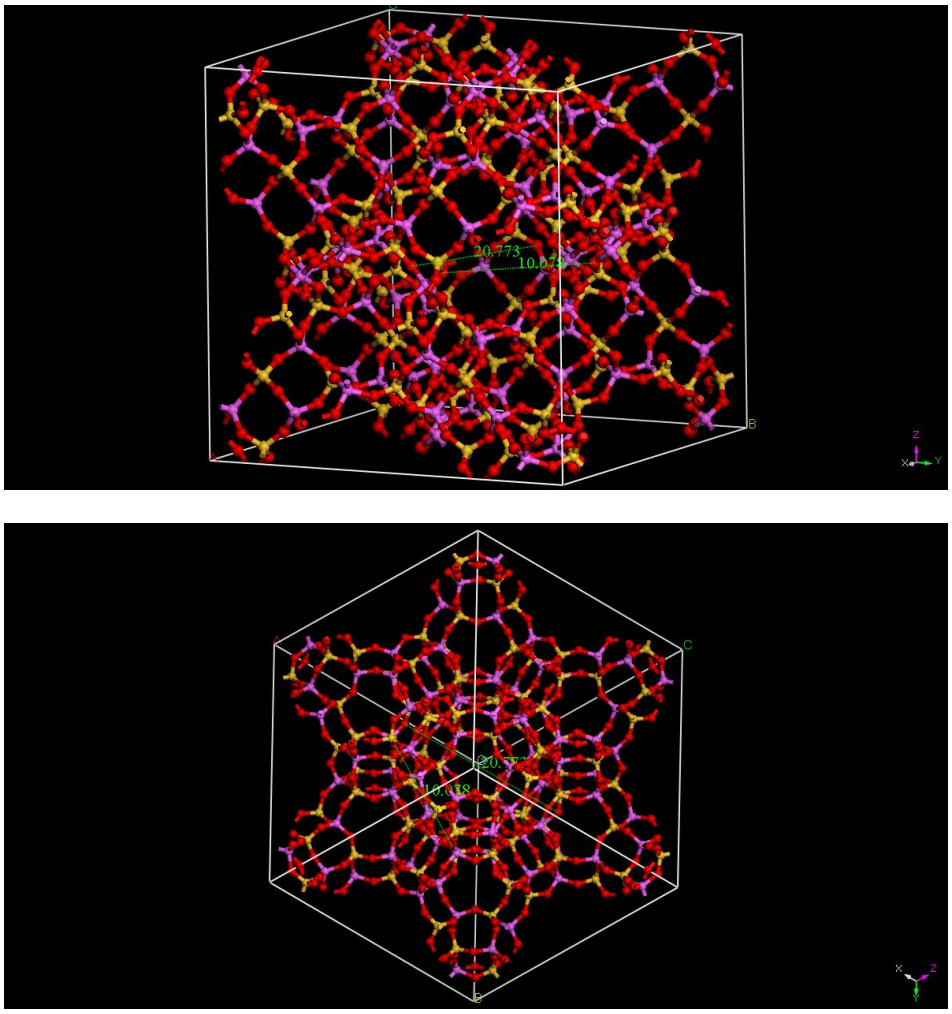


Figure **A-3**: Zeolite Y Structure from Material Studio ver.5.0

**Mordenite**

Mordenite zeolite has a channel-like pore structure with side-pockets with small 8-ring pores (5.7 × 2.6 Å) that open off the main channels with 12-ring pore (7.0 × 6.5 Å). Adsorption and diffusion of molecules readily occurs in the main channels. Mordenite is practically one-dimensional large pore zeolite and transport of most large molecules within the zeolite occurs only along the c axis. Therefore, diffusion in one dimension of mordenite is inherently a slower process than diffusion in two or three dimension.

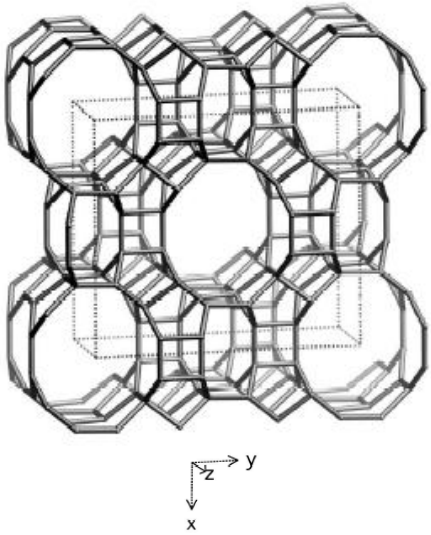


(a) Mordenite framework viewed along [0 0 1].

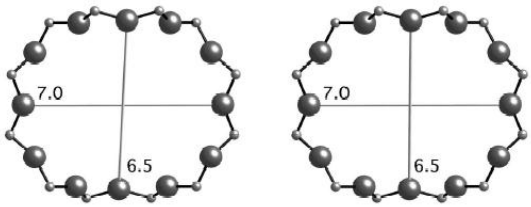


(b) 12-membered channels viewed along [0 0 1].

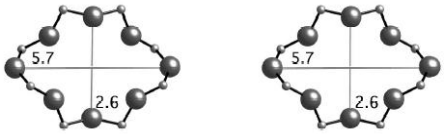


(c) 8-membered side-pockets viewed along [0 0 1].

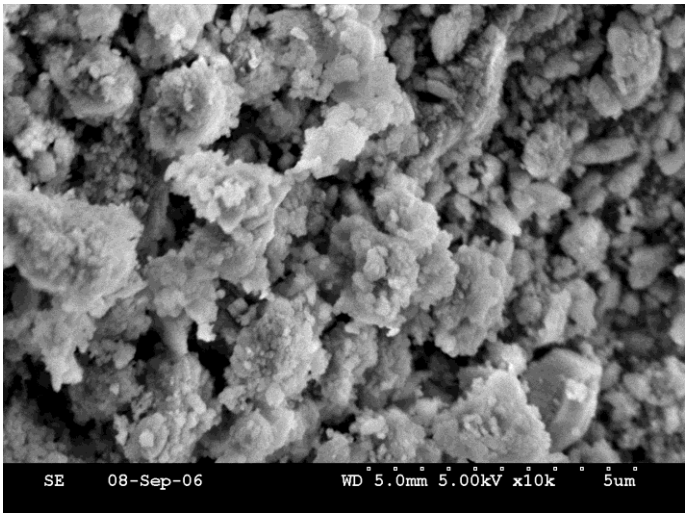


(d) SEM image

Figure A-4: (a) and (b) Crystalline structure with dimensions in Angstroms (Å) [87] and (c) SEM image of mordenite obtained by a JEOL6700F FE-SEM at 5 kV. Samples were iridium sputter coated for 15 seconds/20mA

**Zeolite-A**

Zeolite-A has a 3-dimensional pore structure and molecules can enter into all three x, y, and z-dimension. The pore diameter of the window with eight membered ring is approximately 4.1 Å. The pore opening leads into a larger cavity (α-cage) of minimum free diameter of 11.4 Å. The cavity is surrounded with eight β-cages connected by their square faces in a cubic structure.

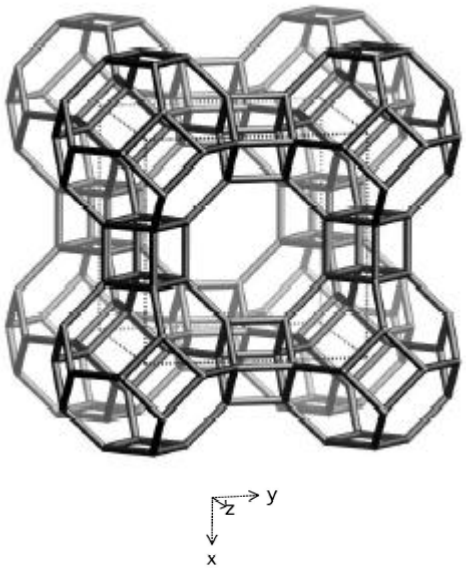


(a) Zeolite-A framework viewed alon [0 0 1].

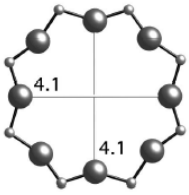


(b) 8-membered pore opening along [1 0 0].

Figure **A-5**: Crystalline structure of zeolite-A. Dimensions in Angstroms (Å). [87]

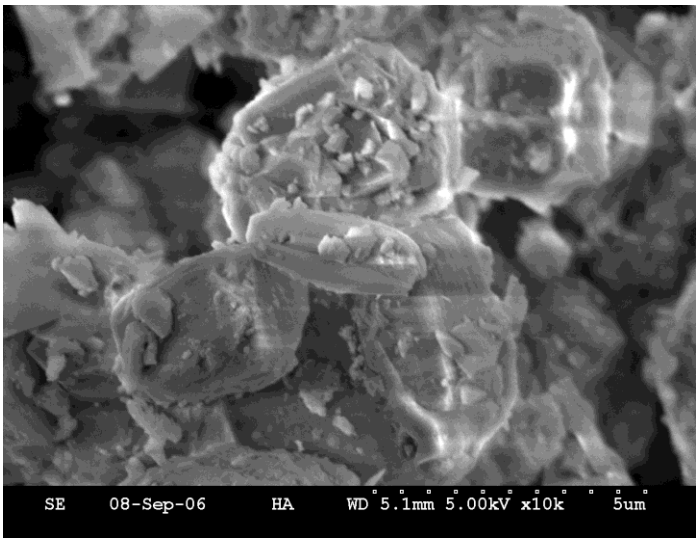


Figure **A-6**: SEM image of Zeolite A obtained by a JEOL6700F FE-SEM at 5 kV. Samples were iridium sputter coated for 15 seconds/20mA

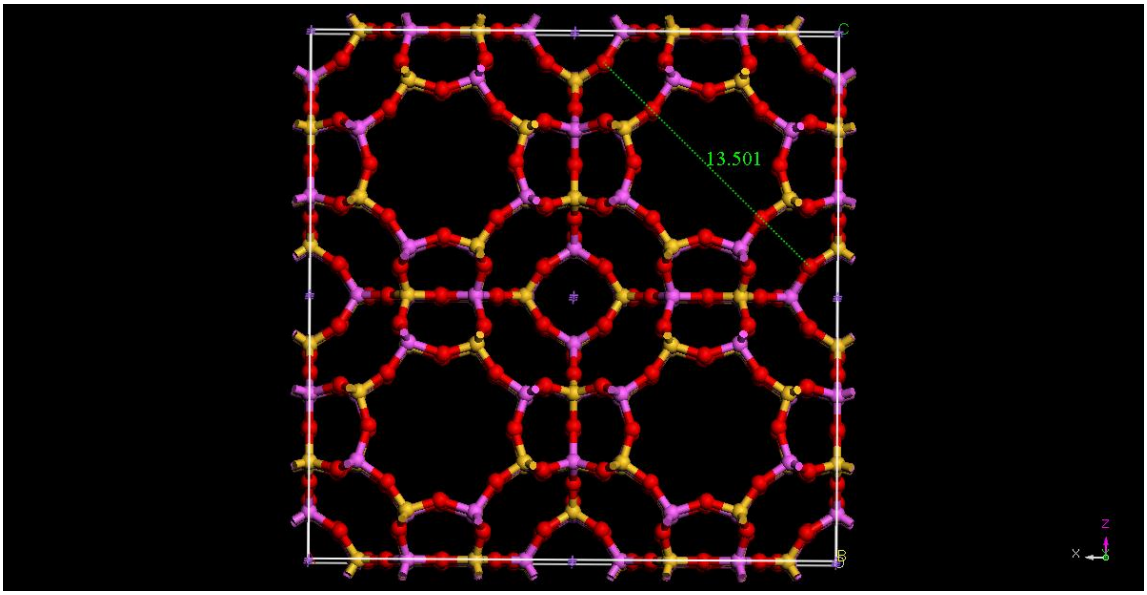


Figure **A-7**: Zeolite A Structure from Material Studio ver.5.0

## Appendix B

## Reactor System

**Batch reactor**

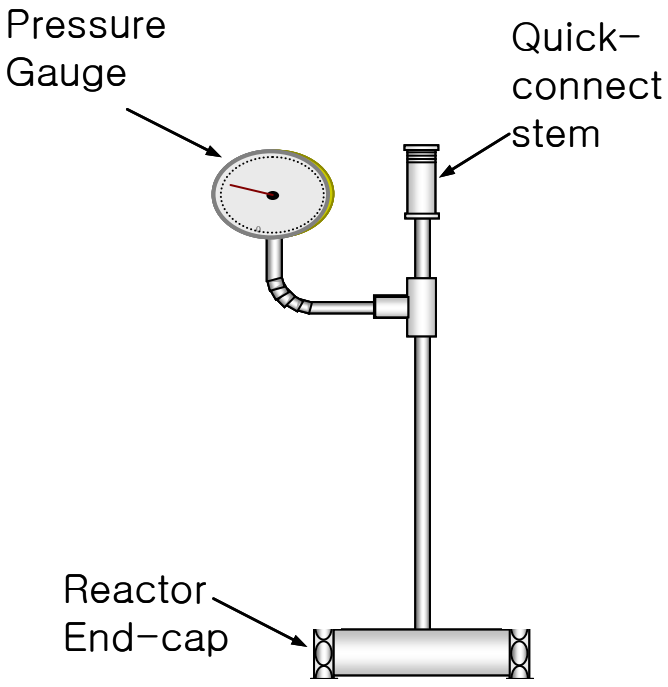


Figure **B-1**: Schematic of batch reactor (horizontal tubing bomb reactor)

**Fixed-bed flow reactor for hydrogenation**

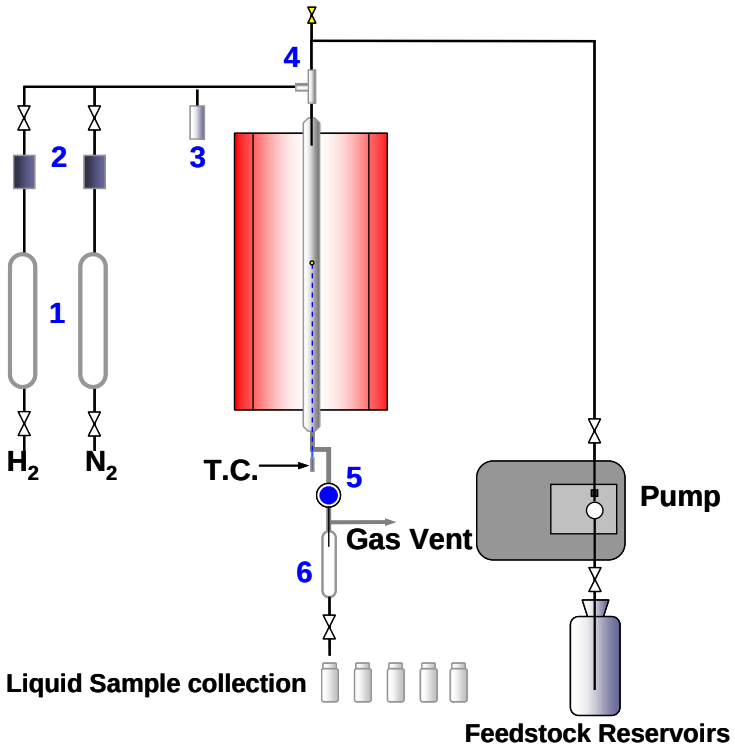


**1 Moisture/oxygen traps** **2 Mass flow controllers**
**3 Digital pressure transducer** **4 Pressure relief valve**
**5 Back pressure regulator** **6 Gas-liquid separator**

Figure **B-2**: Schematic diagram of the fixed bed flow reactor system for hydrogenation

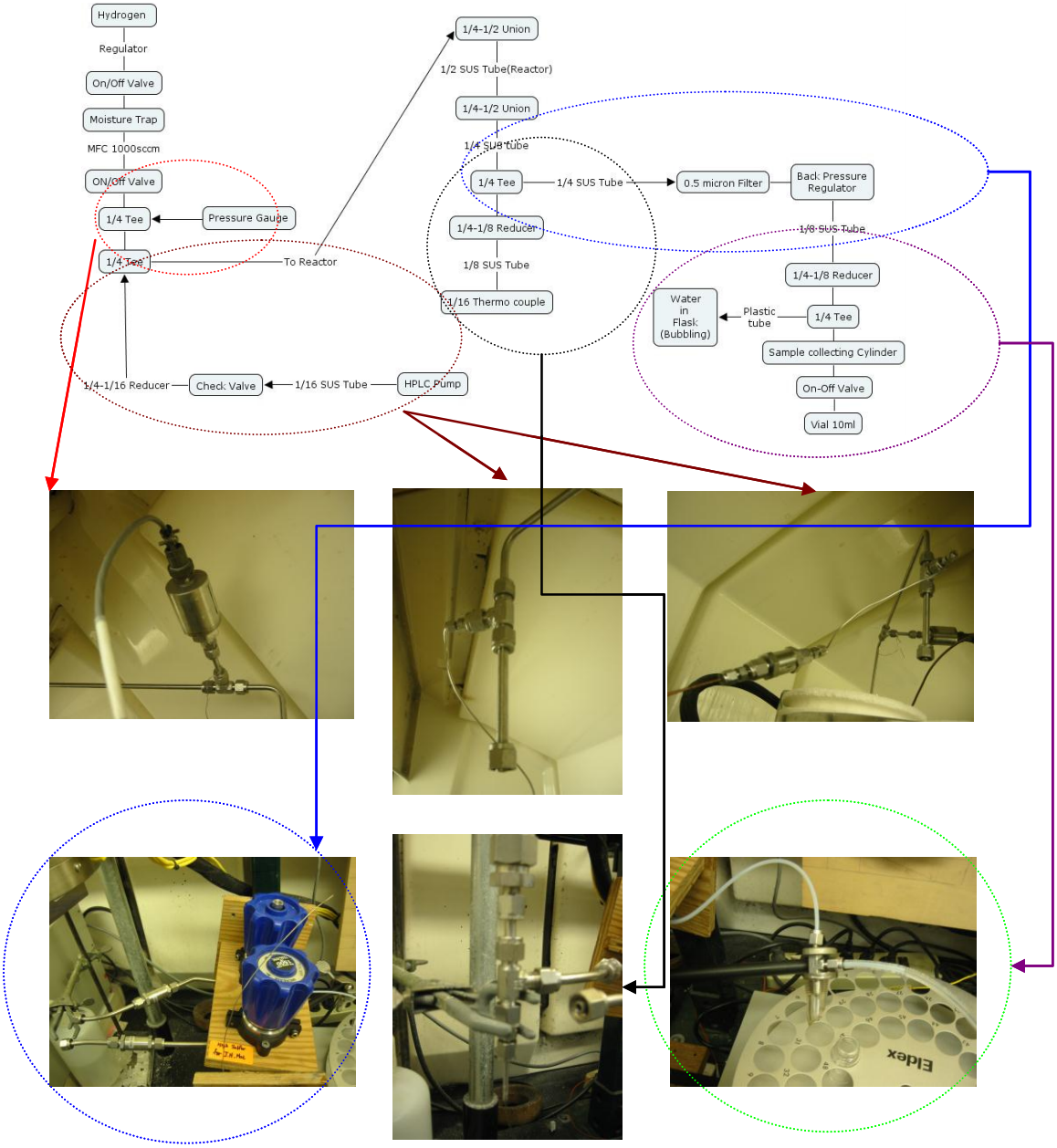


Figure **B-3:** Detailed reactor scheme and picture of the parts in fixed bed flow system

The stainless steel reactor tube is 24 inches (61cm) in length, has an internal diameter of approximately 0.37 inches (0.94cm), and has a wall thickness of approximately 0.065 inches (0.17cm). It is housed in a three zone tubular electric furnace (Applied Test Systems, Series 3210) capable of heating to 900$^{o}$C. Reactor temperature was monitored and controlled by a digital control system (Applied Test Systems, Series XT-16)

An HPLC pump (Alltech Series 426) was used to accurately measure (±0.01ml/min) and pump the liquid feedstock into the reactor at high pressure. The top section of the reactor was used as a pre-heating zone to ensure reactants were well mixed with hydrogen and at the desired temperature upon contact with the catalyst bed. A Brooks mass flow controller (5850TR) calibrated for 0-1000ml/min flow was used to measure and control hydrogen gas flow. A Tescom backpressure regulator was used to maintain system pressure. System pressure was measured by a Coopers Instruments pressure transducer (TPG 135) equipped with an electronic read-out panel. Independent measurement of reactor pressure was obtained from a Bourdon pressure gauge near the reactor inlet.

Temperature in the reactor was monitored and maintained using four K-type omega thermocouples. Three were used to control the heating zones of the tubular furnace. The fourth thermocouple was housed a thermocouple guide tube(thermo-well) designed such that a thermocouple could be moved vertically up or down in order to measure temperature along the length of the catalyst bed.

**Procedure of catalyst preparation, loading and reaction preparation**

(1) Catalyst preparation

Zeolite supports (zeolite A, Y and mordenite) and silica-alumina were obtained from Zeolyst International (formerly PQ Corporation) and Aldrich, respectively. All supports were first calcined in air flow (~60 ml/min) for 4 h at 450 $^{o}$C, with a heating rate of 1.5 $^{o}$C/min.

As zeolite A was sodium form, it needs pretreatment for ion exchange to get proton form (A) or potassium form (KA). In preparation of proton form zeolite A, 30 g of zeolite A as received was dispersed in 330 ml of 0.4 M ammonium chloride ($NH_4Cl$, Aldrich, 99.5%) solution. The zeolite and supernatant solution were then agitated by magnetic stirrer at 80$^{o}$C for 3h and then separated by vacuum filtration. This procedure was repeated 3 times for zeolite to change to ammonium form thoroughly. After three times of ion exchange, the zeolite was rinsed with de-ionized water to remove excess ammonium solution until the filtered water was pH 7 by using pH test paper. The ammonium ion exchanged zeolite was dried in an oven at 120 $^{o}$C and calcined in air flow (~60 mL/min) for 4 h at 450 °C, with a heating rate of 1.5 °C/min. Thus, ammonia ion was decomposed and ammonia form of zeolite A was converted to the proton form. Likewise, potassium form zeolite A (KA) was also prepared by ion exchange of sodium form of zeolite A. Likewise, 30 g of zeolite was dispersed in 0.4 M potassium chloride (KCl, Aldrich, 99.0%) solution 330 ml then agitated by magnetic stirrer at 80 $^{o}$C for 3h to come to equilibrium and then separated by vacuum filtration. This procedure was repeated 3 times for zeolite to change to potassium form thoroughly. After three times of ion exchange, the zeolite was rinsed with de-ionized water to remove excess potassium and chloride ion until the filtered water was pH 7 by using pH test paper. The potassium ion exchanged zeolite was dried in an oven at 120 $^{o}$C and calcined in air flow (~60 mL/min) for 4 hours at 450 °C, with a heating rate of 1.5 °C/min.

The potassium form zeolite Y (KY) followed the same procedure as the potassium form zeolite KA.

All catalysts were prepared by the incipient wetness impregnation (IWI) method. The volume of solution needed to reach the stage of incipient wetness was determined by measuring the volume of water added dropwise to a known weight of the support until the support changed appearance from dry to slightly liquid. The metal precursors used in this study were: $PdCl_2$ (Sigma Aldrich, 99.999%). In order to dissolve $PdCl_2$ in water, it is necessary to add HCl to form soluble $PdCl_4^{2-}$ species. The amount of HCl added to dissolve the $PdCl_2$ is approximately 2.05 of $HCl/PdCl_2$ ratio (theoretical ratio is 2). The appropriate amount of metal precursor, calculated for the desired metal loading, was dissolved in a total volume of diluted hydrochloric acid aqueous solution equal to the pore volume for the support being impregnated. All catalysts in this work were prepared with a nominal metal loading of 2 wt%. The precursor metal salt dissolved solution was then added dropwise to the support. After a few drops were added to the support, metal solution added support was stirred thoroughly, then a few more drops were added and the mixture was stirred again. Impregnation continued in this manner until all of the metal solution was loaded on the support. After the impregnation completed, the metal loaded support was dried at 100 °C overnight. After drying, the catalysts were placed on boat-shaped crucibles and calcined in air flow (~60 ml/min) at 450 °C for 4 hours, with a heating rate of approximately 1.5 °C/min. The calcined catalysts were then again mixed thoroughly.

(2) loading

Borosilicate glass beads were used as inert packing material above and below the catalyst bed. Noble-metal supported catalysts were prepared in powder form, but utilized in flow reactor test as particles. All powder catalysts were first pressed into pellets which were then crushed and

sieved to particles of 0.5-1.0 mm diameter(18-35 mesh). A typical catalyst evaluation experiment used 0.5g of catalyst which was mixed with α- alumina as a diluent material.

Table **B-1**: Catalyst loading

| **Filler** | **type and amount** |
|---|---|
| Borosilicate – Inert packing Material<br>(Lower part of Catalyst bed) | Φ=3mm : 22.525g<br>Φ=2mm : 1.5g<br>Φ=1mm : 1.5g |
| Catalyst and Inert material<br>-Catalyst Bed<br>(should be mixed well) | α- alumina : 3.0g<br>Catalyst : 0.5g |
| Borosilicate – Inert packing Material<br>(Upper part of Catalyst bed) | Φ=1mm : 1.5g<br>Φ=2mm : 1.5g<br>Φ=3mm : Proper amount |

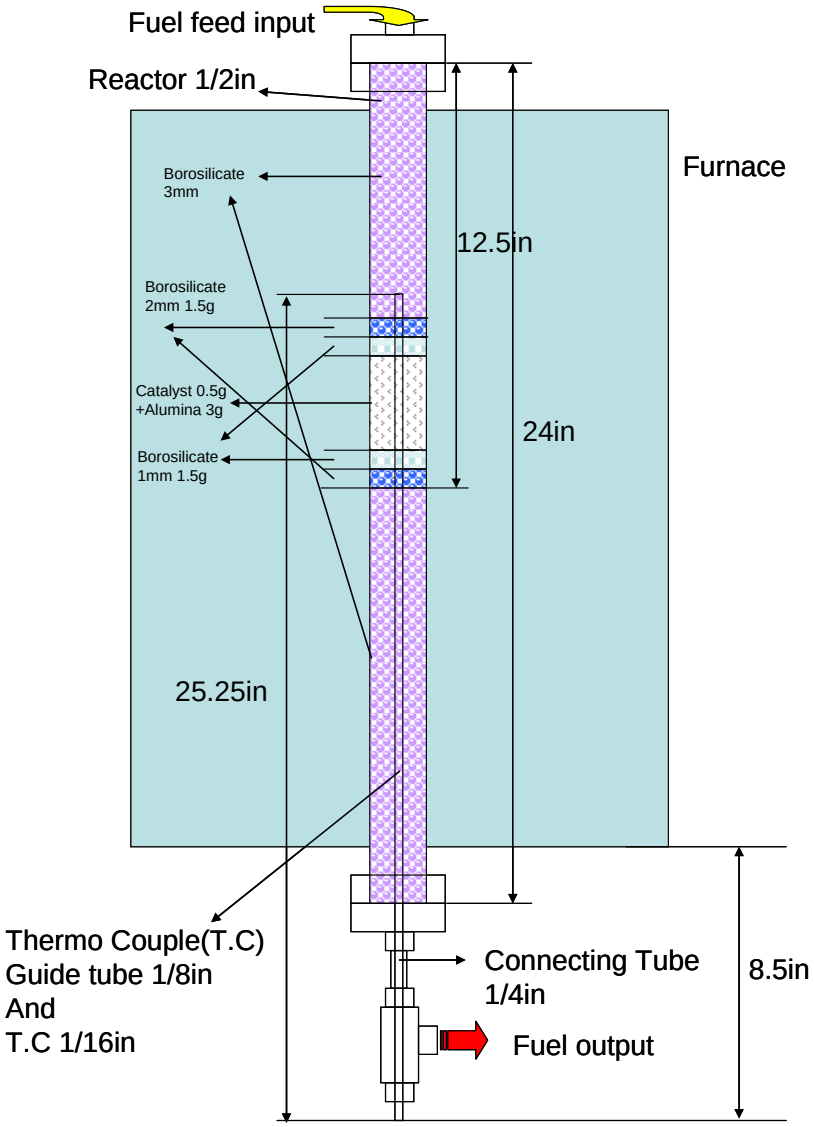


Figure **B-4**: Schematic of reactor and catalyst loading.

(2) Before mounting the reactor

The feed inlet tube via HPLC pump is rinsed with the model fuel for 10 min at 1 ml/min of flow rate. The balance of the reactor is checked when the reactor is mounted. Once the reactor

is mounted, it is checked for leakage by increasing the reactor pressure to 100 psi of hydrogen before the furnace turns on.

(3) Preparation of reaction

The catalyst is reduced in situ overnight under a hydrogen flow of 100 ml/min and 100 psig of $H_2$ pressure at 225 $^oC$ (setting time to reach the temperature is 120min). After reduction, the reactor is pressurized to 600psig of hydrogen and the hydrogen flow was set to 80 ml/min. The temperature of the catalyst bed is checked using a thermocouple introduced into the reactor and the temperature of the bed is kept constant by regulating the temperature of the furnace. The feed is firstly introduced into the reactor and then the system is allowed to be stabilized for 90 min. Therefore, 90 min after the introduction of feedstock was designated as time-on-stream (TOS) equal to zero. Since hydrogenation is exothermic, the bed temperature increases when the feed is introduced and reaction starts. The temperature across the bed of the catalyst (225 $^oC$) keeps constant by lowering the controller setting temperature to the required value. The final setting temperature is varied by the fuel feed rate, fuel composition or reactor condition. For example, the final setting temperature for 20% tetralin in hexadecane with 0.08 ml/min is around 210-215 $^oC$. Care is taken to ensure that the pressure of the reactor doesn't exceed the required pressure by more than 5 psi and is regulated using the back pressure regulator.

(4) After reaction

When the reaction is over, change the fuel to hexadecane and feed with the flow rate of 0.64 ml/min for 30 min to clean the liquid fuel line. The pressure of the reactor is released to atmospheric pressure. Shut down the HPLC pump as well as the furnace. Open the furnace door a little to let the furnace to cool down. Hydrogen gas is allowed to pass through the reactor for 30 min before shutting the valve to allow residual liquid to pass through. Once the reactor has cooled down sufficiently, unload the reactor from the furnace and open to collect the catalyst. The catalyst is collected and washed with acetone. The reactor should be firstly cleaned with detergent and the brush, then cleaned with acetone and paper towel to remove any residual feed sticking to the sides of the reactor. Clean the reactor until the residue is totally removed.

**Procedure**

1. Reduction of Catalytic bed

(1) Introduce 100ml/min of hydrogen to the reactor until reactor pressure reach to 100psi.

(2) Stir the fuel feedstock using magnetic stirrer overnight.

(3) Furnace set up

**Furnace Instruction Manual**

(1) Turn on Power

(2) Hold/Press Enter button until SPTT appears

(3) Enter Target time in minutes (200 min≈1 $^{o}$C/min)

(4) Press Ξ (mode)

(5) Hold/Press Enter buton until Ac.Cd appears. (Check #3 is set)

(6) Press Ξ

(7) Enter Final temperature(225 $^{o}$C)

(8) Turn off power

2. Start Experiment

(1) Increase the $H_2$ pressure inside the reactor to 600 psi. when the pressure reaches to 600 psi, decrease hydrogen flow rate to 80 ml/min.

(2) Place the model fuel bottle into the sonicator bath for 20 min to remove the air dissolved in the fuel.

(3) Fill the model fuel inside HPLC inlet tube by using syringe.

(4) Press start button for Fuel injection (0.08 ml/min)

(5) Decrease the setting temperature to meet the reaction temperature

(6) Make sure the location of Vial and tag for all vials in the automatic sampler are ready to collect the liquid sample

(7) After 1.5 h of fuel injection to stabilize the reaction temperature and pressure, start to collect the liquid sample in the prepared vial

3. After Experiment

(1) Change the fuel to hexadecane and feed with the flow rate of 0.64ml/min to clean the liquid fuel line.
(2) Stop Furnace operation and release the pressure
(3) Stop the hydrogen flow and fuel injection(Hexadecane) after 30min.

**Fuel Feed Flow rate**

| | |
|---|---|
| Test | 0.08ml/min |
| Clean up | 0.64ml/min |

**MFC for hydrogen gas**

| Scale | Real Flow |
|---|---|
| 98 | 100ml/min |
| 79 | 80ml/min |

**Appendix C**

# Kinetic study of tetralin hydrogenation

In this work, the kinetic expression is based on a simple power law equation with the following assumptions:

(1) The reactor is a plug flow reactor. (2) The reactions run in isothermal and isobaric condition. (3) The volume change of liquid flow is ignored. (4) The diffusion limitation is negligible (4) the kinetics of tetralin hydrogenation was first-order (5) The reverse reactions such as tetralin dehydrogenation to naphthalene, decalin dehydrogenation to tetralin and conformational isomerization of trans- to cis-decalin is neglected [80, 99]. The pseudo first order kinetics is applied for the description of the reaction, and thus following pseudo-kinetics is obtained.

$$THN \xrightarrow{k_1} cis-DHN \qquad r_1 = k_1 C_{THN} \qquad \text{Eq. (C.1)}$$

$$THN \xrightarrow{k_2} trans-DHN \qquad r_2 = k_2 C_{THN} \qquad \text{Eq. (C.2)}$$

$$cis-DHN \xrightarrow{k_3} trans-DHN \qquad r_3 = k_3 C_{c-DHN} \qquad \text{Eq. (C.3)}$$

If we model the stand-alone differential equation, we get

$$\frac{dC_{THN}}{d\tau} = -k_1 C_{THN} - k_2 C_{THN} \qquad \text{Eq. (C.4)}$$

$$\frac{dC_{c-DHN}}{d\tau} = k_1 C_{THN} - k_3 C_{c-DHN} \qquad \text{Eq. (C.5)}$$

$$\frac{dC_{t-DHN}}{d\tau} = k_2 C_{THN} + k_3 C_{c-DHN} \qquad \text{Eq. (C.6)}$$

By solving Eq. (C.4),

$$C_{THN} = C_{THN0}\left[e^{-(k_1+k_2)\tau} - 1\right] \qquad \text{Eq. (C.7)}$$

From Eq. (C.5) and Eq. (C.7),

$$\frac{dC_{c-DHN}}{d\tau} = k_1 C_{THN} - k_3 C_{c-DHN} = k_1 C_{THN0} e^{-(k_1+k_2)\tau} - k_3 C_{c-DHN}$$

$$\frac{dC_{c-DHN}}{d\tau} + k_3 C_{c-DHN} = k_1 C_{THN0} e^{-(k_1+k_2)\tau}$$

$$\frac{d\left(C_{c-DHN} e^{k_3\tau}\right)}{d\tau} = k_1 C_{THN0} e^{-(k_1+k_2-k_3)\tau}$$

$$C_{c-DHN} = -\frac{k_1 C_{THN0}}{k_1+k_2-k_3} \frac{e^{-(k_1+k_2-k_3)\tau} - 1}{e^{k_3\tau}} \quad \text{Eq. (C.8)}$$

From Eq. (C.6), Eq. (C.7) and Eq. (C.8),

$$\frac{dC_{t-DHN}}{d\tau} = k_2 C_{THN} + k_3 C_{c-DHN} \quad \text{Eq. (C.6)}$$

$$= k_2 C_{THN0} e^{-(k_1+k_2)\tau} - \frac{k_1 k_3 C_{THN0}}{k_1+k_2-k_3} \frac{e^{-(k_1+k_2-k_3)\tau} - 1}{e^{k_3\tau}}$$

$$C_{t-DHN} = C_{THN0}\left[1 - \frac{(k_2-k_3)}{k_1+k_2-k_3} e^{-(k_1+k_2)\tau} - \frac{k_1}{k_1+k_2-k_3} e^{-k_3\tau}\right] \quad \text{Eq. (C.9)}$$

$k_1$, $k_2$ and $k_3$ were obtained by solving these equations, Eq. (C.7), Eq. (C.8) and Eq. (C.9).

## Appendix D

# Supplementary Data

### Chapter 4

#### Temperature programmed oxidation

The thermal gravimetric analysis of the spent catalysts was performed in air flow for temperature-programmed oxidation (TPO) by Perkin-Elmer thermo-gravimetric instrument with 10 $^{o}$C/min of heating rate up to 1000 $^{o}$C in air.

The temperature programmed oxidation (TPO) profiles of the spent catalysts after naphthalene hydrogenation with 560 ppmw sulfur fuel are presented in Figure D-1. There are 3 distinctive weight losses detected during the oxidation of Pd/Y at the temperature ranges, 25-220$^{o}$C, 220-420$^{o}$C and 420-600 $^{o}$C, which is consistent with the TPO result from our previous study [14]. The weight loss above 600 $^{o}$C due to zeolite dehydroxylation is excluded from our study [106]. The weight loss in the temperature region between 25-220 $^{o}$C is attributed to the desorption of adsorbed water and oxidation of metal sulfide, poisoned metal into PdO [107]. The weight loss at the temperature range 220-420 $^{o}$C and 420-600 $^{o}$C might be related to oxidation of adsorbed aromatic or dicyclic compounds and deposited carbon species, respectively. In the case of Pd/A, there was no significant weight loss detected in whole temperature ranges. It is likely that the amount of adsorbed aromatic compounds on Pd/A is too low to be detected in TGA analysis since the fraction of surface metal sites exposed to bulky aromatic are meager comparing to the metal located inside zeolite A frameworks. The experimental result of the hybrid catalyst was compared with a calculated fit derived from experimental result of Pd/Y and Pd/A at the ratio

of 2:1. The experimental TPO profile of the hybrid catalyst also shows similar trend as that of Pd/Y, but weight losses in all ranges are much milder than the calculated fit. In particular, the weight loss in the temperature range for deposited carbon species are almost negligible, suggesting that hydrogen spillover from Pd/A prevent from carbon deposition on Pd/Y, the catalyst for aromatic hydrogenation. This result is also supportive on that spillover hydrogen prevents coke formation on acid sites of zeolite Y, suggested by Kikuchi and Matsuda in their IR Spectroscopic studies of hydrogen spillover [108]. Although the interpretation of the TGA result might not be accurate in distinguishing between adsorbed aromatics and deposited carbon species, the comparison between the experimental and the calculated fit demonstrates that the hybrid catalyst lowers the amount of adsorbed species and carbon deposition. Therefore, the TPO analysis result, together with the batch reaction test in this study, also substantiates that the metal sites in small pores of Pd/A catalyst possibly play a key role in improving the catalytic activity of hybrid catalyst.

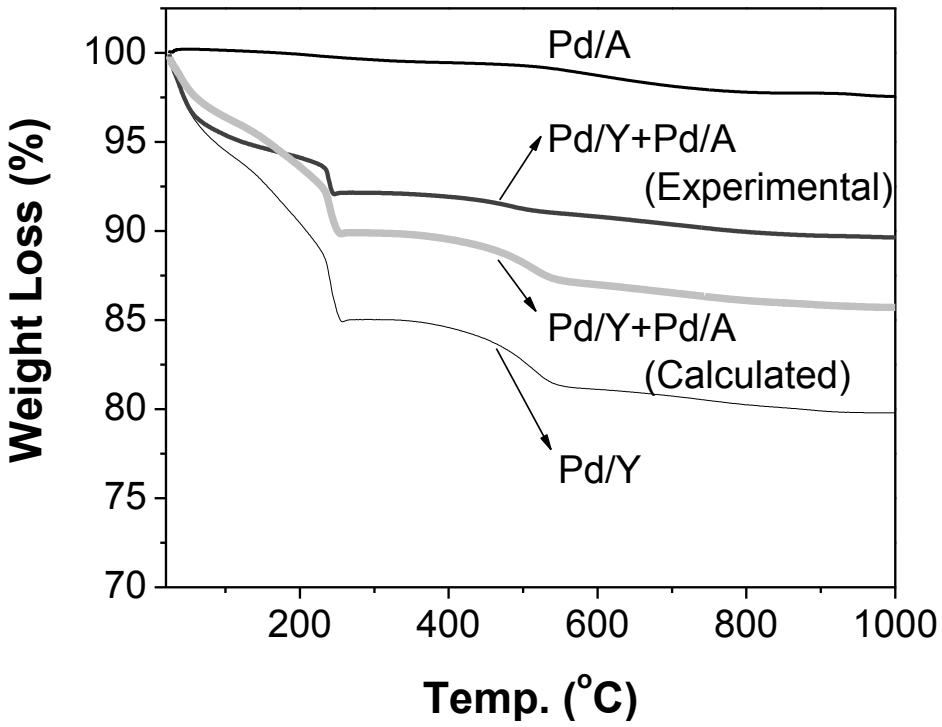


Figure **D-1**: TPO profiles of used Pd catalysts in air after naphthalene hydrogenation in the presence of 560ppmw sulfur as BT

**Hydrogen Spillover**

Hydrogen spillover test was conducted using the same equipment at the same condition with the same procedure mentioned in chapter 5.

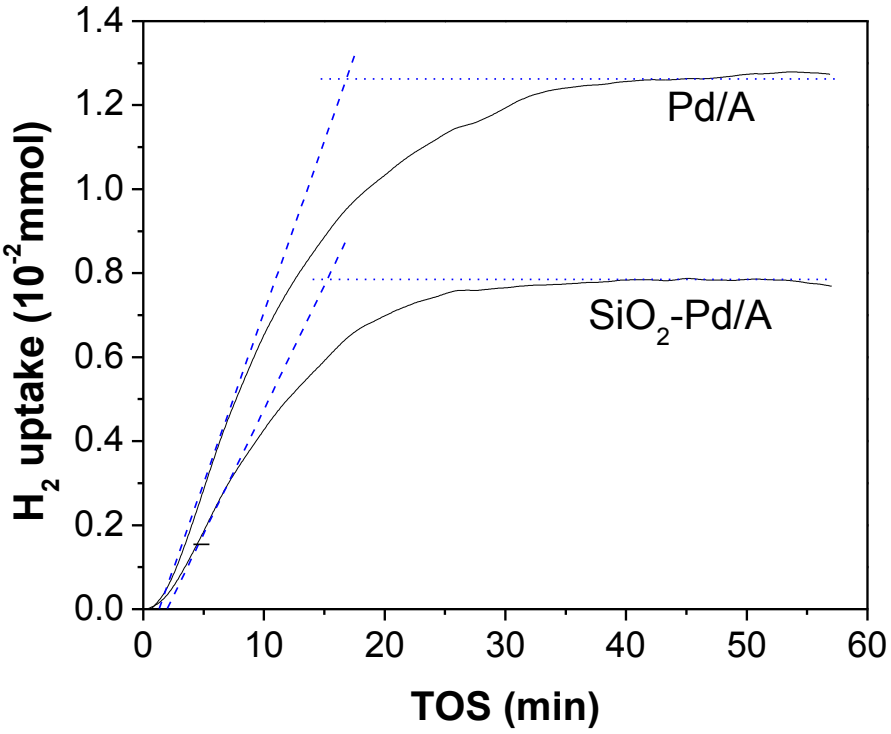


Figure **D-2**: Extent of hydrogen uptake on $WO_3$ by hydrogen spillover

Spillover phenomenon was defined as follows; "spillover involves the transport of an active species which are adsorbed or formed on a first phase onto another phase that does not adsorb or form the species under the same condition.". [109] For hydrogen Hydrogen, hydrogen molecule dissociates on metal active sites and migrates in the form of atoms or $H^+$. The influence of hydrogen spillover on catalytic process was described as (1) spilled-over species keep catalyst

clean, (2) create or regenerate selective sites through a remote controlling mechanism, and (3) as a result, catalytic reactions are accelerated and catalyst deactivation is inhibited effectively [110]. In this study, qualitative and quantitative study of hydrogen spillover phenomenon was tried to investigate the role of small pore catalyst by utilization of tungsten trioxide ($WO_3$) as a sorbent for spilt over hydrogen. The direct evidence of hydrogen spillover was obtained by color change of $WO_3$ when it adsorb hydrogen atom. When the batch reactor system was filled with hydrogen passed over the small pore catalyst-$WO_3$ mixture, the original color of $WO_3$ was changed to dark blue due to the formation of the so called tungsten bronze. This can be explained by the fact that hydrogen dissociates on Pd clusters and migrates via support onto $WO_3$. Quantification of hydrogen spillover was also attempted to inspect the effect of silica coating on hydrogen spillover from Pd/A. It was expressed as the extent of hydrogen uptake onto tungsten trioxide by secondary spillover. Figure D-2 shows hydrogen uptake on $WO_3$+Pd/A and $WO_3$+$SiO_2$-Pd/A mixtures. Apparently, the hydrogen uptakes on both mixtures progress rapidly, but the $SiO_2$-Pd/A catalyst shows approximately 0.7 times lower uptake than that uncoated one. One possible reasone could be lower metal dispersion of $SiO_2$-Pd/A. When compared with metal dispersions of both catalysts, $SiO_2$-Pd/A showed 16.8%, around 10% lower dispersion than Pd/A catalyst. Surface metal passivation by CVD can be another reason of decline on hydrogen spillover, which may cause the lower concentration of hydrogen species on the external surface of $SiO_2$-Pd/A. Hydrogen spillover is the diffusion phenomenon of dissociated hydrogen species on the support, thus the main driving force is concentration differences of hydrogen species between donor (Pd/A or $SiO_2$-Pd/A in this study) and acceptor ($WO_3$). In the case of Pd/A catalyst, as Pd metal on the external surface is highly saturated by dissociated hydrogen atom, the concentration of dissociated hydrogen species on Pd/A catalyst should be higher than that on the silica coated Pd/A catalyst.

It is also possible that the silica coated surface on Pd/A catalyst negatively affect surface diffusion of spillover hydrogen. There is another issue that should be considered on hydrogen spillover, surface properties on the support. The surface composition could be another controlling factor for surface diffusion of the dissociated hydrogen species [83, 111]. It was previously reported that the diffusion coefficients of hydrogen was varied by support types. For example, diffusion coefficient on $SiO_2$-supported Rh catalyst is $9.3\times10^{-11} cm^2 s^{-1}$, which value is lower than that on $Al_2O_3$-supported Rh catalyst, $1.7\times10^{-10} cm^2 s^{-1}$ [83]. The differences of the diffusion coefficients between the supports are possibly associated with differences of hydrogen spillover uptake.

Even though there are several issues that should be considered on hydrogen spillover, the result demonstrates that silica coating on Pd/A catalyst was well performed without blocking the pore opening, maintaining the catalytic activity of Pd inside the pore of zeolite A, i.e. hydrogen spillover.

**Chapter 5**

**Temperature programmed reduction**

TPR test was conducted using the same equipment at the same condition with the same procedure mentioned in chapter 3 and 5.

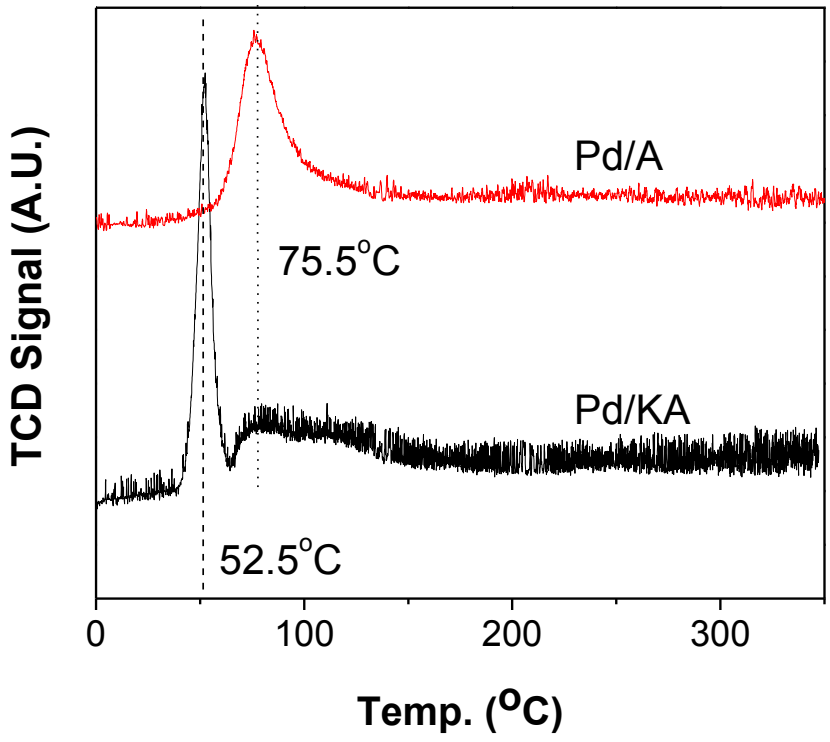


Figure **D-3**: TPR profiles of Pd/A and Pd/KA catalysts

Figure D-3 presents comparison of the TPR profiles of Pd catalysts supported on zeolite A and zeolite KA. The TPR profile of Pd/KA catalyst has two distinguished peaks, the sharp positive peak around 52.5 $^{o}$C and small broad peak around 75 $^{o}$C which is located at almost same position as Pd/A. It is most likely the reduction temperature of Pd on zeolite KA support is shifted to lower temperature. This trend suggests K ion exchange of zeolite A support changes the electron charge density of palladium metal particle. It was previously mentioned that addition of basic promoter such as potassium or strontium to the catalyst improves the dispersion and net charge density of the metal.

# References


1. Cooper, B.H. and B.B.L. Donnis, *Aromatic saturation of distillates: An overview.* Applied Catalysis, A: General, 1996. **137**(2): p. 203-223.
2. Stanislaus, A. and B.H. Cooper, *Aromatic hydrogenation catalysis - A Review.* Catalysis Reviews - Science and Engineering, 1994. **36**(1): p. 75-123.
3. Whitehurst, D.D., T. Isoda, and I. Mochida, *Present State of the Art and Future Challenges in the Hydrodesulfurization of Polyaromatic Sulfur Compounds.* Advances in Catalysis, 1998. **42**: p. 345-471.
4. Song, C. and X.L. Ma, *New design approaches to ultra-clean diesel fuels by deep desulfurization and deep dearomatization.* Applied Catalysis, B: Environmental, 2003. **41**(1-2): p. 207-238.
5. Barbier, J., et al., *Role of Sulfur in Catalytic Hydrogenation Reactions.* Advances in Catalysis, 1990. **37**: p. 279-318.
6. Yang, H., et al., *Shape selective and hydrogen spillover approach in the design of sulfur-tolerant hydrogenation catalysts.* Journal of catalysis, 2006. **243**(1): p. 36-42.
7. Yasuda, H., T. Sato, and Y. Yoshimura, *Influence of the acidity of USY zeolite on the sulfur tolerance of Pd-Pt catalysts for aromatic hydrogenation.* Catalysis Today, 1999. **50**(1): p. 63-71.
8. Venezia, A.M., et al., *Hydrogenation of aromatics over Au-Pd/SiO2-Al2O3 catalysts; support acidity effect.* Applied Catalysis, A: General, 2004. **264**(1): p. 43-51.
9. Simon, L.J., et al., *Sulfur-tolerant Pt-supported zeolite catalysts for benzene hydrogenation I. Influence of the support.* Journal of catalysis, 2001. **201**(1): p. 60-69.
10. Simon, L.J., et al., *Sulfur-tolerant Pt-supported catalysts for benzene hydrogenation II. Influence of cation exchange level for Pt/MOR-based catalysts.* Journal of catalysis, 2001. **203**(2): p. 434-442.
11. Lin, S.D. and M.A. Vannice, *Hydorgenation of aromatic-hydrocarbons over supported Pt catalysts.1. Benzene hydrogenation.* Journal of catalysis, 1993. **143**(2): p. 539-553.
12. Lin, S.D. and M.A. Vannice, *Hydrogenation of aromatic-hydrocarbons over supported Pt catalysts 2. Toluene hydrogenation.* Journal of catalysis, 1993. **143**(2): p. 554-562.
13. Lin, S.D. and M.A. Vannice, *Hydrogenation of aromatic-hydrocarbons over supported Pt catalysts 3. Reaction models for metal-surfaces and acidic sites on oxide supports.* Journal of catalysis, 1993. **143**(2): p. 563-572.
14. Zheng, J., M. Guo, and C. Song, *Characterization of Pd catalysts supported on USY zeolites with different SiO2/Al2O3 for the hydrogenation of naphthalene in the presence of benzothiophene.* Fuel Processing Technology, 2008. **89**(4): p. 467-474.
15. Yasuda, H. and Y. Yoshimura, *Hydrogenation of tetralin over zeolite-supported Pd-Pt catalysts in the presence of dibenzothiophene.* Catalysis Letters, 1997. **46**(1-2): p. 43-48.
16. Yasuda, H., et al., *Confirmation of sulfur tolerance of bimetallic Pd-Pt supported on highly acidic USY zeolite by EXAFS.* Catalysis Letters, 1998. **54**(1-2): p. 23-27.
17. Navarro, R.M., et al., *Hydrogenation of Aromatics on Sulfur-Resistant PtPd Bimetallic Catalysts.* Journal of catalysis, 2000. **189**(1): p. 184-194.
18. Barrio, V.L., et al., *Hydrodesulfurization and hydrogenation of model compounds on silica-alumina supported bimetallic systems.* Fuel, 2003. **82**(5): p. 501-509.

19. Jongpatiwat, S., et al., *Competitive hydrogenation of poly-aromatic hydrocarbons on sulfur-resistant bimetallic Pt-Pd catalysts.* Applied Catalysis, A: General, 2004. **262**(2): p. 241-253.
20. Albonetti, S., et al., *Nanosized Pd/Pt and Pd/Rh catalysts for naphthalene hydrogenation and hydrogenolysis/ring-opening.* Catalysis Letters, 2006. **108**(3-4): p. 197-207.
21. Pawelec, B., et al., *AuPd alloy formation in Au-Pd/Al2O3 catalysts and its role on aromatics hydrogenation.* Applied Surface Science, 2005. **242**(3-4): p. 380-391.
22. Rocha, A.S., et al., *Tetralin hydrogenation on dealuminated Y zeolite-supported bimetallic Pd-Ir catalysts.* Catalysis Today, 2008. **133-135**: p. 394-399.
23. Simon, L.J., et al., *Effect of Co and Ni on benzene hydrogenation and sulfur tolerance of Pt/H-MOR.* Applied Catalysis, A: General, 2003. **252**(2): p. 283-293.
24. Lin, T.B., C.A. Jan, and J.R. Chang, *Aromatics reduction over supported platinum catalysts. 2. Improvement in sulfur resistance by addition of pallaium to supported platinum catalysts.* Industrial & Engineering Chemistry Research, 1995. **34**(12): p. 4284-4289.
25. Song, C.S. and A.D. Schmitz, *Zeolite-supported Pd and Pt catalysts for low-temperature hydrogenation of naphthalene in the absence and presence of benzothiophene.* Energy & Fuels, 1997. **11**(3): p. 656-661.
26. Guo, M., *Hydrogenation of Naphthalene over Noble-metal Catalysts at Low Temperature in the presence of Sulfur*, in *Material Science and Engineering*. 2000, The Pennsylvania State University: University Park.
27. Sprague, M., *Sulfur-induced Deactivation of Zeolite supported Noble-metal Hydrogenation catalysts at Low Temperature*, in *Energy and Geo-Environmental Engineering*. 2001, The Pennsylvania State University: University Park.
28. Jiang, H., et al., *Effect of palladium on sulfur resistance in Pt-Pd bimetallic catalysts.* Catalysis Today, 2007. **125**(3-4): p. 282-290.
29. Song, C.S., *Designing sulfur-resistant, noble-metal hydrotreating catalysts.* Chemtech, 1999. **29**(3): p. 26-30.
30. Song, C., *A Proposed New Concept for Design of Sulfur-Resistant Noble Metal Catalysts Based on Shape-Selective Exclusion and Hydrogen Spillover*, in *Shape-Selective Catalysis, Chemical Synthesis and Hydrocarbon Processing*. 1999, American Chemical Society: Washington, DC. p. 381-389.
31. Topsoe, H., Clausen, B.S., and Massoth, F.E., *Hydrotreating Catalysis Science and Technology*. 1996, Berlin Heidelberg: Springer-Verlag.
32. Stanislaus, A. and B.H. Cooper, *Aromatic Hydrogenation Catalysis: A Review.* Catalysis Reviews: Science and Engineering, 1994. **36**(1): p. 75 - 123.
33. Ali, S. and M. Siddiqui, *Dearomatization, cetane improvement and deep desulfurization of diesel feedstock in a single-stage reactor.* Reaction Kinetics and Catalysis Letters, 1997. **61**(2): p. 363-368.
34. Stork, W.H.J., *Performance testing of hydroconversion catalysts.* Deactivation and Testing of Hydrocarbon-Processing Catalysts, 1996. **634**: p. 379-400.
35. Song, C. and X.L. Ma, *New design approaches to ultra-clean diesel fuels by deep desulfurization and deep dearomatization.* Applied Catalysis B-Environmental, 2003. **41**(1-2): p. 207-238.
36. Stanislaus, A. and B.H. Cooper, *Aromatic Hydrogenation Catalysis - a Review.* Catalysis Reviews-Science and Engineering, 1994. **36**(1): p. 75-123.
37. Cooper, B.H. and B.B.L. Donnis, *Aromatic saturation of distillates: An overview.* Applied Catalysis a-General, 1996. **137**(2): p. 203-223.

38. Stanislaus, A., A. Marafi, and M.S. Rana, *Recent advances in the science and technology of ultra low sulfur diesel (ULSD) production.* Catalysis Today. **153**(1-2): p. 1-68.
39. UOP. *MQD Unionfining Process*. [cited 2011 Feb. 17th]; Available from: http://www.uop.com/objects/24%20MQD%20Unionfining.pdf.
40. Maxwell, I.E., *Innovation in Applied Catalysis.* Cattech, 1997. **1**: p. 5-13.
41. Suchanek, A., *How to make low sulfur, low aromatics, high cetane diesel fuel.* Abstracts of Papers of the American Chemical Society, 1996. **212**: p. 23-Petr.
42. ABB Lummus Global, I., *Hydrotreating.* Hydrocarbon Processing, 1998. **77**(11): p. 90.
43. EPA, *Regulatory Impact Analysis: Heavy-Duty Engine and Vehicle Standards and Highway Diesel Fuel Sulfur Control Requirements*. 2000, United States Environmental Protection Agency, Air and Radiation.
44. Bartholomew, C.H., P.K. Agrawal, and J.R. Katzer, *Sulfur poisoning of metals.* Advances in Catalysis, 1982. **31**: p. 135-242.
45. Maxted, E.B., et al., *The Poisoning of Metallic Catalysts*, in *Advances in Catalysis*. 1951, Academic Press. p. 129-178.
46. Satterfield, C.N. and G.W. Roberts, *Kinetics of thiophene hydrogenolysis on a cobalt molybdate catalyst.* AIChE Journal, 1968. **14**(1): p. 159-164.
47. Maxted, E.B. and H.C. Evans, *135. Catalytic toxicity and chemical structure. Part I. The relative toxicity of sulphur compounds in catalytic hydrogenation.* Journal of the Chemical Society (Resumed), 1937: p. 603-606.
48. Gallezot, P., *The State and Catalytic Properties of Platinum and Palladium in Faujasite-type Zeolites.* Catalysis Reviews: Science and Engineering, 1979. **20**(1): p. 121 - 154.
49. Mills, G.A., et al., *(Houdriforming Reactions) Catalytic Mechanism.* Industrial & Engineering Chemistry, 1953. **45**(1): p. 134-137.
50. Dalla Betta, R.A. and M. Boudart. in *Proc. 5th Int. Cong. on Catalysis*. 1973: North Holland, Amsterdam.
51. Karpinski, Z., H.P. D.D. Eley, and B.W. Paul, *Catalysis by Supported, Unsupported, and Electron-Deficient Palladium*, in *Advances in Catalysis*. 1990, Academic Press. p. 45-100.
52. Sachtler, W.M.H. and A.Y. Stakheev, *Electron-deficient palladium clusters and bifunctional sites in zeolites.* Catalysis Today, 1992. **12**(2-3): p. 283-295.
53. Sachtler, W.M.H. and Z.C. Zhang, *Zeolite-supported Transition-metal catalysts.* Advances in Catalysis, 1993. **39**: p. 129-220.
54. Simon, L.J., et al., *Sulfur tolerance of Pt/mordenites for benzene hydrogenation Do Bronsted acid sites participate in hydrogenation?* Catalysis Today, 2002. **73**(1-2): p. 105-112.
55. Sabatier, P., *Hydrogénations et déshydrogénations par catalyse.* Berichte der deutschen chemischen Gesellschaft, 1911. **44**(3): p. 1984-2001.
56. Rylander, P.N., *Catalytic hydrogenation over platinum metals*. 1967: Academic P.
57. Albertazzi, S., et al., *Hydrogenation of naphthalene on noble-metal-containing mesoporous MCM-41 aluminosilicates.* Journal of Molecular Catalysis A: Chemical, 2003. **200**(1-2): p. 261-270.
58. Baetzold, R.C., *Calculated Properties of Metal Aggregates. II. Silver and Palladium.* The Journal of Chemical Physics, 1971. **55**(9): p. 4363-4370.
59. Hu, L.J., et al., *Strong effect of transitional metals on the sulfur resistance of Pd/HY-Al2O3 catalysts for aromatic hydrogenation.* Journal of Molecular Catalysis a-Chemical, 2001. **171**(1-2): p. 169-179.

60. Niquille-Roethlisberger, A. and R. Prins, *Hydrodesulfurization of 4,6-dimethyldibenzothiophene and dibenzothiophene over alumina-supported Pt, Pd, and Pt-Pd catalysts.* Journal of catalysis, 2006. **242**(1): p. 207-216.
61. Schmitz, A.D., G. Bowers, and C.S. Song, *Shape-selective hydrogenation of naphthalene over zeolite-supported Pt and Pd catalysts.* Catalysis Today, 1996. **31**(1-2): p. 45-56.
62. Reddy, K.M. and C.S. Song, *Mesoporous zeolite-supported noble metal catalysts for low-temperature hydrogenation of aromatics in distillate fuels.* Am. Chem. Soc. Div. Fuel Chem. Prepr., 1996. **41**(3): p. 906-910.
63. Albertazzi, S., et al., *New Pd/Pt on Mg/Al basic mixed oxides for the hydrogenation and hydrogenolysis of naphthalene.* Journal of catalysis, 2004. **223**(2): p. 372-381.
64. Lai, W.C. and C.S. Song, *Conformational isomerization of cis-decahydronaphthalene over zeolite catalysts.* Catalysis Today, 1996. **31**(1-2): p. 171-181.
65. Weitkamp, A.W., *Deuteriation and deuterogenation of naphthalene and 2 octalins.* Journal of catalysis, 1966. **6**(3): p. 431-&.
66. Frye, C.G., *Equilibria in the Hydrogenation of Polycyclic Aromatics.* Journal of Chemical & Engineering Data, 1962. **7**(4): p. 592-595.
67. Frye, C.G. and A.W. Weitkamp, *Equilibrium hydrogenations of multi-ring aromatics.* Journal of Chemical & Engineering Data, 1969. **14**(3): p. 372-376.
68. Anderson, R.B. and P.T. Dawson, *Experimental methods in catalytic research*. Vol. 2. 1976: Academic Press.
69. Lerner, B.A., B.T. Carvill, and W.M.H. Sachtler, *Microgeometry of Pt/Mordenite and stereoselectivity of methylcyclopentane ring-opening catalysis.* Journal of Molecular Catalysis, 1992. **77**(1): p. 99-108.
70. Satterfield, C.N., *Heterogeneous catalysis in practice*. 1980: McGraw-Hill.
71. Zhou, F., et al., *Hydrodesulfurization of dibenzothiophene catalyzed by Pd supported on overgrowth-type MCM-41/HY composite.* Catalysis Today, 2010. **150**(3-4): p. 218-223.
72. Zhang, H., et al., *MCM-41 Overgrown on Y Composite Zeolite as Support of PdPt Catalyst for Hydrogenation of Polyaromatic Compounds.* Industrial & Engineering Chemistry Research, 2007. **46**(12): p. 4186-4192.
73. Meng, X.C., Y.X. Wu, and Y.D. Li, *Tailoring the pore size of zeolite Y as the support of diesel aromatic saturation catalyst.* Journal of Porous Materials, 2006. **13**(3-4): p. 365-371.
74. Ismagilov, Z.R., et al., *Deep desulphurization of diesel fuels on bifunctional monolithic nanostructured Pt-zeolite catalysts.* Catalysis Today, 2009. **144**(3-4): p. 235-250.
75. Chen, H., et al., *Contribution of hydrogen spillover to the hydrogenation of naphthalene over diluted Pt/RHO catalysts.* Applied Catalysis, A: General, 2009. **358**(2): p. 103-109.
76. Reddy, K.M., L. Sun, and C.S. Song, *Effect of physico-chemical properties of ZSM-5 on shape selective methylation of toluene.* Am. Chem. Soc. Div. Petrol. Chem. Prepr., 1998. **43**(2): p. 251-255.
77. Sprague, M., J. Zheng, and C.S. Song, *Effect of sulfur removal from naphthalene on its hydrogenation over mordenite-supported palladium catalyst.* Am. Chem. Soc. Div. Petrol. Chem. Prepr., 2002. **47**(2): p. 103-105.
78. Ceckiewicz, S. and B. Delmon, *Cooperative action of Pt/gamma-Al2O3 catalyst and gamma-Al2O3 diluent in the hydrogenation of benzene.* Journal of catalysis, 1987. **108**(2): p. 294-303.
79. Senger, B.C. and C.S. Song, *Low-temperature hydrogenation of tetralin over supported noble-metal catalysts in the presence of sulfur.* Am. Chem. Soc., Div. Petrol. Chem. Prepr., 2004. **49**(3): p. 297-299.

80. Huang, T.C. and B.C. Kang, *Kinetic-study of naphthalene hydrogenation over Pt/Al2O3 catalyst.* Industrial & Engineering Chemistry Research, 1995. **34**(4): p. 1140-1148.
81. Niquille-Rothlisberger, A. and R. Prins, *Hydrodesulfurization of 4,6-dimethyldibenzothiophene and dibenzothiophene over alumina-supported Pt, Pd, and Pt-Pd catalysts.* Journal of Catalysis, 2006. **242**(1): p. 207-216.
82. Conner, W.C., G.M. Pajonk, and S.J. Teichner, *Spillover of sorbed species.* Advances in Catalysis, 1986. **34**: p. 1-79.
83. Rozanov, V.V. and O.V. Krylov, *Hydrogen spillover in heterogeneous catalysis.* Uspekhi Khimii, 1997. **66**(2): p. 117-130.
84. Levy, R.B. and M. Boudart, *Kinetics and mechanism of spillover.* Journal of catalysis, 1974. **32**(2): p. 304-314.
85. Sermon, P.A. and G.C. Bond, *Studies of hydrogen spillover 4. Factors affecting hydrogen spillover and its reversal.* Journal of the Chemical Society, Faraday Transactions, 1980. **76**: p. 889-900.
86. Auerbach, S.M., K.A. Carrado, and P.K. Dutta, *Handbook of Zeolite Science and Technology*. 2003, New York: Marcel Dekker, Inc.
87. Baerlocher, C., L.B. McCusker, and D. Olson, *Atlas of zeolite framework types*. 2001: Elsevier.
88. Matsui, T., et al., *EXAFS study on the sulfidation behavior of Pd, Pt and Pd-Pt catalysts supported on amorphous silica and high-silica USY zeolite.* Applied Catalysis, A: General, 2005. **290**(1-2): p. 73-80.
89. Gallezot, P., et al., *Location and dispersion of platinum in PtY zeolites.* Journal of Catalysis, 1975. **39**(3): p. 334-349.
90. Anderson, R.B. and P.T. Dawson, *Experimental methods in catalytic research*. 1976: Academic Press.
91. Sugioka, M., et al., *Noble metals supported on mesoporous silicate FSM-16 as new hydrodesulfurization catalyst.* Catalysis Today, 1997. **39**(1-2): p. 61-67.
92. Sugioka, M., et al., *Hydrodesulfurization over noble metals supported on ZSM-5 zeolites.* Catalysis Today, 1998. **45**(1-4): p. 327-334.
93. Sugioka, M., et al., *New hydrodesulfurization catalysts: noble metals supported on USY zeolite.* Catalysis Today, 1996. **29**(1-4): p. 255-259.
94. Fujikawa, T., et al., *EXAFS characterization of bimetallic Pt–Pd/SiO2-Al2O3 catalysts for hydrogenation of aromatics in diesel fuel.* Catalysis Letters, 1999. **63**(1): p. 27-33.
95. Karpinski, Z., *Catalysis by Supported, Unsupported, and Electron-Deficient Palladium.* Advances in Catalysis, 1990. **37**: p. 45-100.
96. Minachev, K.M., et al., *Hydrogenation of aromatic hydrocarbons on nickel catalysts modified with heteropolycompounds.* Petroleum Chemistry U.S.S.R., 1985. **25**(4): p. 221-228.
97. Yoshimura, Y., et al., *Active phases and sulfur tolerance of bimetallic Pd-Pt catalysts used for hydrotreatment.* Applied Catalysis A: General, 2007. **322**: p. 152-171.
98. Jongpatiwut, S., et al., *Competitive hydrogenation of poly-aromatic hydrocarbons on sulfur-resistant bimetallic Pt-Pd catalysts.* Applied Catalysis a-General, 2004. **262**(2): p. 241-253.
99. Weitkamp, A.W., H.P. D.D. Eley, and B.W. Paul, *Stereochemistry and Mechanism of Hydrogenation of Naphthalenes on Transition Metal Catalysts and Conformational Analysis of the Products.* Advances in Catalysis, 1968. **18**: p. 1-110.
100. Papapolymerou, G. and V. Bontozoglou, *Decomposition of NH3 on Pd and Ir Comparison with Pt and Rh.* Journal of Molecular Catalysis A: Chemical, 1997. **120**(1-3): p. 165-171.

101. Rades, T., et al., *Diffuse Reflectance IR Study of CO Adsorption on a Bimetallic PtPd Catalyst Supported on NaY Zeolite. Evidence of Alloy Formation.* The Journal of Physical Chemistry, 1996. **100**(40): p. 16238-16241.
102. Squires, R.R., *Correlation of electron and hydrogen atom binding energies for transition-metal atoms.* Journal of the American Chemical Society, 1985. **107**(15): p. 4385-4390.
103. Levenspiel, O., *Chemical reaction engineering*. 1999: Wiley.
104. Ohgoshi, S., I. Nakamura, and Y. Wakushima, *Hydrogenation of isobutylene by spiltover hydrogen from Pt/KA-zeolite to NaY zeolite* Studies in Surface Science and Catalysis, 1993. **77**: p. 289-292.
105. IZA. *Zeolite Y (FAU) database*. [cited; Available from: http://www.iza-online.org/.
106. Ghosh, A.K. and G. Curthoys, *Characterization of zeolite activity- A thermal study of normal-butylamine and ammonia adsorbed on mordenites.* Journal of Physical Chemistry, 1984. **88**(6): p. 1130-1132.
107. Xiao, T.C., et al., *Effect of the addition of antifoulant agents on the deactivation of NiMoP/Al2O3 catalysts for hydrotreating of residuum.* Industrial & Engineering Chemistry Research, 2000. **39**(10): p. 3679-3687.
108. Kikuchi, E., et al., *The effect of spillover hydrogen on coke formation catalyzed by HY zeolite and pillared montmorillonite*, in *Studies in Surface Science and Catalysis*. 1993, Elsevier. p. 53-60.
109. Fujimoto, K., K.F.T.U. T. lnui, and M. Masai, *Catalyst design based on spillover theory*, in *Studies in Surface Science and Catalysis*. 1993, Elsevier. p. 9-16.
110. Zhang, A., et al., *Isomerization of n-Pentane and Other Light Hydrocarbons on Hybrid Catalyst. Effect of Hydrogen Spillover.* Industrial & Engineering Chemistry Research, 1995. **34**(4): p. 1074-1080.
111. Sermon, P.A. and G.C. Bond, *Hydrogen Spillover.* Catalysis Reviews, 1974. **8**(1): p. 211-239.

# VITA

**Hyun Jae Kim**

## ■ Educational Background

**Doctor of Philosophy** (Ph.D.) in department of energy and geo-environmental engineering , Pennsylvania State university, University Park, USA (Aug.2005 ~ Aug.2011)

**Master of Science** (M.S.) in department of chemical engineering, Yonsei University, Seoul, South Korea (Mar. 2001 ~ Feb. 2003)

**Bachelor of Science** (B.S.) in department of chemical engineering, Yonsei University, Seoul, South Korea (Mar. 1994~ Feb. 2001)

## ■ Awards/Fellowship

1. Student Award for Best Paper at the American Chemical Society national meeting (2008)
   - Division of Petroleum Chemistry, American Chemical Society
2. Anne C. Wilson Graduate Student Research award (2005)
   - College of earth and mineral science, Pennsylvania State University
3. University Graduate Fellowship, Pennsylvania State University (2005)

## ■ Publications during Ph.D. study (Papers and Conference proceedings)

1. Enhanced sulfur tolerance of hybrid zeolite-supported Pd catalyst for low temperature hydrogenation of diaromatics, **Hyun Jae Kim**, Chunshan Song, in preparation

2. Sulfur-tolerant hybrid zeolite-supported Pd catalyst based on Shape-selective Exclusion and Hydrogen Spillover for low-temperature hydrogenation of aromatics, **Hyun Jae Kim**, Chunshan Song, in preparation

3. Aromatic hydrogenation over hybrid zeolite-supported catalyst with sulfur tolerance by shape selective exclusion of sulfur compound, 238$^{th}$ American Chemical Society National Meeting, August, 2009, Washinton D.C

4. Hybrid zeolite-supported Pd catalyst with shape selectivity for aromatic hydrogenation in diesel fuel, 14$^{th}$ International Congress on Catalysis, July, 2008, Seoul, Korea

5. Hybrid zeolite-supported catalyst with shape selectivity and sulfur tolerance for low temperature aromatic hydrogenation, 235$^{th}$ American Chemical Society National Meeting, April, 2008, New Orleans, Louisiana

6. Optimal design for integrating $CO_2$ capture and fuel conversion technologies in a 500MWe Coal-based Power plant, Proceedings 23$^{rd}$ Annual International Pittsburgh Coal Conference, Sep, 2006, Pittsburgh, Pennsylvania